



1-1-2018

Seismic Analysis Of Wind Turbines

Sam Austin

Follow this and additional works at: <https://commons.und.edu/theses>

Recommended Citation

Austin, Sam, "Seismic Analysis Of Wind Turbines" (2018). *Theses and Dissertations*. 2389.
<https://commons.und.edu/theses/2389>

This Dissertation is brought to you for free and open access by the Theses, Dissertations, and Senior Projects at UND Scholarly Commons. It has been accepted for inclusion in Theses and Dissertations by an authorized administrator of UND Scholarly Commons. For more information, please contact zeinebyousif@library.und.edu.

SEISMIC ANALYSIS OF WIND TURBINES

by

Sam Austin
Master of Science, University of Tehran, 2008

A Dissertation

Submitted to the Graduate Faculty

of the

University of North Dakota

in partial fulfillment of the requirements

for the degree of

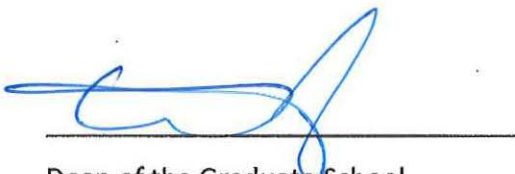
Doctor of Philosophy

Grand Forks, North Dakota
December
2018

This dissertation, submitted by Sam Austin in partial fulfillment of the requirements for the Degree of Doctor of Philosophy from the University of North Dakota, has been read by the Faculty Advisory Committee under whom the work has been done and is hereby approved.

Sukhvarsh Jerath 12-6-2018
SUKHVARSH JERATH
Name of Chairperson
DABA GEDABA 12/6/18
Name of Committee Member
NABIL SULEIMAN
Name of Committee Member
WILLIAM SEMKE
Name of Committee Member
MICHAEL MANN
Name of Committee Member
Nabil Suleiman

This dissertation meets the standards for appearance, conforms to the style and format requirements of the Graduate School of the University of North Dakota, and is hereby approved.



Dean of the Graduate School

December 6, 2018

Date

PERMISSION

Title SEISMIC ANALYSIS AND DESIGN OF WIND TURBINES

Department Civil Engineering

Degree Doctor of Philosophy

In presenting this dissertation in partial fulfillment of the requirements for a graduate degree from the University of North Dakota, I agree that the library of this University shall make it freely available for inspection. I further agree that permission for extensive copying for scholarly purposes may be granted by the professor who supervised my dissertation work or, in his absence, by the chairperson of the department or the dean of the Graduate School. It is understood that any copying or publication or other use of this dissertation or part thereof for financial gain shall not be allowed without my written permission. It is also understood that due recognition shall be given to me and to the University of North Dakota in any scholarly use which may be made of any material in my dissertation.

Typed Name Sam Austin
Date 12/6/2018

TABLE OF CONTENTS

PERMISSION	iii
TABLE OF CONTENTS.....	iv
LIST OF FIGURES.....	vii
LIST OF TABLES.....	x
ABSTRACT.....	xii
CHAPTER 1 INTRODUCTION.....	1
Background.....	1
Problem Statement.....	6
Objectives and Scope.....	9
CHAPTER 2 LITERATURE REVIEW	12
Standards and Guidelines	12
Publications on Earthquake Design and Analysis	14
CHAPTER 3 THEORETICAL FORMULATIONS AND METHODOLOGY	27
Theoretical Formulations.....	27
Time Domain.....	27
Frequency Domain.....	34
Methodology.....	36
Seismic Loads	36
Assumptions and Considerations	44
CHAPTER 4 PARAMETRIC STUDY OF WIND TURBINES	45
Validation of Numerical Method	45
Experimental Model.....	45
Experimental Test	46
Experimental Results	47
Validation Model.....	49

Validation Analysis	55
Validation Results	56
Parametric Models.....	57
Geometry	57
Material Properties.....	58
Meshing.....	59
Parametric Analysis.....	60
Modal Analysis	61
Transient Analysis	62
CHAPTER 5 SOIL-STRUCTURE INTERACTION.....	69
Frequency Based Design	69
Numerical Soil Models	70
Linear Soil Pressure Distribution Model	70
K-Model.....	71
Explicit Model.....	71
Foundation Types.....	72
Spread Foundation.....	72
Mono Pile	73
Pile Group & Cap.....	73
Anchored Spread Foundation	73
Parametric Models.....	74
Geometry	74
Material Properties.....	75
Meshing.....	76
Parametric Analysis.....	77
Modal Analysis	77
Transient Analysis	81
CHAPTER 6 RESULTS.....	84
Damping Effects	84
Load Direction Effects.....	87
Resonance and Load Frequency Effects	88
Turbine Size Effects.....	90

Soil-Structure Interaction Effects.....	91
Response Spectrum vs. Transient Analysis.....	96
CHAPTER 7 SUMMARY AND CONCLUSION	100
Summary	100
Conclusion.....	101
APPENDIX A TRANSIENT ANALYSIS DATA FOR WIND TURBINES WITHOUT FOUNDATIONS	105
65kW Tower	105
1MW Tower	110
5MW TOWER	116
APPENDIX B TRANSIENT ANALYSIS DATA FOR WIND TURBINES WITH FOUNDATIONS.	122
1MW & Foundation	122
REFERENCES	127

LIST OF FIGURES

Figure 1. Three types of vertical axis wind turbines	2
Figure 2. Horizontal axis wind turbine parts	3
Figure 3. Geometrical parameters of horizontal axis wind turbines	4
Figure 4. Different types of towers	5
Figure 5. Horizontal axis wind turbines	6
Figure 6. United States wind map.....	7
Figure 7. System of lumped masses and flexible rods used by Ritschel et al.	14
Figure 8. Finite element model used by Bazeos et al.	15
Figure 9. Finite element model used by Lavassas et al.	16
Figure 10. Multibody system used by X. Zhao et al.	17
Figure 11. Turbine model used by M. Hänler et al.	18
Figure 12. Hybrid model used by X. Zhao et al.	19
Figure 13. Finite element model used by Prowell et al.	20
Figure 14. Experimental wind turbine and shake table	21
Figure 15. Foundation model used by M. Hongwang	22
Figure 16. Finite element model used by R.S. Kourkoulis et al.	23
Figure 17. Model of the 5 MW wind turbine used by R.A. Kjølraug et al	24
Figure 18. Foundation model used by F. Taddeia et al.	25
Figure 19 (a). Input accelerations for Imperial Valley earthquake North-South direction	38
Figure 20. Filtered East-West component of Landers earthquake	47
Figure 21. Recorded acceleration at top of the nacelle	48
Figure 22. Acceleration transfer function from base to top of the nacelle	48
Figure 23. Observed 1st and 2nd mode shapes	49

Figure 24. Nacelle and hub dimensions for the 65 kW wind turbine	50
Figure 25. Blade dimensions for the 65 kW wind turbine	50
Figure 26. Finite element model of the 65 kW wind turbine	52
Figure 27. SHELL181 element []	53
Figure 28. SOLID186 element [53]	55
Figure 29. Experimental and numerical transient results with 0.86% damping	56
Figure 30. First three mode shapes of the validation model.....	56
Figure 31. Blade dimensions for the 1 MW and 5 MW wind turbines	58
Figure 32. Horizontal and vertical mode shapes of parametric model towers	61
Figure 33. Acceleration response at top of the nacelle in the X and Y directions for the 1 MW turbine with 0.5%, 1%, and 2% damping ratios	64
Figure 34. Acceleration response in the Z direction for 0.5%, 1%, and 2% damping ratios	65
Figure 35. Acceleration response at top of the nacelle in the X and Y directions for the 5 MW turbine with 1% damping ratio	65
Figure 36. Displacement at top of the nacelle in the Y direction with 1.0% damping	66
Figure 37. Displacement at top of the nacelle in the Z direction with 1.0% damping	66
Figure 38. $\sigma_{\text{von Mises max}}/\sigma_y$ at tower base.....	67
Figure 39. $\sigma_{\text{von Mises max}}/\sigma_y$ at tower base.....	67
Figure 40. Allowable frequency range	70
Figure 41. Soil pressure distribution in K-model	71
Figure 42. Spread foundation and pedestal	72
Figure 43. Placement of piles and anchors	74
Figure 44. Meshing of 1 MW turbine with different foundation types.....	78
Figure 45. Meshing of pile group & cap foundation and explicit soil.....	78
Figure 46. Comparison of acceleration response at top of the nacelle in the X direction for 1 MW system with K soil and different foundation types	82
Figure 47. Reversal of acceleration in 1S2.0-L analysis	85
Figure 48. Amplitude vs. frequency for Landers, Imperial Valley, and Northridge loads	90
Figure 49. First natural frequency (Hz) of 65 kW system	93

Figure 50. Second natural frequency (Hz) of 65 kW system.....	93
Figure 51. Third natural frequency (Hz) of 65 kW system	94
Figure 52. Third natural frequency (Hz) of 1 MW system	95
Figure 53. Third natural frequency (Hz) of 5 MW system	95
Figure 54. ASCE 7-10 design spectrum for DHS (stiff soil) (5% damping).....	98

LIST OF TABLES

Table 1. PGA and frequency of earthquake loads	37
Table 2. Physical properties of the experimental wind turbine	46
Table 3. Material properties used in the finite element model	51
Table 4. Meshing summary.....	51
Table 5. Natural modes of validation model	57
Table 6. Physical properties of parametric models	59
Table 7. Number of nodes and element of the parametric model parts	59
Table 8. Natural modes of parametric models	60
Table 9. Peak acceleration and deformation response at top of the nacelle and maximum von Mises stress at tower base	68
Table 10. Dimensions of the soil bodies and foundations.....	75
Table 11. Mechanical properties of soil.....	76
Table 12. Meshing summary.....	76
Table 13. Natural frequencies and mode shapes of the 65 kW structure.....	79
Table 14. Natural frequencies and mode shapes of the 1 MW structure	80
Table 15. Natural frequencies and mode shapes of the 5 MW structure	81
Table 16. Peak acceleration and deformation response at top of the nacelle and maximum von Mises stress at tower base for 1 MW system with K soil and different foundation types.....	82
Table 17. Normalized peak acceleration and deformation response at top of the nacelle, and normalized von Mises stress at tower base for all analyses	86
Table 18. Effect of damping on normalized acceleration, deformation, and stress (Landers earthquake).....	87
Table 19. Effect of load direction on normalized acceleration, deformation and stress (Landers earthquake).....	88

Table 20. Effect of earthquake load properties (1% damping)	89
Table 21. Response comparison for different turbine sizes (Landers earthquake)	91
Table 22. Change in acceleration at top of the 1MW nacelle with soil & foundation	96
Table 23. Accelerations based on IEC 61400 design spectrum and transient methods ..	99
Table 24. Moment demands based on IEC 61400 design spectrum and transient analysis	99

ABSTRACT

The goal of this research is to add additional data to an expanding body of knowledge in the field of seismic engineering of wind turbines through a series of numerical analyses and also comparing them to current guidelines. This data can be used to further study the dynamic behavior of wind turbines under seismic loads and also provides answers to some of the questions in this field. This is important considering the expansion of wind farms into seismically active regions, increasing size of wind turbines, and lack of specific guidelines for seismic design of wind turbines. This research also emphasizes the need for a comprehensive research on the seismic behavior of larger turbines. This study will outline the shortcomings of current design guidelines and will result in safer and more economic designs in the wind industry.

In the following chapters, first a review of existing codes and articles on the topic is presented. Then theoretical formulations associated with time and frequency domain methods are presented. These methods will be used in the numerical procedure in the following chapters. Next using experimental shake table results on an industrial scale wind turbine, the finite element model is first validated. Then a series of modal and transient finite element analyses are performed on three horizontal axis tubular steel wind turbines towers on four types of foundations. Effect of soil is added using both implicit and explicit techniques. Seismic response of wind turbines with different sizes is then analyzed and effect of different design parameters including damping ratio, load direction, natural frequencies, size, foundation type, and soil model is investigated. Finally, accuracy of the response spectrum method (first mode approximation) suggested by current design codes is evaluated.

The results of this study show that the acceleration response in the vertical direction is sensitive to damping values and in design of connections for vertical forces, lower damping ratios should be considered. It was also observed that for all turbine sizes, displacement and stress values in the horizontal directions were significantly higher compared to vertical direction which means tower design is governed by horizontal seismic forces. When it comes to critical seismic direction, it was seen that increasing the size of turbine, tends to change this direction therefore, turbines should be designed for both seismic directions. Another observation was that larger turbines (5 MW) with lower damping values can have vertical accelerations higher than horizontal and it shows the need for three dimensional design of connection components. When it comes to seismic resonance, it was shown that natural frequency of the wind turbines can be close enough to earthquake frequencies to cause amplification. Therefore, it's recommended to separate structural natural frequencies of wind turbines from both operational and seismic frequencies. Regarding the seismic design factor of safety, it was shown that factor of safety of wind turbines designed with current guidelines decrease as the wind turbine size increase. This is an important finding and reiterates the need for updated design codes considering the current trend in increasing size of turbines. Analysis results showed that including soil and foundation can increase the acceleration and displacement up to 13%. Therefore, it's recommended to include the soil-structure interaction. When it comes to foundation, it was shown that different foundation types shift the structural frequencies unequally. This shows the importance of foundation type selection to avoid resonance. This study concludes that for wind turbines that have a frequency-based foundation design, the soil can be modeled faster and easier using the K-model. The results of this study also showed that moment demand value for the larger 5 MW turbine calculated based on IEC 61400 design guideline was smaller than what was seen in the transient FEA. This is a significant finding considering that size of modern wind turbines is

increasing and they are being installed more frequently in seismic regions. This suggests the need for reevaluation of the current design standards for wind turbines.

CHAPTER 1

INTRODUCTION

Background

Wind turbines are the world's fastest-growing source of renewable energy across America and around the globe. United States is one of the fastest-growing wind power markets in the world, second only to China. In 2015, the U.S. wind industry installed 8,598 MW of new capacity, a 77% increase over 2014 and the third highest annual total in history. The new installations bring total wind power capacity in the U.S. up to 74,471 MW [1], enough to power 20 million average American homes, accounting for 4.7 percent of the nation's electricity supply. Wind energy has supplied 30% of all new power capacity additions from 2010 to 2015 and 41% of new capacity additions in 2015 alone. Because of advancing technology and domestic manufacturing, wind has become one of the most affordable sources of electricity in the US. From 2009 to 2016 wind power's cost has dropped an impressive 66%. Wind has also become a major economic contributor. Since 2008, over \$114 billion in private investment has flowed into the U.S. wind industry [1,2,3].

Wind turbines can be categorized by the power output into three general classifications; residential, industrial, and utility scale. Residential scale turbines are small turbines with less than 50 kW power and are intended for remote power production. Industrial scale wind turbines are medium sized, with power output of 50 to 250 kW and are intended for remote grid production. Utility scale turbines are large turbines generating over 900 kW power per turbine. They are typically installed in large

arrays called wind energy projects. They can also be installed in small quantities on distribution lines. Utility scale development is the most common form of wind energy development in the U.S. [4].

Modern wind turbines work by taking energy from the wind to turn a rotor, which can rotate around a horizontal or vertical axis. In vertical axis wind turbines, the main rotor shaft is arranged vertically. These turbines do not need to be pointed to the wind direction to rotate. This is an advantage on sites where the wind direction is highly variable. With a vertical axis turbine, the generator and gearbox can be placed near the ground to be more accessible for maintenance. In this case, tower doesn't need to support this excessive weight. Drawbacks are that some designs produce pulsating torque, it is difficult to mount them on towers and therefore, they are often installed closer to the base on which they rest such as the ground or a building rooftop where the wind speed is lower. There are three types of vertical axis wind turbines; Darrieus, Giromill, and Savonius [5, 6, 7]. Figure 1 shows three types of vertical axis wind turbines.



a) Darrieus [5]

b) Giromill [6]

c) Savonius [7]

Figure 1. Three types of vertical axis wind turbines

In horizontal axis wind turbines, the rotor has wing shaped blades attached to a hub. Nacelle that houses a drive train consists of a gearbox, connecting

shafts, brakes, generator and other machinery fixed on top of a tall tower made of steel and/or concrete. At the bottom, tower and ground mounted electrical equipment like transformer are attached to the foundation [8]. Figure 2 shows different parts of a horizontal axis wind turbine.

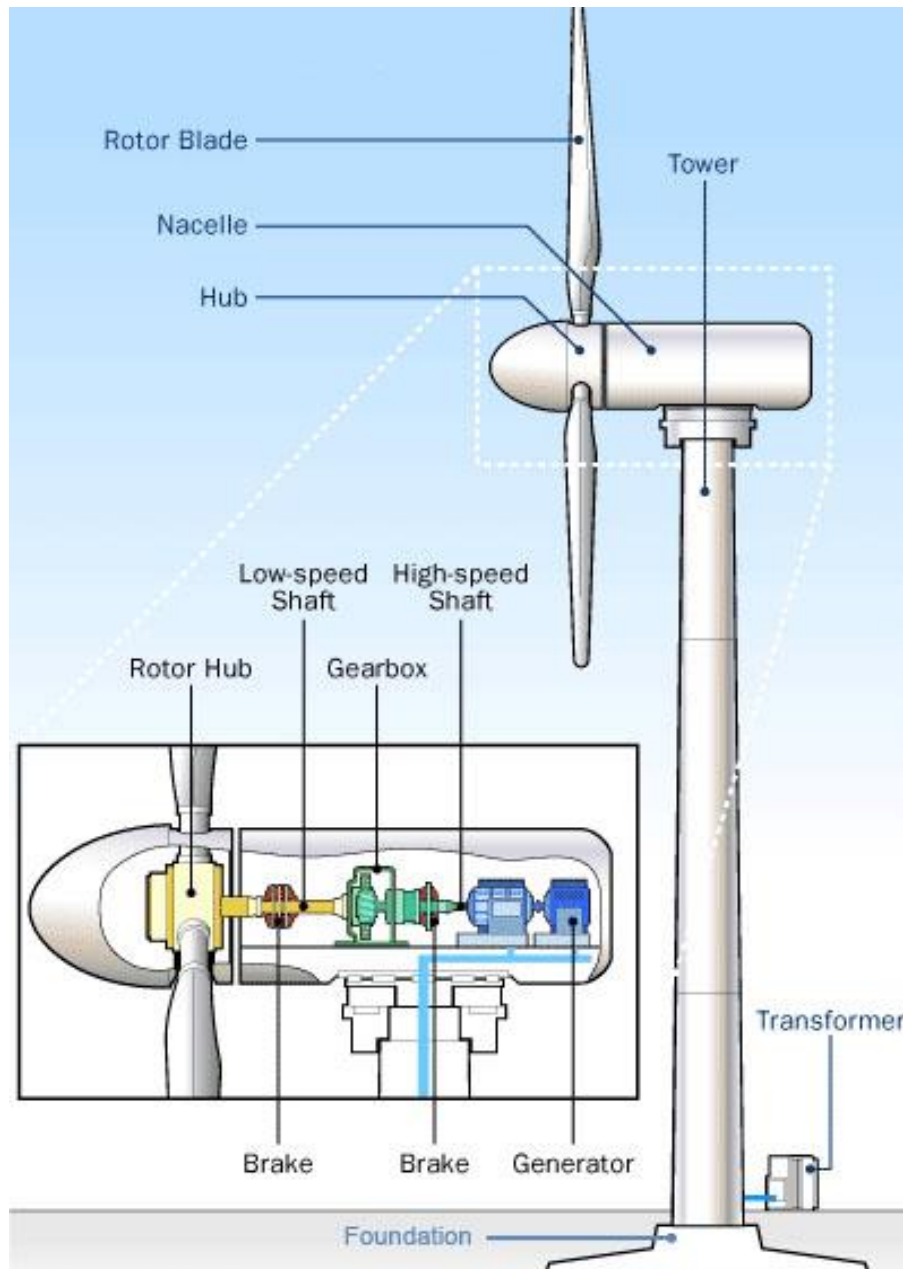


Figure 2. Horizontal axis wind turbine parts [9]

Wind turbines typically start generating electricity once the wind speed reaches 3-4 m/s (10-13 ft/s) and meet their rated output capacity at wind speeds of around 13 m/s (43 ft/s). The low speed, high torque rotation of the rotor is converted into high speed low torque rotation by a gearbox and this motion is then converted into electricity by an on-board generator located in the nacelle. To prevent damage to the generator and other components, wind turbines shutoff at a wind speed of 25 m/s (82 ft/s) [16]. Design geometrical parameters of horizontal axis wind turbines are the maximum height, hub height, and rotor diameter. Maximum turbine height depends on the hub height and the rotor diameter as depicted in Figure 3. There is no standard hub height or ratio of hub height to rotor diameter but in general, turbine hub heights are approximately 1 to 1.4 times the rotor diameter.



Figure 3. Geometrical parameters of horizontal axis wind turbines [4]

Wind turbine towers designs include guyed, truss (lattice), tubular (mono-pole), or a combination of these as shown in Figure 4. Guyed towers are cheaper than other types of towers but occupy a big area of land. These towers are more suitable for residential scale projects. Truss towers are also cheap; they are light and their design is flexible. These towers are usually used only in the design of coastal wind turbines because of the aesthetic aspect. Open section of truss towers allows winds and waves to

flow into and through structure, which can lead to less wind and wave loads [10]. On the down side, numerous connections are exposed to corrosion, weak diagonals are sensitive to wind excitation which creates durability issues [11], and their installation is time consuming due to the large number of different elements. Tubular towers are the most common types of towers. They need a small area of land, their appearance is more appealing, and their fabrication is relatively easy and fast.

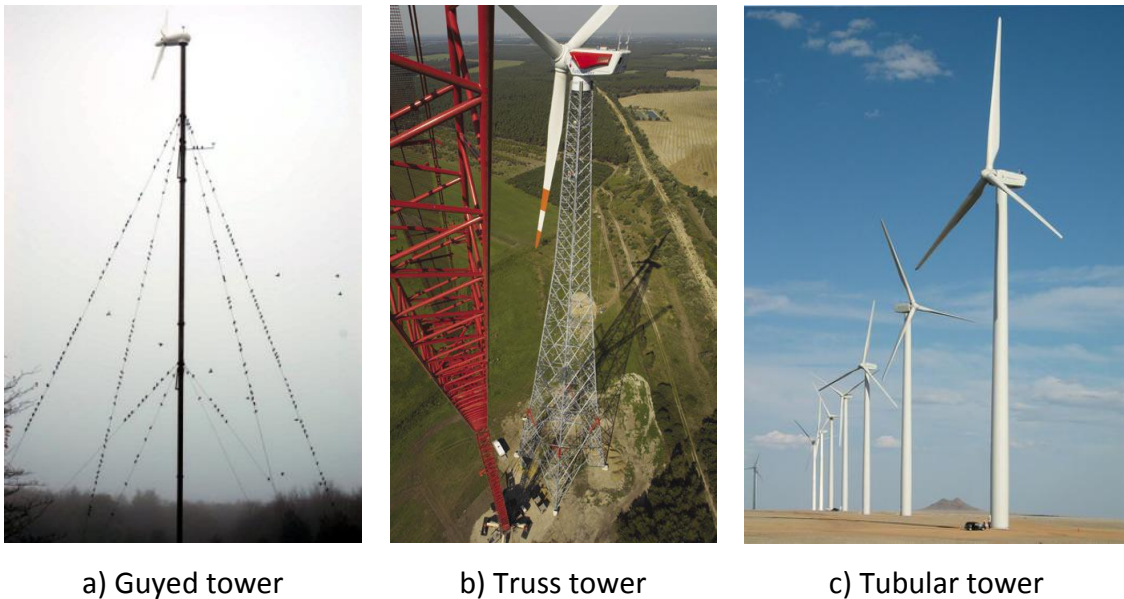


Figure 4. Different types of towers [12]

Wind turbine towers are made of steel, concrete, or a combination of both. Steel has a higher strength-to-weight ratio; it is relatively easy to construct and it can be recycled. Tall tubular towers are usually made of steel, using prefabricated sections that are connected using weld or bolts. The biggest setback in using tubular steel towers is the high price of steel. In the case of towers with tapered hollow sections, each section is a truncated tubular cone. This configuration is economical specially if combined with gradual decrease of thickness along the tower height. The buckling problem in these towers should be avoided properly otherwise the cost of stiffening plates and their installation makes the design uneconomical.

Concrete towers can be either reinforced or pre-stressed. Concrete can deliver large diameter, low maintenance, and economic design in tall towers. It is also a durable material under extreme exposure conditions and it's the reason why concrete towers are popular in off-shore wind turbine farms. Some designers use cast-in-place hybrid towers with concrete at the bottom and steel at the top. If designed well, precast concrete-steel towers can offer easy transportation, rapid erection, high strength, high stiffness, reduced maintenance, and reduced lifetime cost [13]. Figure 5 shows inland and coastal horizontal axis wind turbines.



a) Inland wind turbines



b) Coastal (offshore) wind turbines

Figure 5. Horizontal axis wind turbines [5]

Problem Statement

Decreasing number of prime sites with high wind availability and good access, coupled with increasing demand for higher power output has increased the need to use taller towers with longer blades especially in less windy sites [14]. This is due to the facts that the amount of energy available to a wind turbine increases proportional to the third power of wind speed and that wind speed tends to increase with height. Taller turbines produce energy at a lower price. For example, the world's tallest wind turbine

tower (Fuhrländer Wind Turbine, Laasow, Germany) with a hub height of 160 m (525 ft) would supply 35% to 45% more wind power compared to a 100 m (328 ft) wind turbine [12]. A study on two concrete turbines with hub height of 100 and 120 meter (328 and 394 foot) showed that the cost difference was compensated for in less than 4 years [14]. This is especially important in regions with lower wind speed in which the cost of production tends to be higher. Figure 6 shows the wind map of the United States.

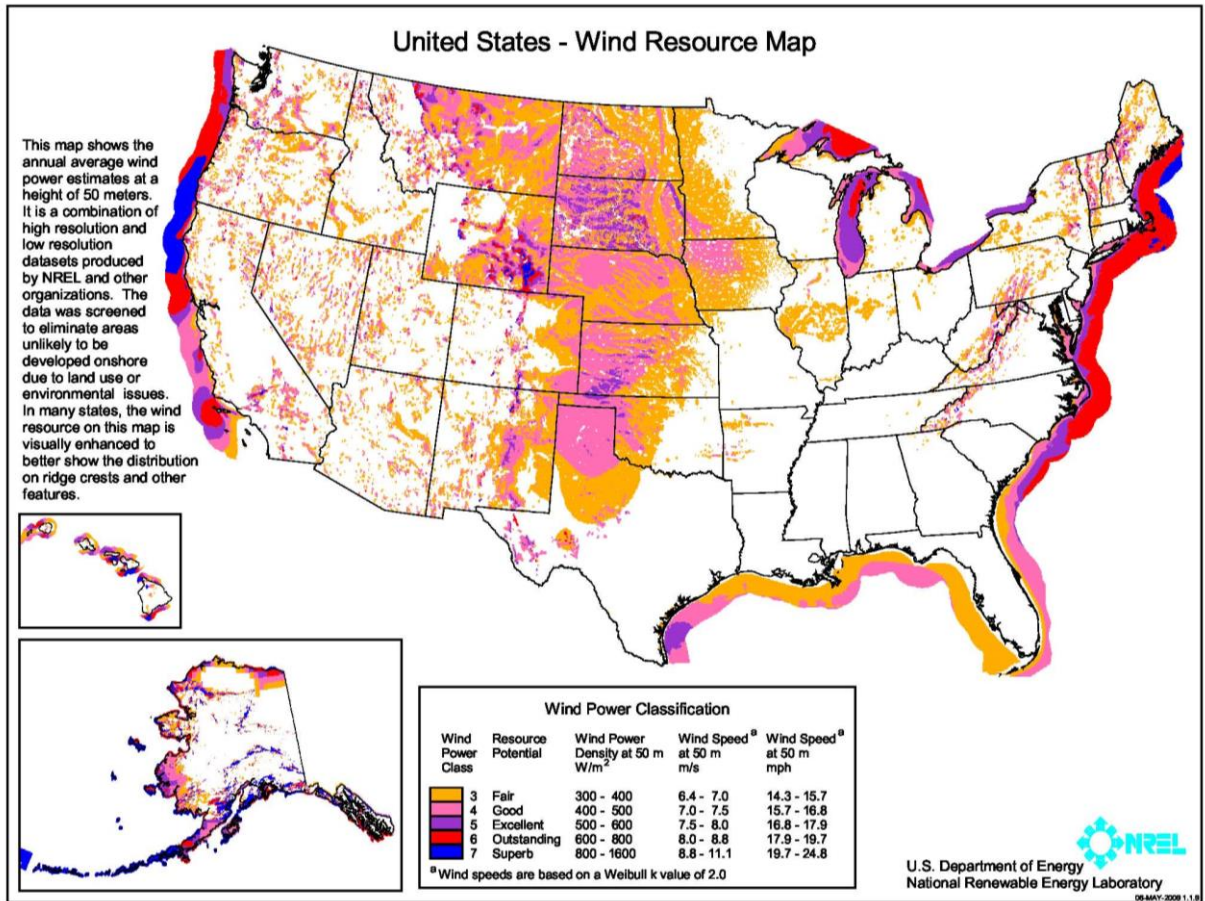


Figure 6. United States wind map [15]

New generation wind farms require turbines in the range of 5 MW and above with blade lengths in the range of 60 m (197 ft) and tower heights of 100 m (328 ft) [16], compared to current 0.5 to 1.5 MW turbines which require 40 m (131 ft) long blades and 60-70 m (197-230 ft) tall towers. Common hub heights used during 2004-2005, fell

in the range of 65 to 80 m (213 to 262 ft). In May 2005, the tallest wind turbine in the U.S. had an 80 m (262 ft) hub height and an 82 m (269 ft) rotor diameter with a maximum height of 121 m (397 ft). As of 2016, the tallest wind turbine in the U.S. has a 2,400 MW capacity and a maximum height of 170 m (557 ft). This turbine has a concrete tower and weights as much as 1,200 tons [17].

Implementing taller wind turbines however, are associated with significant challenges. Transportation of tall towers is difficult. Although using modular designs helps, their construction time can be longer; lengthening return on investment. Taller towers require bigger and more expensive foundations. Their frequencies are close to the frequency of turbine mechanical systems, interfering with their operation. The real limit on the height of wind turbines lays at the economics because the costs per length of tower increases faster than increment in energy output.

Wind turbine towers are subjected to dead loads from self-weight of the structure. The wind load on towers consist of direct wind pressure, gust factor, and force coefficient [16]. Wind forces can be classified as stationary and cyclic. In addition, the rotor is subjected to non-periodic and random loads caused by wind turbulence. The taller the turbine, the higher the wind forces. It's also true for seismic forces. Taller towers in the seismic regions endure higher seismic forces that can even be greater than the wind forces [18]. In such cases, an inaccurate estimate of the seismic force can result in either structural failure or uneconomic design. Traditionally, wind turbines used to be analyzed by modal methods [19] used in the design of buildings, but these methods were not adequate for wind turbines. The behavior of wind turbines is different from ordinary structures under earthquake load because of the presence of a rotating mass at the top of a slender tower and also because of the effect of wind on its damping properties [20]. Therefore, it is advantageous to analyze the wind turbine structures using methods that can incorporate these factors, e.g. the transient analysis method.

Current wind turbine design codes have relatively similar and simplified procedures for calculating the seismic forces. Application of these codes involves a

series of assumptions and simplifications in considering seismic characteristics of the structure including the mass distribution, damping ratio, and frequency. For example, it is not clear how simplifying the mass distribution can alter the frequency of the structure and therefore, an engineer can't compare this alteration in a short turbine with a taller heavier turbine which itself results in more assumptions in calculating the optimum height of the turbine; or it is not known how much damping ratio should be adopted which can result in higher seismic forces and a conservative design. The other unknown is whether application of response spectra in current codes can accurately estimate the demand on the taller towers. This is because the heavy mass of the larger blades and their different stiffness and frequencies can reduce the significance of the first mode. What also is not addressed in these codes is the direction of seismic forces and whether assuming a specific direction is conservative or not. There are other uncertainties involving the effects of structural parameters, e.g. the relation between the turbine size and the effects of seismic force direction. Also, how different turbine parameters including foundation type change the structure frequencies. It is important from the design perspective because engineers should shift structural frequencies far from the range of load frequencies. Another important factor is the effects of soil-structure interaction on the overall seismic behavior of wind turbines; whether it's safe to input load at the tower base level or should it be applied to the foundation/soil.

Objectives and Scope

This research intends to help design process by investigating the problems described above and providing answers to the following questions:

1. Considering the uncertainties in the damping values, how much effect does damping have on the seismic response?
2. How does load direction affect the seismic response?
3. How do load frequency amplitudes and resonance affect the seismic response?

4. How does the effect of seismic forces increase when wind turbine height is increased?
5. Is soil-structure interaction analysis necessary in seismic design of wind turbines?
6. Can the response spectrum method described in design codes calculate the seismic forces on wind turbines accurately and how many modal frequencies should be considered?

To do so, the seismic behavior of wind turbines is analyzed using numerical techniques. First experimentally obtained response data of a 65 kW wind turbine under Landers earthquake is compared to the results of the time history analysis of a similar turbine performed using finite element method (FEM) in the ANSYS program. It is shown that the experimental and numerical values compare well at the experimentally obtained damping ratio of 0.86 establishing the validity of the numerical method. Next, performing a parametric study, the effects of each parameter on the seismic response is investigated. It includes wind turbine size (65 kW, 1 MW, 5 MW), damping ratio (0.5%, 1%, 2%), base acceleration directions (vertical, horizontal parallel to the rotor axis, horizontal perpendicular to the rotor axis), earthquake characteristics (Landers, Imperial Valley, Northridge), and foundation type (spread, mono pile, pile group & cap, anchored spread). The responses studied are natural frequencies, the peak accelerations and deformations at the top of the nacelle, and the maximum von Mises stresses at the base of the wind turbine towers. Finally, the accuracy of mass distribution method, and response spectrum method is investigated.

This dissertation is divided into seven chapters. Current chapter provides introduction to the wind turbines and states the objectives of the research. Chapter two is a review of the published literature on the subject. Chapter three discusses the theoretical formulation of the problem, methods, and assumptions used. It also presents selected earthquakes and their properties. Chapter four includes the experimental data used in the validation of the numerical method. It describes the

numerical method used to analyze the seismic behavior of wind turbines, as well as detailed descriptions of the procedure and validation results. Chapter five investigates the effects of wind turbine foundations and soil-structure interaction. Chapter six presents results of the parametric study, in addition to validation of response spectrum method. Chapter seven summarizes the results of this study and draws conclusions. Recommendations for future work is given at the end of this chapter. Complete transient analyses data is given in the appendix, followed by the references.

CHAPTER 2

LITERATURE REVIEW

Since 2000, numerous experimental and analytical studies have been performed to investigate the seismic behavior of wind turbines and to come up with a sound and simple method to estimate the seismic demand on these structures. Most of the data are generated using finite element analysis (FEA) on small wind turbines with simplified geometrical properties. Unfortunately, there are not many experimental data on the subject except for a recent real size shake table test performed on an industrial scale wind turbine [36]. A review of the existing literature on the subject is presented in this chapter. The first part is a summary of current engineering codes and specifications. The second part presents a summary of research publications and their findings.

Standards and Guidelines

The International Electro-Technical Commissions (IEC) is a non-profit, non-governmental international standards organization that prepares and publishes International Standards for all electrical, electronic and related technologies. IEC 61400 (2005), which is a series of guidelines related to wind turbines, addresses the design requirements for the wind turbines in its part 1. This part specifies minimum requirements for the design of wind turbines and classifies the earthquake load as “extreme other environmental conditions”. IEC 61400 (2005) recommends using the response spectrum based on local codes. For cases where an analysis can't be

performed, IEC suggests using the first natural mode of the turbine with 1% damping ratio and total mass of rotor and nacelle plus 50% of the tower mass [21].

Another specification is GL 2010. It is a standard by Germanischer Lloyd SE, a classification society located in the city of Hamburg, Germany. GL services include wind turbine type certification, design consultancy, energy yield assessments, project management, site assessments, permitting, front end engineering, due diligence, software solutions for wind parks, solar plants and turbine design, wind and solar forecasting and renewable plant operations improvement services. GL 2010, A Guideline for the Certification of Wind Turbines, describes design procedure for different components of wind turbines. To estimate the seismic demand on wind turbines, GL 2010 allows using both frequency and time domain methods provided at least three natural modes are used in the frequency domain and minimum six analyses are performed in the time domain. GL assumes a linear behavior for towers and allows assuming a nonlinear behavior for lattice towers. In doing so, GL suggests using local regulations [22].

Det Norske Veritas (DNV) located in Oslo, Norway, is a classification society with the objective of "Safeguarding life, property, and the environment". DNV-OS-J101, Design of Offshore Wind Turbine Structures [23], was created through cooperation of DNV and Risø National Laboratory. For calculating the seismic force on wind turbines, DNV-Risø [24] and DNV-OS-J101 recommend application of the pseudo response spectra that estimates the maximum displacement, velocity, and acceleration based on the structural frequency and damping ratio. DNV-OS-J101 recommends analyzing the structure in two horizontal and one vertical direction and allows the turbine to be modeled as a concentrated mass atop of a vertical rod.

Publications on Earthquake Design and Analysis

Ritschel et al. (2000) [25] analyzed the seismic behavior of a 60 m (197 ft) hub height wind turbine using a system of lumped masses and flexible rods shown in Figure 7 under peak ground acceleration (PGA) of 0.3 g. Two methods were used; modal and time domain. In the modal approach, four modes were considered and mass of nacelle and rotor was modeled as one point on top of the tower. In the time domain method, two tower modes were considered. Results were relatively conservative near the tower base in the modal approach and near the top in the time domain method. Also, the third and fourth modes were found to be not influential. They concluded that an envelope of both approaches was a reliable measure in estimating the design load on the tower.

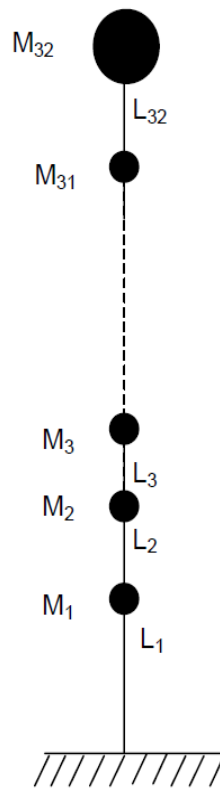


Figure 7. System of lumped masses and flexible rods used by Ritschel et al. [25]

Bazeos et al. (2002) [26] studied the load bearing capacity of a 450 kW wind turbine with a 38 m (125 ft) tower shown in Figure 8. They used both simplified analytical model recommended by Eurocode 3 [27] and refined finite element model. Gravity, seismic loads, and site-dependent seismic motions were considered. Results showed that simplified methods can be used if appropriate boundary conditions are incorporated.



Figure 8. Finite element model used by Bazeos et al. [26]

Kiyomya et al. (2002) [28] investigated effects of wind and earthquake load combination from a probabilistic point of view. Using dynamic response analysis to find sectional forces, it was shown that wind towers have enough seismic capacity when they are designed for wind forces.

Lavassas et al. (2003) [29] performed a finite element analysis of a 1-MW wind turbine tower shown in Figure 9 with a hub height of 44.075 m (145 ft). The tower was tubular steel with variable cross section and variable thickness. The results showed that a simplified linear procedure can accurately estimate the response to seismic and gravity load but is inaccurate in an ultimate limit state design because it ignores the stress concentration. The seismic load effects were found to be more severe than wind in a seismically hazardous area zone III and IV (Eurocode).

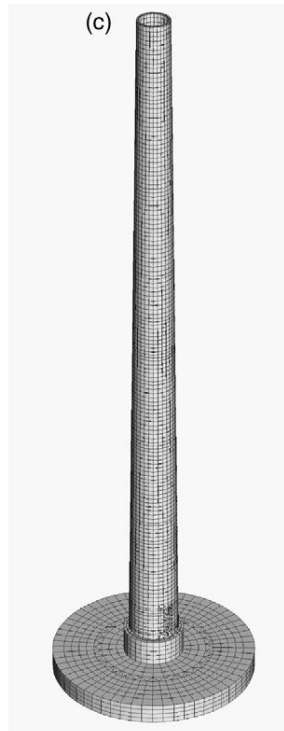


Figure 9. Finite element model used by Lavassas et al. [29]

Witcher et al. (2005) [30] presented a new method to perform seismic calculation in the time domain. This method allows both modelling of the dynamic motion of the wind turbine with wind loading acting on the rotor blades and the response of the turbine controller.

Zhao et al. (2005) [31] investigated a multibody model considering the soil-structure interaction in the time domain. The soil-structure interaction was analyzed using a frequency-independent discrete parameter model shown in Figure 10. The governing motion equations were derived by the application of Lagrange formalism.

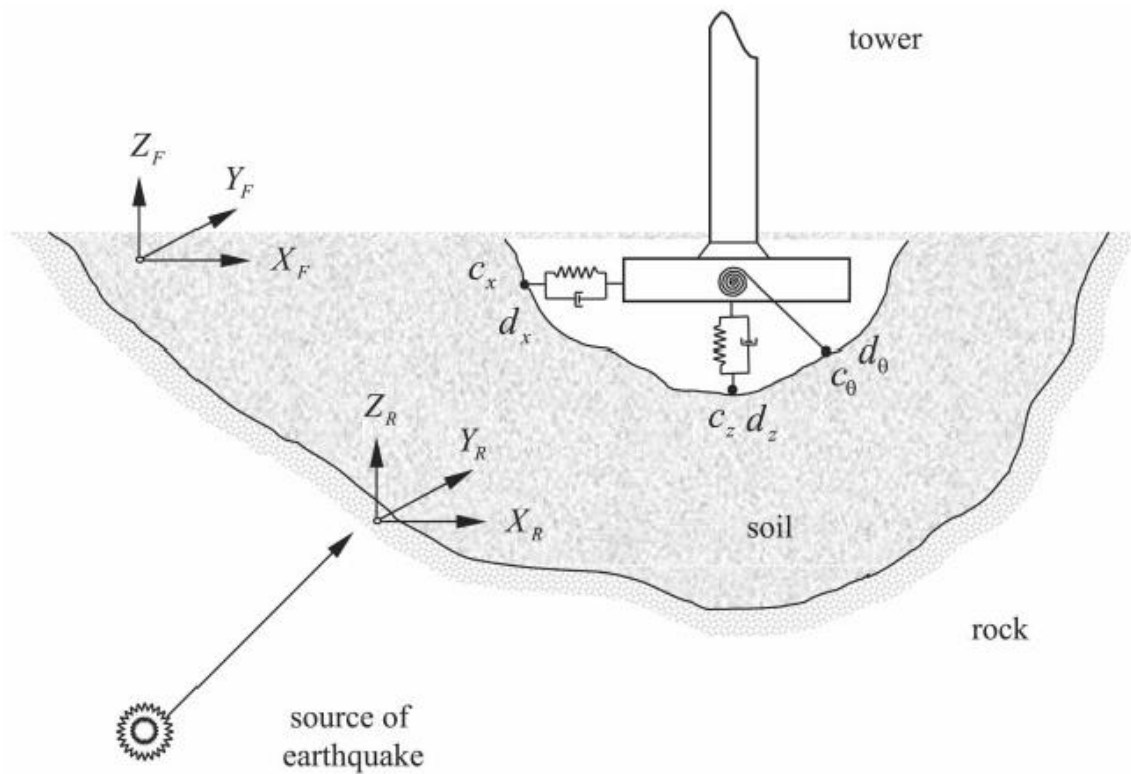


Figure 10. Multibody system used by X. Zhao et al. [31]

Hänler et al. (2006) [32] reported results on their simulation program (SIWEC) for the dynamic analysis of horizontal axis wind turbine represented in Figure 11. The program is based on a multi-body system with a modular structure in which blades are modeled by a variable number of input modes. The interaction of foundation and ground is also considered. The solver is using differential equation with variable step and effective error control. The program is validated with measured data and results showed that tower modes that are higher than normal operation excitation modes, are more important in earthquake analysis.

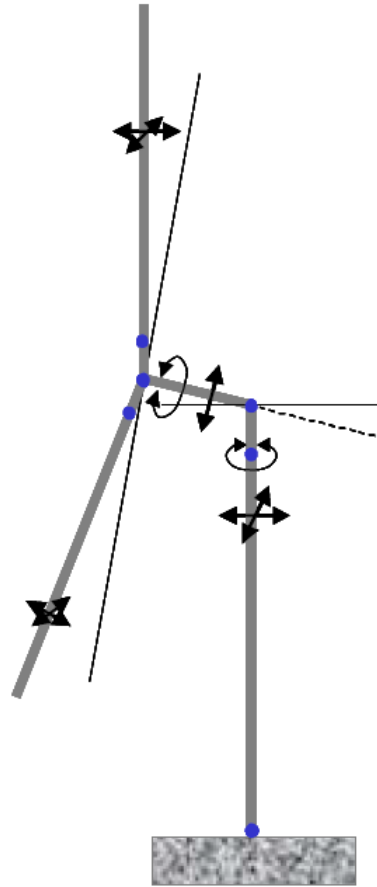


Figure 11. Turbine model used by M. Hänler et al. [32]

Zhao et al. (2006) [33] presented a new multibody modeling method based on a hybrid system of rigid and flexible bodies, force elements, and joints shown in Figure 12. Using the concepts of differential geometry, the Lagrange's motion equations of multibody were represented in explicit form and all dynamic characteristics of the wind turbine were captured with a low degree of freedom model.

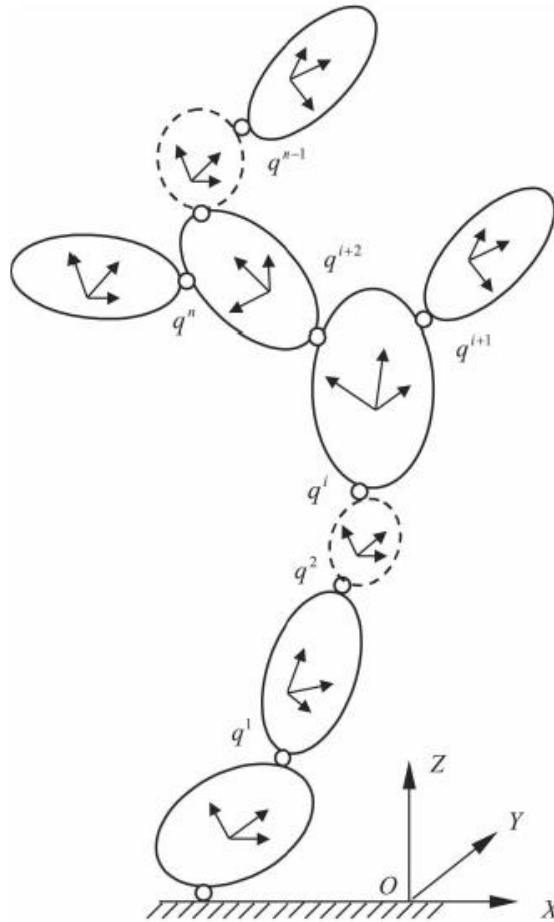


Figure 12. Hybrid model used by X. Zhao et al. [33]

Bir et al. (2007) [34] examined the aeroelastic stability of a 5 MW wind turbine for both onshore and offshore situations. Results showed that parked wind turbines can become unstable with side to side motion of the tower, edgewise motion of the rotor blades, and yawing of the platform. Two strategies are suggested to mitigate these instabilities; feathering the blade at non 90 degree angles and applying generator break.

Prowell et al. (2009) [35] performed a seismic hazard study on wind turbine towers to understand the relation between tower moment demand and rated power. This study suggested that seismic loading may impact more than just the tower and it was recommended that full system models be considered in seismic demand

calculations. It was also shown that soil-structure interaction has a strong influence on higher modes.

Prowell et al. (2009) [36] presented the experimental results on a full scale shake table test on a relatively small 65 kW wind turbine shown in Figure 14 and a finite element model that was developed to study the earthquake response characteristics. The wind turbine with a hub height of 23 m (75 ft) was tested in parked situation under five historical earthquakes of California, both uni-axially and bi-directionally. The experimental results showed that the first mode is the dominating mode and higher modes are more effective in higher frequency motion (more than 10 Hz). The viscous damping ratio is between 0.5% and 1% for the first mode. In finite element analysis, two beam-column models are studied. One is a vertical column with a lumped mass at top representing the weight of rotor and hub and the other with whole rotor and hub modeled as shown in Figure 13. Results showed that the moment capacity of tower was close to the capacity of an idealized slender tube. It was also found that damping can have a significant effect depending on the earthquake characteristics. Higher modes were found to be important in taller turbines. Finally, the implication of a bi-directional loading was found to be conservative.

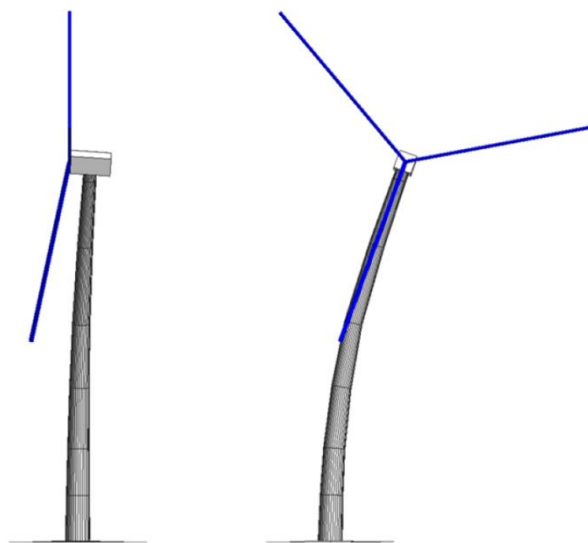


Figure 13. Finite element model used by Prowell et al. [36]



Figure 14. Experimental wind turbine and shake table [37]

Prowell et al. (2010) [38] analyzed a full soil-structure system with a 5 MW wind turbine with a hub height of 90 m (295 ft) and a 126 m (413 ft) rotor diameter. A detailed finite element model of the turbine was created, including a full three-dimensional soil mesh to study the influence of soil-structure interaction (SSI) on the dynamic properties and response. The turbine was modeled on 3-15 m (9.8-49 ft) thick soil profiles of varying stiffness and subjected to a 1994 Northridge Earthquake record. The investigation found that for these soil profiles, ground motion, and wind turbine size, SSI influence on the first and second longitudinal bending modal parameters was relatively minor, while maximum moment and shear demand distribution along the tower height was more significant. Prowell et al. recommended the selection of a range of carefully chosen ground motions to match the anticipated shaking for the proposed site in SSI analyses.

M. Hongwang (2012) [39] analyzed the seismic response of two 1.65MW and 3 MW wind turbine models including SSI and P- Δ effects under horizontal and vertical components of six historical earthquake time histories. The SSI was modeled by connecting the turbine base to a rigid support mounted on translational and rotational springs and dampers showed in Figure 15. The results showed that the SSI caused a 7% decrease in the first natural frequency, 10% decrease in horizontal acceleration at top of the tower, 10-12% decrease in the towers base moment, and 5-6% decrease in the tower base shear force. The SSI had no significant effect on the vertical acceleration and axial force of the towers and P- Δ effect increased the tower base moment slightly.

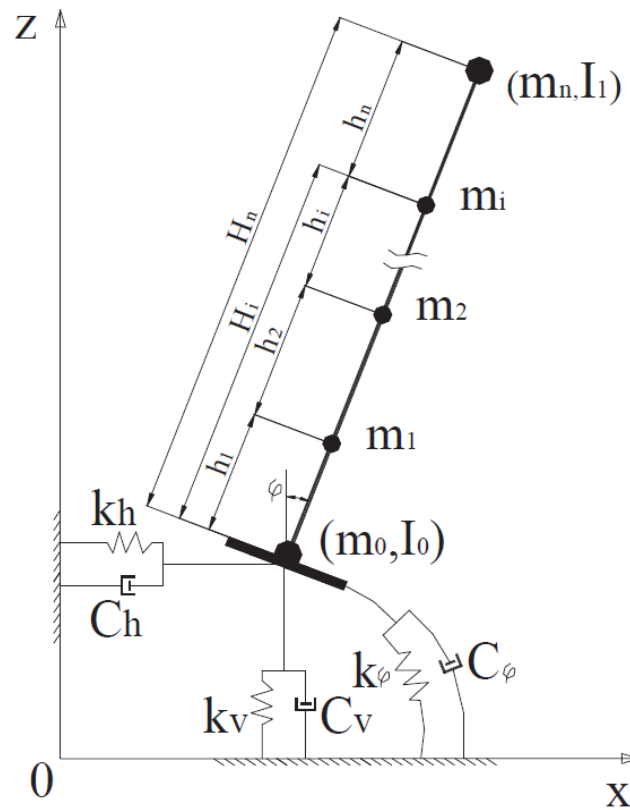


Figure 15. Foundation model used by M. Hongwang [39]

R.S. Kourkoulis et al. (2012) [40] performed a parametric seismic analysis on two 2 MW and 3.5 MW wind turbines with suction caisson foundations under static cyclic and earthquake loads. The analysis included non-linear SSI caused by sliding between the caisson skirt and the soil and gap formation. The model included 3D soil elements with shell elements representing the interface, beam elements for tower, and a concentrated mass representing the rotor blades and nacelle, as shown in Figure 16. The results showed that the interface failure could reduce the capacity of suction caisson foundations especially in foundations with deep caissons. It was also shown that foundation rotation made by interfaces problems could cause irrecoverable displacement on the nacelle level. Increasing the caisson diameter was found to be a better solution compared to increasing the depth of embedment.

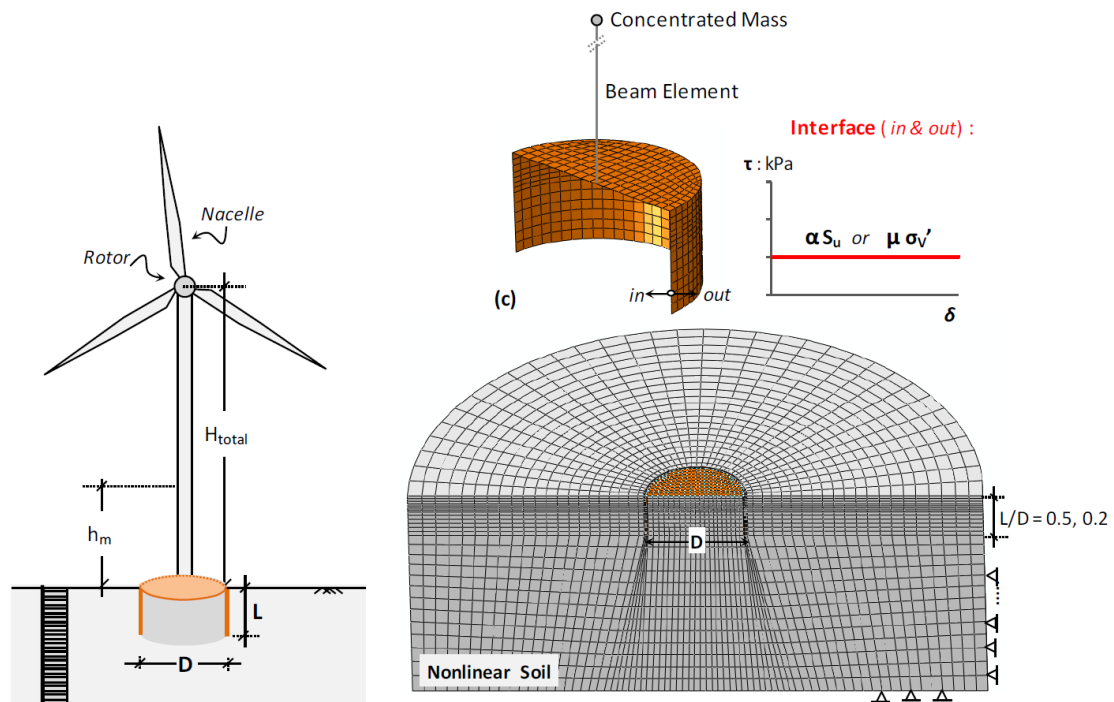


Figure 16. Finite element model used by R.S. Kourkoulis et al. [40]

R.A. Kjølraug et al. (2014) [41] evaluated dynamic response of a 5 MW wind turbines including the soil-structure interaction shown in Figure 17. It was shown that the vertical earthquake excitation can produce severe vertical accelerations in upper

parts of a wind turbine. It was also shown that earthquake is not expected to govern the design for small to moderate earthquakes in stiff soils, however, for softer soils, the displacement and base moment demand from earthquake could very well match the response from wind-induced forces.

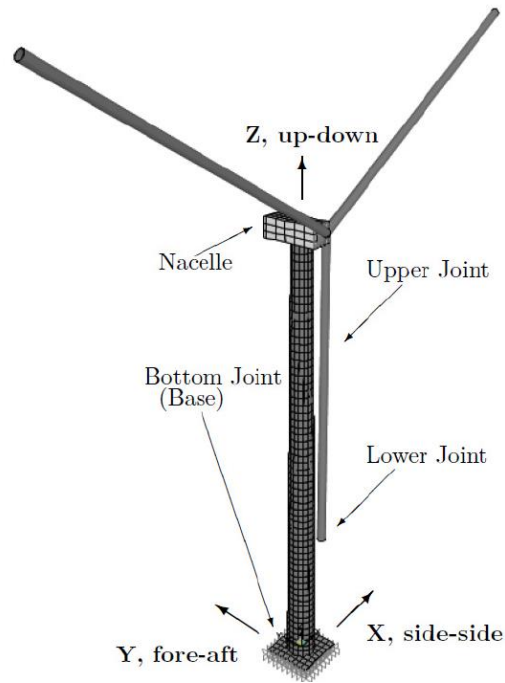


Figure 17. Model of the 5 MW wind turbine used by R.A. Kjølraug et al [41]

F. Taddeia et al. (2017) [42] presented a practical model for the analysis of the soil-structure interaction effects on the seismic behavior of a 5 MW wind turbine, during normal power production and emergency shutdown. The model shown in Figure 18 was based on a simplified lumped parameter model for the soil-foundation sub-system and allowed a significant model size reduction and accurate approximation of the soil-structure behavior in time domain.

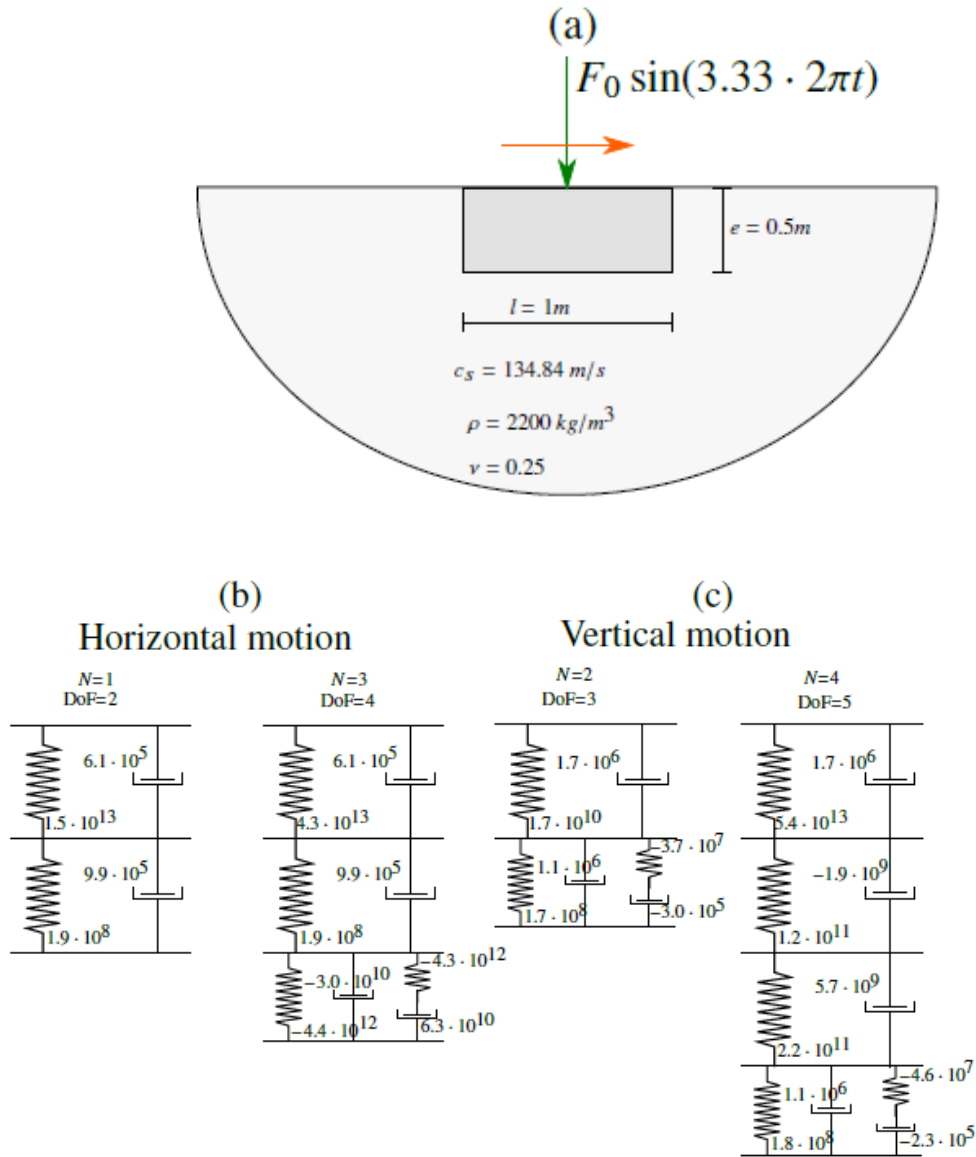


Figure 18. Foundation model used by F. Taddeia et al. [42]

It can be seen that there are still a lot of questions that haven't been answered in the literature. For example, how much damping should be used? With lack of experimental data to answer this question, we need to investigate the damping significance in the meantime to help engineers make a justified assumption in choosing a damping value. What's also missing from the literature is how the load direction effect, damping value, and turbine size changes relative to each other. It's also not known how different the effects of different foundation types are. Another unknown is the best way to model the

soil and relationship between soil-structure interaction importance and other design parameters. Considering the increasing size of the wind turbines, it is also not clear if current design guidelines are appropriate for designing these larger turbines.

CHAPTER 3

THEORETICAL FORMULATIONS AND METHODOLOGY

Equations of motion of a dynamic system can be solved using different techniques. These techniques can be categorized under two major categories; time domain and frequency domain methods.

Theoretical Formulations

Time Domain

In the time domain methods, the equations of motion are solved in a step-by-step procedure using numerical integration techniques. The response is calculated during each step, using the initial displacement, initial velocity, and the history of loading during the step. The structural properties within each step are assumed to remain constant, but could vary from one step to another (nonlinear analysis) or remain the same during all time-steps (linear analysis). If the calculated response for each step depends on the response quantities from the last step, the method is called explicit and the analysis proceeds directly from one step to the next. If the calculated response depends on some of the quantities from the same step, the method is called implicit and involves initial trial values and iterative analysis. Important factors in selecting a time domain method include efficiency, round-off and truncation errors, instability, phase shift or apparent change of frequency, and artificial damping [43]. Time domain methods are time intensive and often used for the analysis purposes.

Two common time domain methods are:

- Mode superposition

In a linear analysis, the mode superposition method can be used to uncouple the equations of motion. The dynamic response is first obtained separately for each vibration mode and then superimposed for all significant modes to obtain the total response. In other words, the time domain integration of equation (1) is applied separately to several independent single degree of freedom (SDOF) equations and the resulting responses are then superimposed to compute the total response of the structure. The main task in this method is the computation of eigenvalue problems, followed by modal coordinate transformation to uncouple a multi degrees of freedom (MDOF) dynamic analysis to the solution of a series of SDOF systems. It is important to note that the equations of motion will be uncoupled only if the damping can be represented by a mass proportional and stiffness proportional damping matrix known as Rayleigh damping. The Rayleigh damping, described below, is suitable when the damping mechanism is distributed rather uniformly throughout the structure [43].

- Direct step-by-step method

In this method, the step-by-step integration is applied directly to the original equations of motion with no need for modal coordinate transformation to uncouple them. Thus, there is no need to obtain natural mode shapes and frequencies or to limit damping to the proportional type. The method can be used for both linear and nonlinear response analyses.

Equation of Motion

In obtaining a solution to a time dependent (dynamic) problem, a finite difference procedure is usually utilized by discretization of time over the history of dynamic action and reaction. For a SDOF system with linear damping and stiffness, dynamic equation governing the motion of a spring-damper-mass system is:

$$M \ddot{u}(t) + C \dot{u}(t) + K u(t) = F^a \quad (1)$$

in which M is mass, C is damping, and K is the stiffness of spring and $\ddot{u}(t)$, $\dot{u}(t)$, and $u(t)$ are acceleration, velocity, and displacement vector at time t, respectively. F^a is the applied force e.g. earthquake force at time t. In a finite element representation of a system with MDOF, the governing dynamic equation is

$$[M] \{\ddot{u}(t)\} + [C] \{\dot{u}(t)\} + [K]\{u(t)\} = \{F^a\} \quad (2)$$

in which [M], [C], and [K] are mass, damping, and stiffness matrix and $\{\ddot{u}(t)\}$, $\{\dot{u}(t)\}$, and $\{u(t)\}$ are nodal acceleration, velocity, displacement, and force vectors at time t, respectively. $\{F^a\}$ is the applied force vector. To calculate the response of MDOF system over the duration of an earthquake load or earthquake time history, solution of this equation should be calculated over a series of time steps that start from the beginning of the earthquake load. Ending time depends on the damping properties of the system and whether the free vibration phase should be studied or not.

Newmark Method

A popular solution to equation (2) which is also used in the ANSYS program, is the Newmark time integration method. This method uses finite difference expansions in the time interval Δt , in which it is assumed that

$$\{\dot{u}_{n+1}\} = \{\dot{u}_n\} + [(1 - \delta) \{\ddot{u}_n\} + \delta \{\ddot{u}_{n+1}\}] \Delta t \quad (3)$$

$$\{u_{n+1}\} = \{u_n\} + \{\dot{u}_n\} \Delta t + \left[\left(\frac{1}{2} - \alpha \right) \{\ddot{u}_n\} + \alpha \{\ddot{u}_{n+1}\} \right] \Delta t^2 \quad (4)$$

where α and δ are the Newmark integration parameters; $\{u_n\}$, $\{\dot{u}_n\}$, and $\{\ddot{u}_n\}$ are nodal displacement, velocity, and acceleration vector at time t_n , respectively. Similarly, $\{u_{n+1}\}$, $\{\dot{u}_{n+1}\}$, and $\{\ddot{u}_{n+1}\}$ are the nodal displacement, velocity, and acceleration vector at the

time t_{n+1} . In this equation $\Delta t = t_{n+1} - t_n$. The governing Eq. (2) is written at time t_{n+1} to calculate $\{u_{n+1}\}$ as follows:

$$[M] \{\ddot{u}_{n+1}\} + [C] \{\dot{u}_{n+1}\} + [K] \{u_{n+1}\} = \{F_{n+1}^a\} \quad (5)$$

The $\{u_{n+1}\}$ is calculated by rearranging Eqs. (4 and 5) as follows [44]:

$$\{\ddot{u}_{n+1}\} = a_0(\{u_{n+1}\} - \{u_n\}) - a_2 \{\dot{u}_n\} - a_3 \{\ddot{u}_n\} \quad (6)$$

$$\{\dot{u}_{n+1}\} = a_5 \{\dot{u}_n\} + a_6 \{\ddot{u}_n\} + a_7 \{\dot{u}_{n+1}\} \quad (7)$$

Where $a_0 = \frac{1}{\alpha \Delta t^2}$, $a_1 = \frac{\delta}{\alpha \Delta t}$, $a_2 = \frac{1}{\alpha \Delta t}$, $a_3 = \frac{1}{2\alpha} - 1$, $a_4 = \frac{\delta}{\alpha} - 1$, $a_5 = \frac{\Delta t}{2} \left(\frac{\delta}{\alpha} - 2 \right)$,

$a_6 = \Delta t(1 - \delta)$, and $a_7 = \delta \Delta t$.

$\{\ddot{u}_{n+1}\}$ in Eq. (4) can be substituted from Eq. (3). The equations for $\{\ddot{u}_{n+1}\}$ and $\{\dot{u}_{n+1}\}$ are thus expressed in terms of unknown displacements $\{u_{n+1}\}$ and the known displacements $\{u_n\}$, velocities $\{\dot{u}_n\}$, and accelerations $\{\ddot{u}_n\}$ at the time t_n . The equations for $\{\ddot{u}_{n+1}\}$ and $\{\dot{u}_{n+1}\}$ are then substituted in Eq. (5) to get

$$\begin{aligned} (a_0[M] + a_1[C] + [K]) \{u_{n+1}\} &= \{F_{n+1}^a\} + [M](a_0 \{u_n\} + a_2 \{\dot{u}_n\} + a_3 \{\ddot{u}_n\}) + \\ &[C] (a_1 \{u_n\} + a_4 \{\dot{u}_n\} + a_5 \{\ddot{u}_n\}) \end{aligned} \quad (8)$$

Next, the unknown displacements $\{u_{n+1}\}$ are obtained from Eq. (8). Then Eqs. (6 and 7) are used to update the velocities and accelerations. The amount of numerical algorithm dissipation can be controlled by one of Newmark's parameters as follows:

$$\alpha \geq \frac{1}{4} \left(\frac{1}{2} + \delta \right)^2, \text{ and } \delta \geq \frac{1}{2} \quad (9)$$

By introducing the amplitude decay factor γ , Eq. (9) can be written as:

$$\alpha = \frac{1}{4} (1 + \gamma)^2, \text{ and } \delta = \frac{1}{2} + \gamma \quad (10)$$

If $\gamma \geq 0$, the solutions of Eq. (5) are stable [44].

In the Newmark method, the amount of numerical dissipation can be controlled by the parameter δ in Eq. (9 and 10). However, in low frequency modes the Newmark method fails to retain the second-order accuracy as $\delta > \frac{1}{2}$. Note that the Newmark implicit method (constant average method; namely, $\delta = \frac{1}{2}$ and $\alpha = \frac{1}{4}$), which is unconditionally stable and second-order accurate, has no numerical damping. If other sources of numerical damping are not introduced, the lack of numerical damping can be undesirable so that the higher frequencies of the structure can produce unacceptable levels of numerical noise [45].

Generalized HHT- α method

To circumvent the drawbacks of the Newmark family of methods, the ANSYS program implements the generalized HHT- α (Hilber-Hughes-Taylor) method [46] which sufficiently damps out spurious high-frequency response via introducing controllable numerical dissipation in higher frequency modes, while maintaining the second-order accuracy. It should be noted that the generalized HHT- α method incorporated in the program can recover the WBZ- α (Wood-Bossak-Zienkiewicz) method [47] and the HHT- α method as well as the Newmark family of time integration algorithms, depending upon the user's input. To solve for the three unknowns $\{u_{n+1}\}$, $\{\dot{u}_{n+1}\}$, and $\{\ddot{u}_{n+1}\}$, along with Eq. (3 and 4) the generalized HHT- α method uses the algebraic equation:

$$[M] \{ \dot{u}_{n+1-\alpha_m} \} + [C] \{ \dot{u}_{n+1-\alpha_f} \} + [K] \{ u_{n+1-\alpha_f} \} = \{ F_{n+1-\alpha_f}^a \} \quad (11)$$

Where [46]:

$$\{ \ddot{u}_{n+1-\alpha_m} \} = (1 - \alpha_m) \{ \ddot{u}_{n+1} \} + \alpha_m \{ \ddot{u}_n \},$$

$$\{ \dot{u}_{n+1-\alpha_f} \} = (1 - \alpha_f) \{ \dot{u}_{n+1} \} + \alpha_f \{ \dot{u}_n \},$$

$$\{ u_{n+1-\alpha_f} \} = (1 - \alpha_f) \{ F_{n+1}^a \} + \alpha_f \{ F_n^a \},$$

$$\{ F_{n+1-\alpha_f}^a \} = (1 - \alpha_f) \{ F_{n+1}^a \} + \alpha_f \{ F_n^a \}.$$

Eq. (11) gives the finite difference form:

$$\begin{aligned} & (a_0[M] + a_1[C] + (1 - \alpha_f) [K]) \{ u_{n+1} \} = \\ & (1 - \alpha_f) \{ F_{n+1}^a \} + \alpha_f \{ F_n^a \} - \alpha_f [K] \{ u_n \} + [M] (a_0 \{ u_n \} + a_2 \{ \dot{u}_n \} + a_3 \{ \ddot{u}_n \}) \\ & + [C] (a_1 \{ u_n \} + a_4 \{ \dot{u}_n \} + a_5 \{ \ddot{u}_n \}) \end{aligned} \quad (12)$$

Where

$$a_0 = \frac{1-\alpha_m}{\alpha \Delta t^2}, \quad a_1 = \frac{(1-\alpha_f) \delta}{\alpha \Delta t}, \quad a_2 = a_0 \Delta t, \quad a_3 = \frac{1-\alpha_m}{2\alpha} - 1, \quad a_4 = \frac{(1-\alpha_f) \delta}{\alpha} - 1,$$

$$a_5 = (1 - \alpha_f) \left(\frac{\delta}{2\alpha} - 1 \right) \Delta t$$

Analogous to the Newmark method, the generalized HHT- α method calculates the unknown $\{u_{n+1}\}$ at time t_{n+1} by making use of Eq. (12). Then, the program computes the two unknowns $\{\dot{u}_{n+1}\}$ and $\{\ddot{u}_{n+1}\}$ by using Eqs. (6 and 7). Since the generalized HHT- α method is also an implicit time scheme, the structural stiffness matrix must be factorized to solve for $\{u_{n+1}\}$ at time t_{n+1} .

As mentioned in the literature [48], the generalized HHT- α method is unconditionally stable and second-order accurate if the parameters meet the conditions of equation (13):

$$\begin{aligned} \delta &= \frac{1}{2} - \alpha_m + \alpha_f \\ \alpha &\geq \frac{1}{2} \delta \\ \alpha_m &\leq \alpha_f \leq \frac{1}{2} \end{aligned} \tag{13}$$

where $\alpha_m \leq 0$ [47] and $\alpha_m \leq \alpha_f \leq \frac{1}{2}$ [46]. By introducing the amplitude decay factor $\gamma \geq 0$, the program also allows the user to control the amount of numerical damping. This method allows to control the amount of numerical damping. The amplitude decay factor is recommended to be set as $\gamma = 0.05$ [45], with which any spurious participation of the higher modes can be damped out and the lower modes are not affected. A significant amount of numerical damping may be introduced by setting $\gamma = \frac{1}{3}$ but it is not recommended.

Rayleigh Damping

In finite element method, different methods are available to include damping in the analysis. One of these methods is Rayleigh formulation in which damping is assumed to be proportional to a linear combination of the mass and stiffness matrices [53]:

$$[C] = \alpha [M] + \beta [K] \quad (14)$$

In this equation α and β are the mass and stiffness damping coefficients respectively. The values of α and β are not generally known directly and are calculated from modal damping ratios ξ_i , which are the ratio of actual damping to critical damping for each mode:

$$\xi_i = \frac{\alpha}{2\omega_i} + \frac{\beta\omega_i}{2} \quad (15)$$

ω_i is the natural circular frequency of the i^{th} mode.

As an example, for a damped system with $\omega_0 = 20 \frac{\text{rad}}{\text{sec}}$ and $\omega_1 = 40 \frac{\text{rad}}{\text{sec}}$, and a modal damping value of $\xi_0 = \xi_1 = 0.01$, equation (15) gives:

$$\begin{pmatrix} \frac{1}{2\omega_0} & \frac{\omega_0}{2} \\ \frac{1}{2\omega_1} & \frac{\omega_1}{2} \end{pmatrix} \begin{pmatrix} \alpha \\ \beta \end{pmatrix} = \begin{pmatrix} \xi_0 \\ \xi_1 \end{pmatrix}$$

$$\begin{pmatrix} \frac{1}{40} & \frac{20}{2} \\ \frac{1}{80} & \frac{40}{2} \end{pmatrix} \begin{pmatrix} \alpha \\ \beta \end{pmatrix} = \begin{pmatrix} 0.01 \\ 0.01 \end{pmatrix}$$

$$\alpha = 0.2667 \text{ and } \beta = 0.333 \times 10^{-3}$$

In many structural problems $\alpha = 0$ and therefore, $\beta = 2\xi_i/\omega_i$. This is usually referred to as β damping.

Frequency Domain

An alternative approach to solving the equations of motion for linear systems is to perform the analysis in the frequency domain. Specially, when the equation of

motion contains frequency-dependent parameters such as foundation stiffness and damping, the frequency domain approach is much superior to the time domain approach. In a seismic analysis, the frequency domain solution involves expressing the ground motion in terms of its harmonic components, evaluating the response of the structure to each harmonic component, and superposing the harmonic responses to obtain total structural response. In this process, the harmonic amplitudes of the ground motion (the first step) and superposed harmonic responses (the third step) are obtained using the Fast Fourier Transform (FFT) algorithm. Frequency domain methods are faster and useful for the design purposes.

Block Lanczos Method

Block Lanczos is a frequency domain method used by the ANSYS program. In this method, eigenvalue solver uses the Lanczos algorithm where the Lanczos recursion is performed with a block of vectors. Block Lanczos uses the sparse matrix solver and is especially powerful when searching for eigen-frequencies in a given part of the eigenvalue spectrum of a given system. The convergence rate of the eigen-frequencies, when extracting modes in the midrange and higher end of the spectrum, will be about the same as when extracting the lowest modes. This method is recommended to find many modes of large models and it can handle poorly shaped solid and shell elements [53]. To obtain accurate results using Block Lanczos method, number of considered modes should be enough to include at least 90% of the effective mass. The effective mass for the i^{th} mode (which is a function of excitation direction) is:

$$M_{ei} = \frac{\gamma_i^2}{\{\phi\}_i^T [M]_i \{\phi\}_i}$$

in which $\{\phi\}_i$, $[M]_i$, and γ_i are mode shapes, mass matrix, and shape factor for the i^{th} mode respectively. Note that if $\{\phi\}_i^T [M]_i \{\phi\}_i = 1$, the effective mass reduces to γ_i^2 . The cumulative mass fraction for the i^{th} mode is:

$$\widehat{M}_{ei} = \frac{\sum_{j=1}^i M_{ej}}{\sum_{j=1}^N M_{ej}}$$

where N is the total number of modes.

Methodology

To achieve the objectives mentioned in Chapter 1, a parametric study is performed in both time and frequency domains. A series of wind turbines with different sizes and capacities are analyzed using Block Lanczos method for modal analysis and generalized HHT- α method with different Rayleigh damping for transient analysis. In the time domain, based on NEHRP recommendations [49], a minimum of three earthquake time history loads should be selected. Selected loads should have frequencies close to the frequency of turbines so that they can excite natural modes of the turbine. This is necessary to study the effects of resonance in the event of an earthquake. Each load is comprised of vertical and horizontal components applied as uni-axial excitations at the base of the turbine towers. To study the effects of direction, horizontal component is applied both parallel and perpendicular to the rotor axis separately. Gravity acceleration is also added on the turbine mass. Parametric results including displacement, velocity, acceleration, and stress are recorded at all points.

Seismic Loads

Based on NEHRP recommendations, three earthquake loads are selected. Dominant frequency of these loads are ranging from 0.59 to 1.06 Hz in the horizontal

direction, similar to the main frequency of the selected turbines, and 4.2 to 6.95 Hz in the vertical direction.

1. North-South and vertical component of Imperial Valley earthquake (May 19th, 1940) with PGA (peak ground acceleration) equal to 0.3g and 0.21g respectively (USGS station 117), and dominant frequency of 0.59 Hz and 4.2Hz, respectively.
2. North-South and vertical component of Northridge earthquake (January 17th, 1994) with PGA=0.34g and 0.55g respectively (CDMG station 24087), and dominant frequency of 0.85Hz and 6.95Hz, respectively.
3. East-West and vertical component of Landers earthquake (June 28th, 1992) with PGA=0.15g and 0.17g respectively recorded at Desert Hot Springs station (DHS), with moment magnitude of 7.3 at DHS. Located on deep alluvium, DHS is 23 km (14.3 miles) far from the Landers Earthquake fault. The ground is classified as stiff soil, site class D with a shear wave velocity at 30 m depth of $V_{s30}=345$ m/s (1,132 ft/s) [50] and dominant frequency of 1.06 Hz and 6.74 Hz, respectively.

Figure 19 shows input accelerations in both time and frequency domain. PGA of earthquake loads are given in Table 1.

Table 1. PGA and frequency of earthquake loads

Earthquake		PGA (g)	Dominant Freq. (Hz)
Imperial Valley	NS	0.313	0.59
	Up	0.205	4.2
Landers	EW	0.154	0.85
	Up	0.167	6.95
Northridge	NS	0.344	1.06
	Up	0.552	6.74

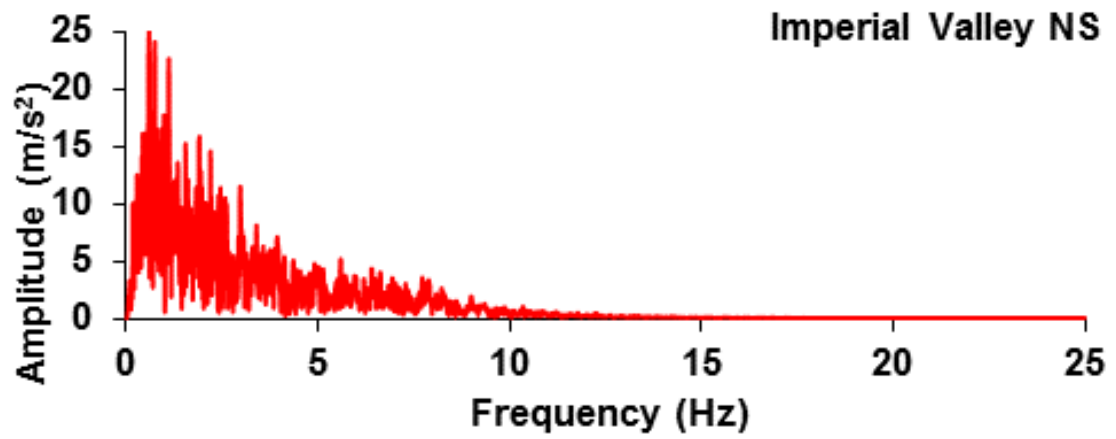
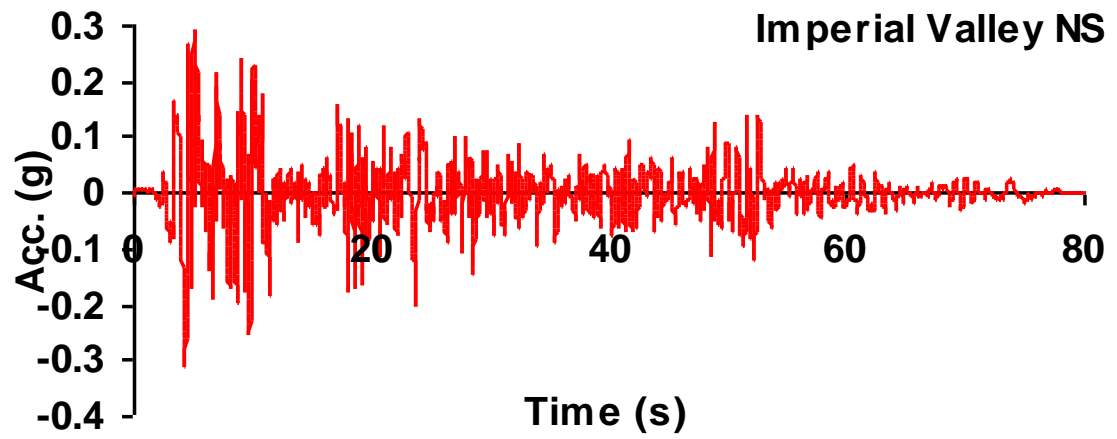


Figure 19 (a). Input accelerations for Imperial Valley earthquake North-South direction

Figure 19 cont.

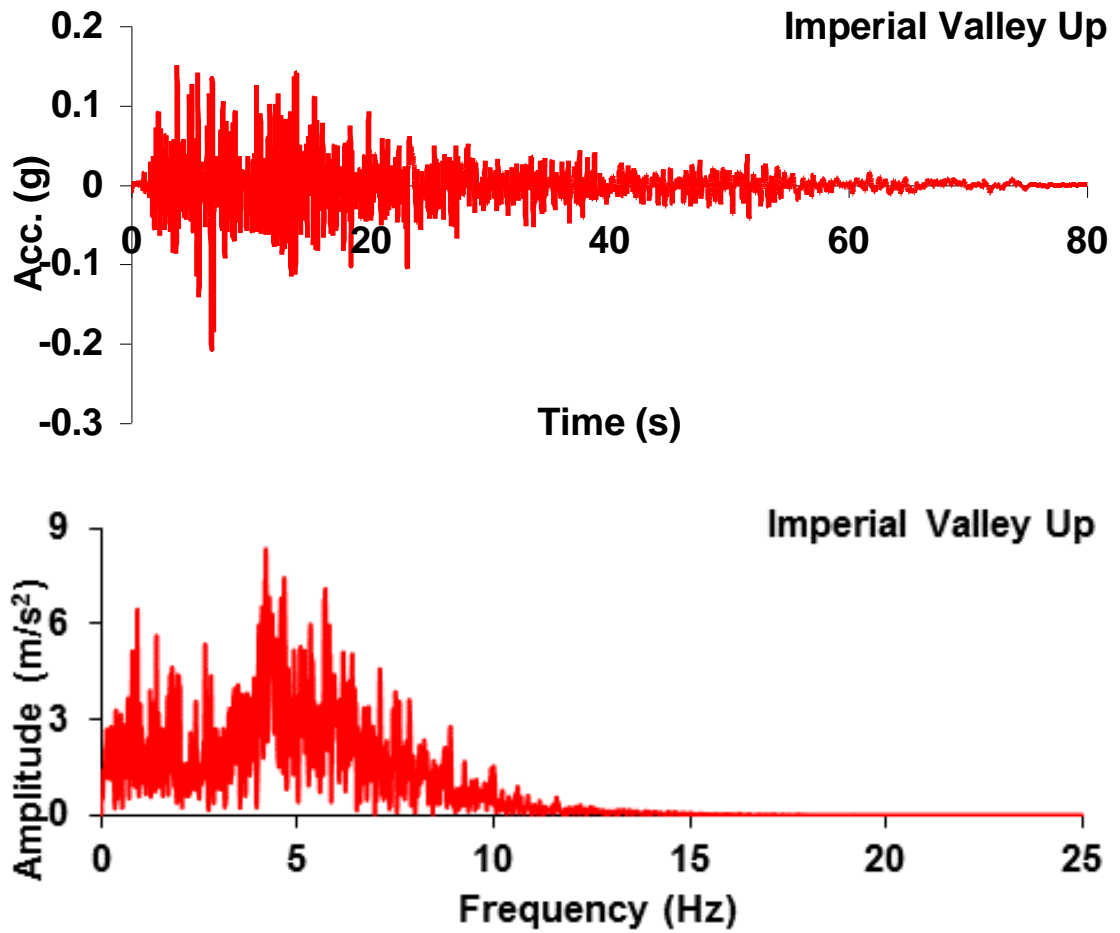


Figure 19 (b). Input accelerations for Imperial Valley earthquake vertical direction

Figure 19 cont.

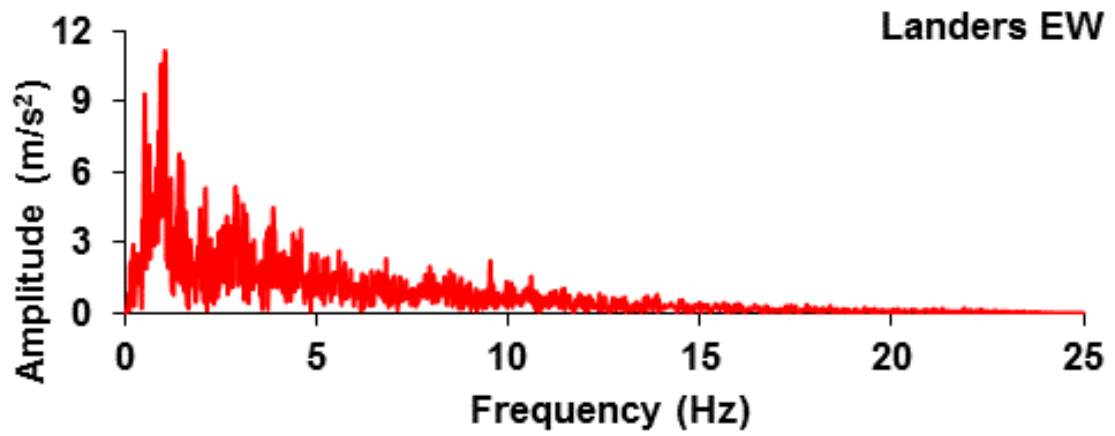
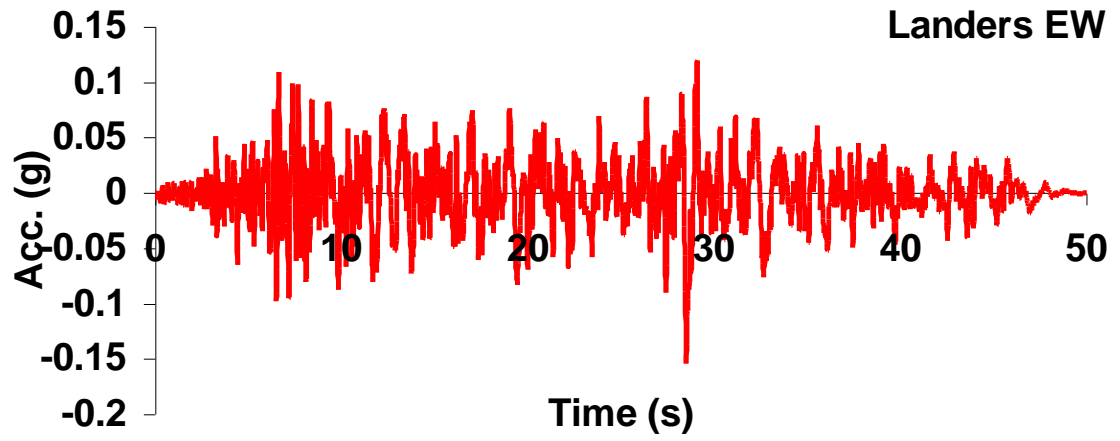


Figure 19 (c). Input accelerations for Landers earthquake East-West direction

Figure 19 cont.

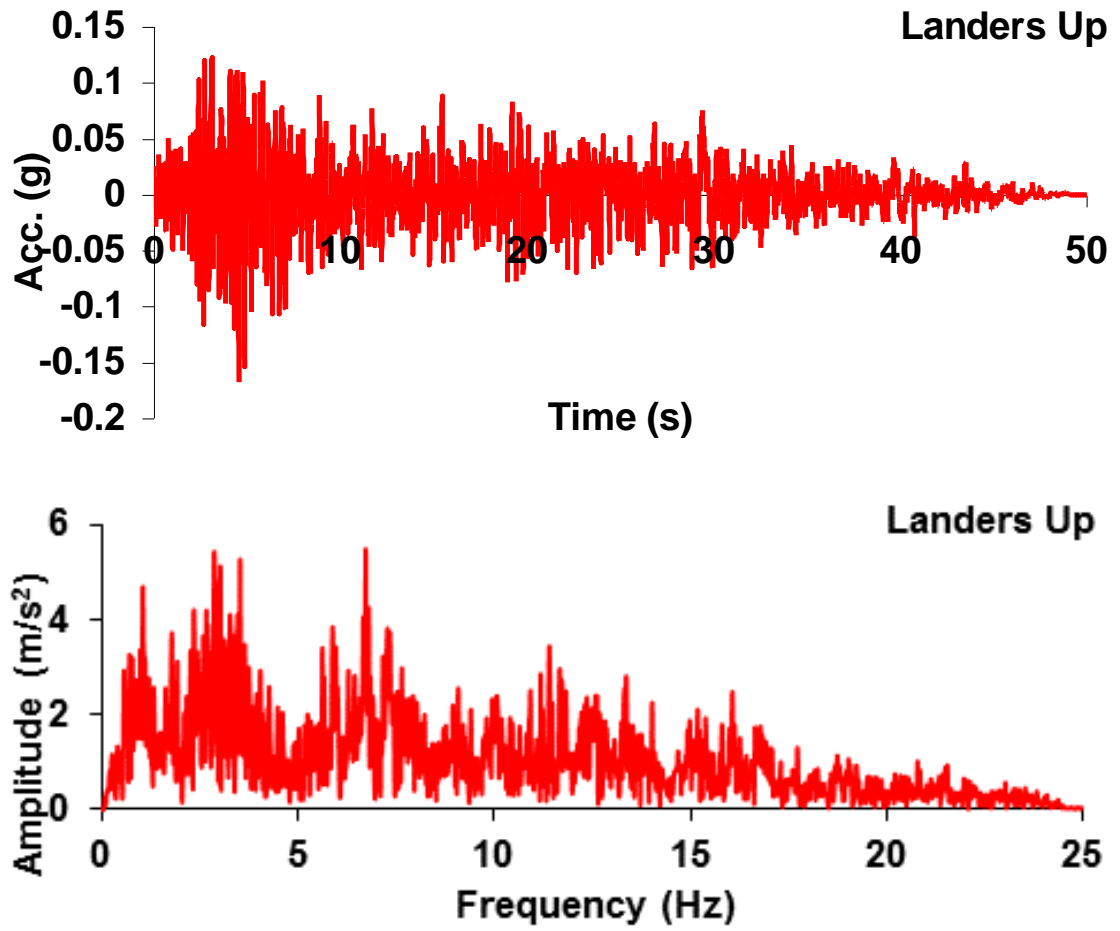


Figure 19 (d). Input accelerations for Landers earthquake vertical direction

Figure 19 cont.

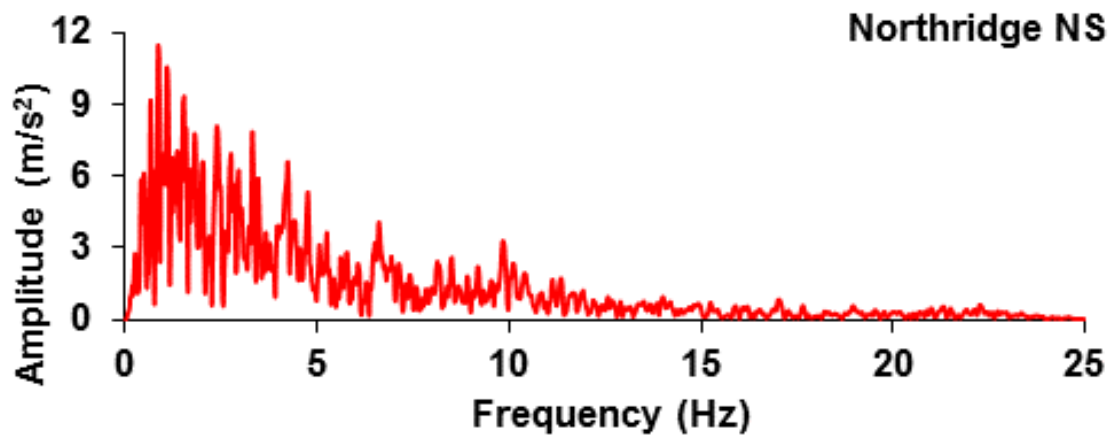
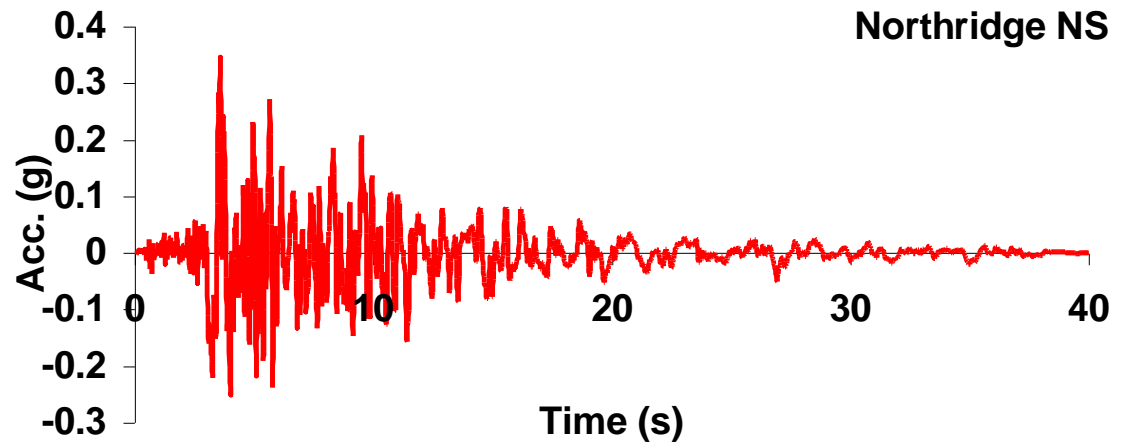


Figure 19 (e). Input acceleration for Northridge earthquake North-South direction

Figure 19 cont.

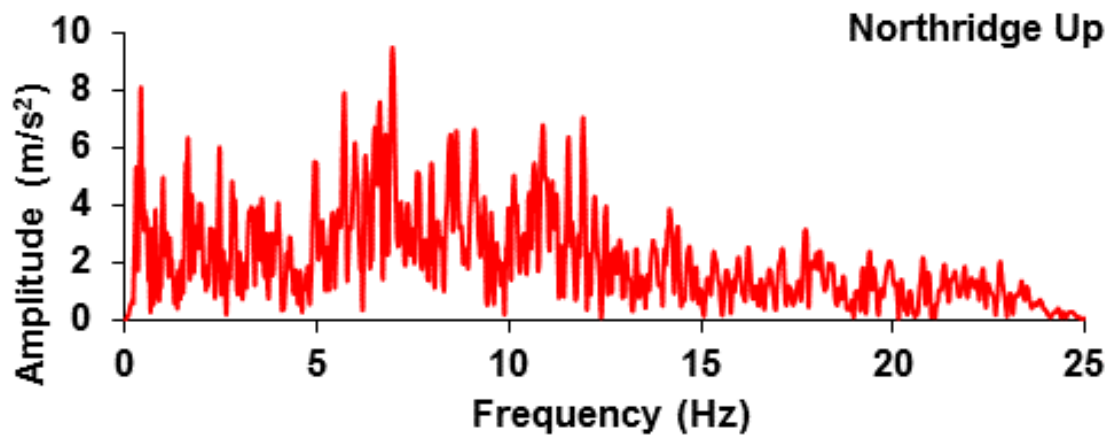
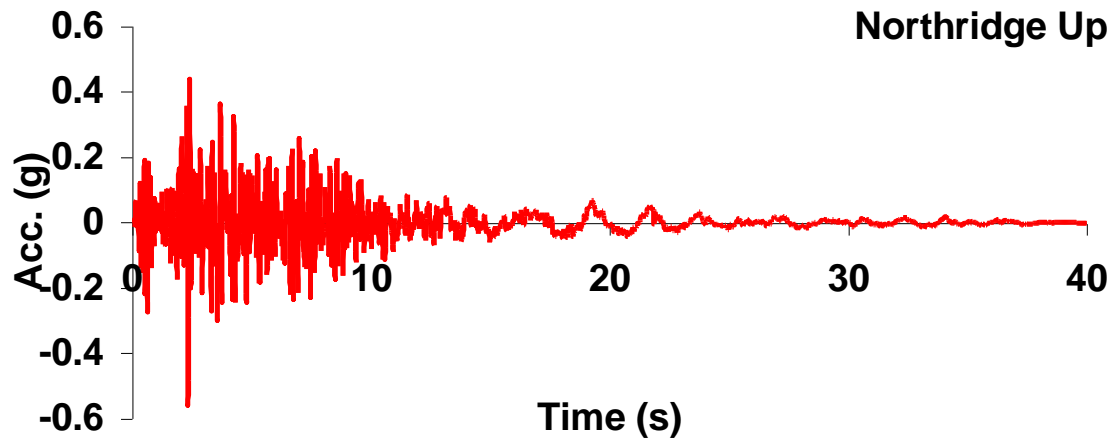


Figure 19 (f). Input accelerations for Northridge earthquake vertical direction

Assumptions and Considerations

1. X direction is parallel to the rotor's axis, Y direction is perpendicular to the rotor axis, and Z direction is parallel to the tower.
2. Wind turbines are assumed to be parked, which means blades are locked to prevent excessive force on the mechanical parts.
3. Tower and nacelle connection is bonded in all DOFs.
4. Global and local buckling modes of towers are neglected assuming they are designed to resist buckling. In practice, it is usually achieved by using stiffeners along the tower length. Preventing local buckling without modeling the stiffeners reduces the number of the nodes and elements and increases the analysis speed drastically.
5. In models without foundations, towers are fixed at the bottom in all translational and rotational DOFs.
6. In all finite element models, all parts are flexible. These include foundations, tower, rotor blades, and nacelle.
7. Material, and geometrical nonlinearities are ignored and all models are assumed to perform linearly.
8. Damping variations due to soil-structure interaction and air-structure interaction is included. Negative damping values due to special wind conditions (suggested by some sources) is not included.
9. Duration of each transient analysis is chosen to be more than the duration of earthquake load so that the free vibration phase is captured.
10. Acceleration responses are given as a fraction of gravity (g).
11. In finite element method, stiffness is higher than experimental values. Increasing the number of elements reduces the stiffness and mesh size-stiffness curvature is asymptotic to experimental stiffness.
12. Foundations are designed in a way that structural and performance failures are eliminated.

CHAPTER 4

PARAMETRIC STUDY OF WIND TURBINES

Validation of Numerical Method

Like any numerical method, finite element method should be validated before any application. It is to insure accuracy of material models, element formulations, and mathematical calculations. In this study, experimental data obtained from testing a full scale wind turbine on a shake table [36] is used to validate the ANSYS program. The test was performed on an industrial scale 65 kW turbine with 23 m (75 ft) height and 10,700 kg (733 slug) mass. Although the model is small compared to modern turbines that are subjects of this study with heights of up to 100 m (328 ft), it's similar to modern wind turbines and the data can be used to validate the FEM.

Experimental Model

The turbine tower is made of three tubular steel sections with two frustum transitional regions as shown in Figure 14 and is similar to modern conical towers. Rotor is parked during the test, with one blade oriented downward. Different accelerometers are placed at different heights of the tower, base, lower joint, upper joint, and top of the nacelle. Table 2 gives physical properties of the experimental turbine.

Table 2. Physical properties of the experimental wind turbine [36]

Property	Value
Hub height	22.60 m (890 in.)
Nacelle mass	2,400 kg (164.5 slug)
Rotor blades diameter	16 m (905 in.)
Rotor blades and hub mass	1,900 kg (130.2 slug)
Tower diameter-outer, lower section	2.02 m (80 in.)
Tower diameter-outer, middle section	1.58 m (62 in.)
Tower diameter-outer, upper section	1.06 m (41.7 in.)
Tower length, total	21.90 m (862 in.)
Tower length, lower section	7.96 m (313 in.)
Tower length, middle section	7.94 m (313 in.)
Tower length, upper section	6.05 m (238 in.)
Tower length, transition regions	1.91 m (75 in.)
Tower mass	6,400 kg (438.5 slug)
Tower thickness	5.3 mm (0.21 in.)

$$1 \text{ slug} = 32.17 \text{ lbm} = 14.62 \text{ kg}$$

Experimental Test

Earthquake load is a uni-axial horizontal excitation perpendicular to the rotor's axis, applied to the basement of the tower through a 7.6x12.2 m² (25x40 ft²) outdoor shaking table with a stroke of ±0.75 m (±29.5 in.) as seen in Figure 14. The table can exert a peak horizontal velocity of 1.8 m/s (3.9 ft/s), a horizontal force of 6.8 MN (1.53E6 lbf), and a vertical force of 20 MN (4.5E6 lbf). Shake table is capable of simulating frequencies of up to 33Hz. Input acceleration, is the East-West component of Landers earthquake (June 28th, 1992). The input acceleration is filtered for DC offset and high frequency noise using a 0.05-25 Hz band-pass filter. This filter acts as a combination of low and high-pass filter and passes frequencies within a certain range.

DC offset is the mean amplitude of the waveform and can cause saturation or change in the operating point of an amplifier. It can be reduced by a high-pass filter. High frequency noise is also unwanted and caused by different sources and can be cancelled using a low-pass filter. Figure 20 shows the filtered acceleration used as input excitation for experimental test. As shown on the graph, duration of excitation is 50 seconds and $PGA = 0.15 \text{ g}$ (gravity acceleration) happens at $t=28.52 \text{ s}$.

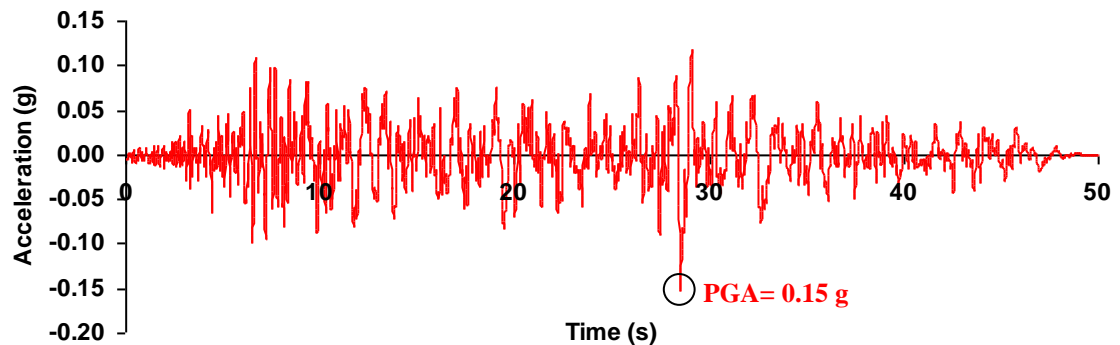


Figure 20. Filtered East-West component of Landers earthquake [36]

Experimental Results

Accelerometer located at top of the nacelle records the peak acceleration response of 0.28 g at $t=30.48 \text{ s}$. Graph presentation of this record is given in Figure 21. The structure effect on the input acceleration can be quantified using the acceleration transfer function along two points of the structure. This function measures the amplification for each frequency between these two points. Figure 22 shows the transfer function from base to top of the nacelle. Maximum amplification is found to be 21.02 for frequency of 1.66 Hz. Observed first and second natural frequencies are 1.7 Hz and 11.7-12.3 Hz, respectively. Mode shapes are constructed using an average of the amplitude and phase of the transfer function and are depicted in Figure 23. Equivalent viscous damping at the first natural frequency is also calculated using the log decrement method [51] and is found to be 0.86%.

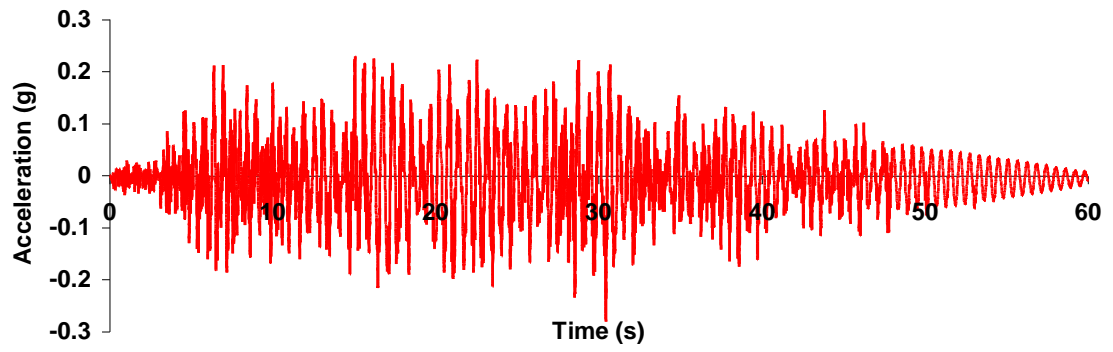


Figure 21. Recorded acceleration at top of the nacelle [36]

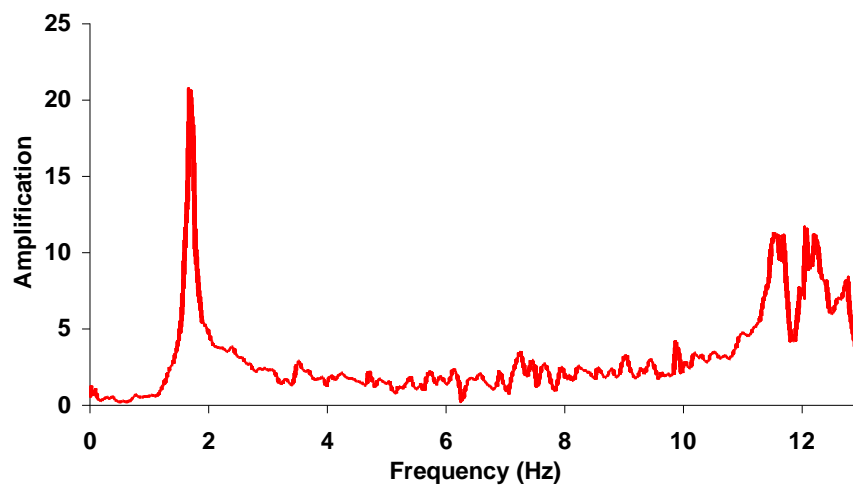


Figure 22. Acceleration transfer function from base to top of the nacelle [36]



Figure 23. Observed 1st and 2nd mode shapes [36]

Validation Model

Geometry

To validate the numerical method, a simplified 3D finite element model of the experimental test is studied. This model consists of tower, nacelle, rotor blades, and hub. Nacelle and hub are solid and tower is a shell with a uniform thickness of 60 mm (2.36 in.) along the length. Simplifying the blade geometry will not cause a problem if the mass distribution of the whole system is not altered. It's due to the fact that local modes of rotor blades are very different from tower modes. Correct mass distribution is accounted for by adjusting the blade width along the length. Mass of miscellaneous tower parts (flanges, bolts, etc.) is 1929 kg (132.2 slug) and is added to the tower as a distributed mass along the length of the tower. Dimensions of nacelle, hub, and rotor blades are given in Figure 24 and Figure 25.

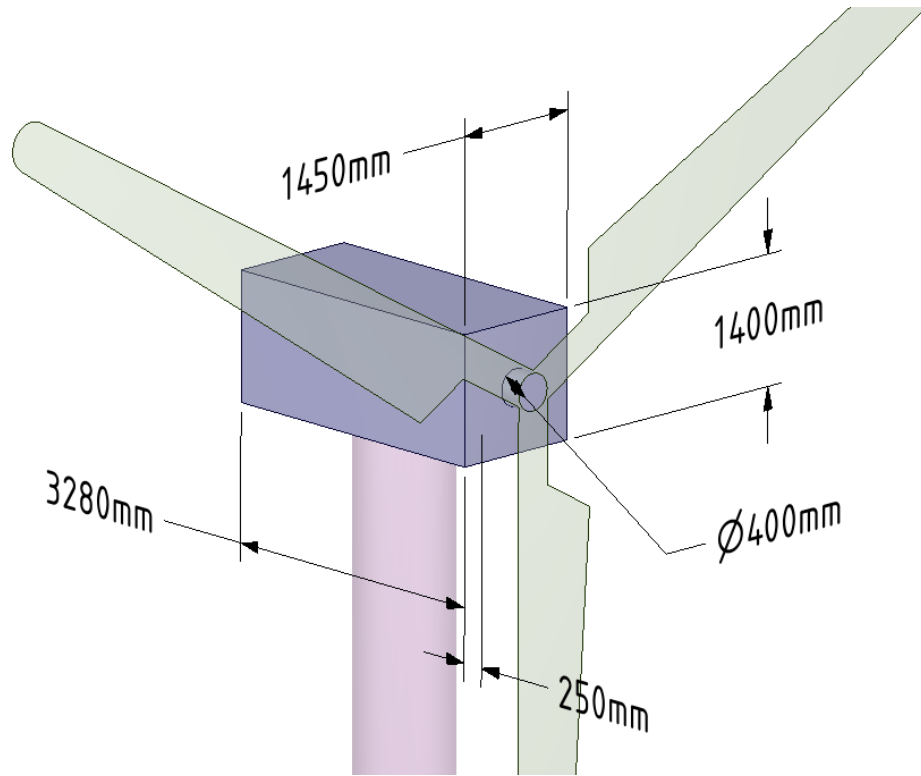


Figure 24. Nacelle and hub dimensions for the 65 kW wind turbine

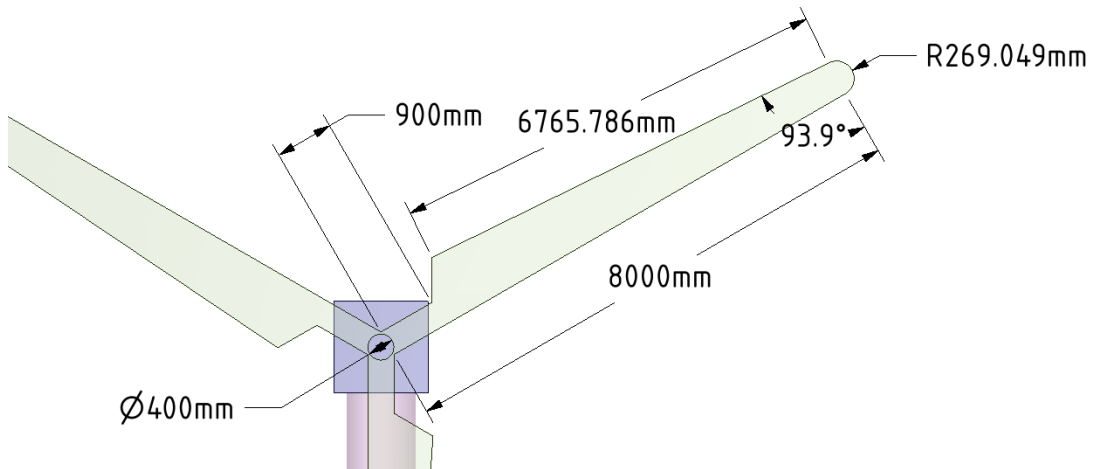


Figure 25. Blade dimensions for the 65 kW wind turbine

Material Properties

Two different materials are defined; a composite material (fiberglass and carbon fibers) [52] for rotor, and structural steel for tower, nacelle, and hub. Because experimental nacelle is lighter than a solid steel box with the same volume, an equivalent lower density is used for the nacelle model. Steel density for other parts is 7860 kg/m^3 (15.25 slug/ft^3). All materials are assumed to be linear. Table 3 gives material properties used in the numerical model.

Table 3. Material properties used in the finite element model

Property	Composite	Steel
Density	648 kg/m^3 (1.26 slug/ft^3)	$7,860 \text{ kg/m}^3$ (15.25 slug/ft^3)
Young's modulus	235,000 MPa (34,084 ksi)	200,000 MPa (29,000 ksi)
Poisson's ratio	0.3	0.3
Tensile yield strength	3,920 MPa (569 ksi)	250 MPa (36,000 psi)
Tensile ultimate strength	3,920 MPa (569 ksi)	460 MPa (66,700 psi)

Table 4. Meshing summary

Part	Elements	Nodes	Element Type
Tower	1760	12430	Shell181
Nacelle	579	2073	Solid186
Hub	28	199	Solid186
Blades	278	387	Shell181
Total	2645	15089	-

Meshing

Tower and blades are meshed using shell181 elements. Nacelle and hub are meshed with solid186 elements. Resulting finite element model is shown in Figure 26. Table 4 gives the number of elements and nodes for each part. The meshing of nacelle and rotor blades is not fully mapped and elements have different sizes. Refinement is

done in extremities. Further refinement is found to have no significant effect on the results.

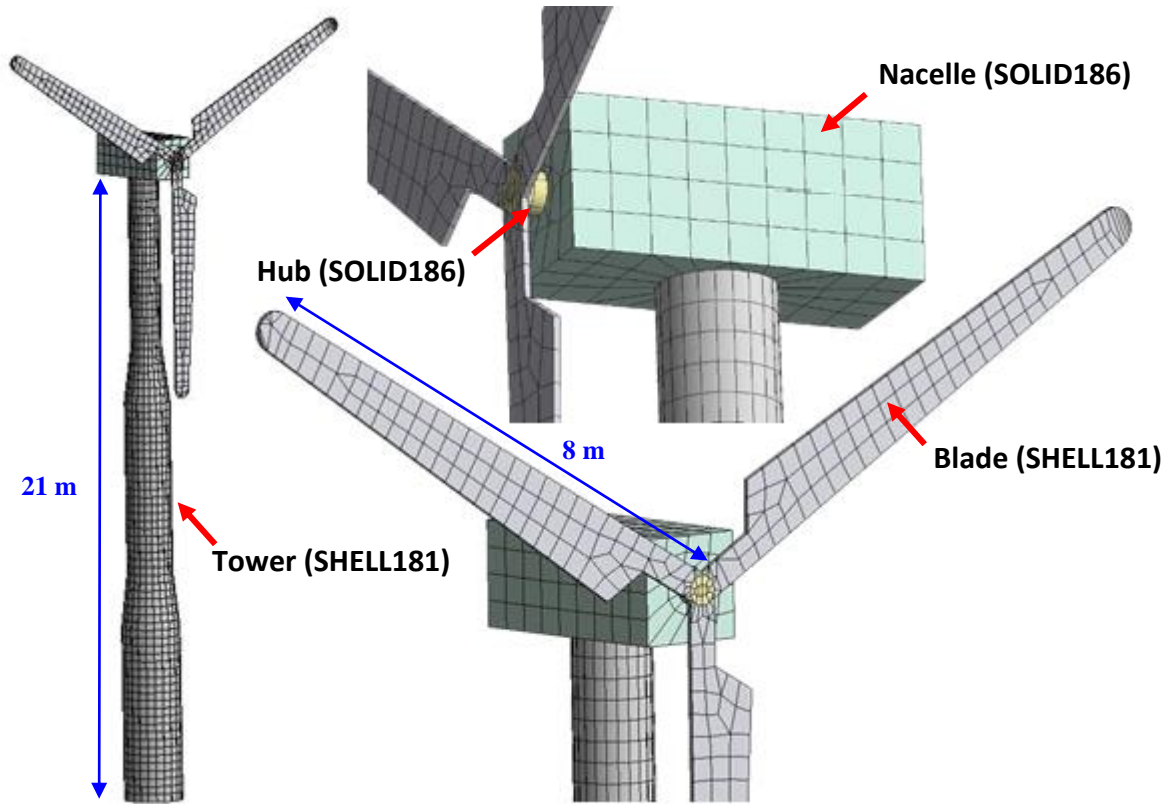


Figure 26. Finite element model of the 65 kW wind turbine

SHELL181 is suitable for analyzing thin to moderately-thick shell structures. It is a 4-node element with six degrees of freedom at each node; translations in the x, y, and z directions, and rotations about the x, y, and z-axes. If the membrane option is used, the element will have translational degrees of freedom only. The degenerate triangular option should only be used as filler elements in mesh generation. SHELL181 is well-suited for linear, large rotation, and/or large strain nonlinear applications. Change in shell thickness is accounted for in nonlinear analyses. In the element domain, both full and reduced integration schemes are supported. SHELL181 accounts for follower (load stiffness) effects of distributed pressures.

Shape functions for stiffness matrix, consistent mass, and for stress stiffness matrices of SHELL181 are as follow:

$$u = \frac{1}{4}(u_I(1-s)(1-t) + u_J(1+s)(1-t) + u_K(1+s)(1+t) + u_L(1-s)(1+t))$$

$$v = \frac{1}{4}(v_I(1-s)(1-t) + v_J(1+s)(1-t) + v_K(1+s)(1+t) + v_L(1-s)(1+t))$$

$$w = \frac{1}{4}(w_I(1-s)(1-t) + w_J(1+s)(1-t) + w_K(1+s)(1+t) + w_L(1-s)(1+t))$$

$$\theta_x = \frac{1}{4}(\theta_x(1-s)(1-t) + \theta_x(1+s)(1-t) + \theta_x(1+s)(1+t) + \theta_x(1-s)(1+t))$$

$$\theta_y = \frac{1}{4}(\theta_y(1-s)(1-t) + \theta_y(1+s)(1-t) + \theta_y(1+s)(1+t) + \theta_y(1-s)(1+t))$$

$$\theta_z = \frac{1}{4}(\theta_z(1-s)(1-t) + \theta_z(1+s)(1-t) + \theta_z(1+s)(1+t) + \theta_z(1-s)(1+t))$$

Geometry of SHELL181 is shown in Figure 27.

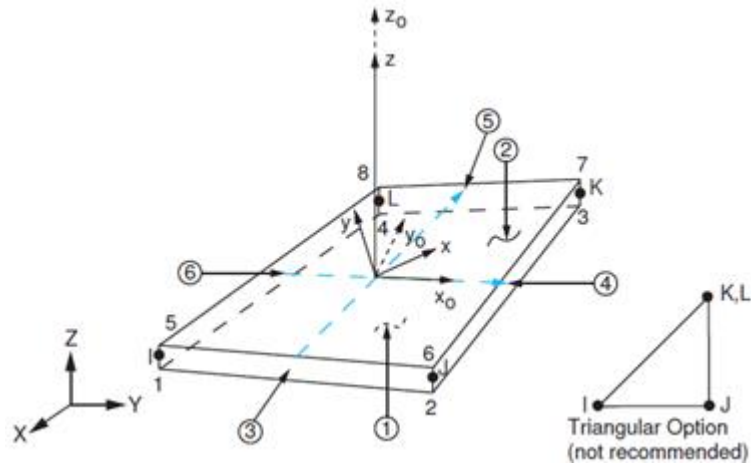


Figure 27. SHELL181 element [53]

SOLID186 is a higher order 3-D 20-node solid element that exhibits quadratic displacement behavior. The element is defined by 20 nodes having three degrees of freedom per node; translations in the nodal x, y, and z directions. The element supports plasticity, hyper-elasticity, creep, stress stiffening, large deflection, and large strain

capabilities. It also has mixed formulation capability for simulating deformations of nearly incompressible elasto-plastic materials, and fully incompressible hyper-elastic materials. SOLID186 Homogenous Structural Solid is well suited for modeling irregular meshes. The element may have any spatial orientation.

Shape functions for stiffness and stress stiffness matrices and for mass matrix of SOLID186 are as follow:

$$\begin{aligned}
 u = & \frac{1}{8}(u_I(1-s)(1-t)(1-r)(-s-t-r-2) + u_J(1+s)(1-t)(1-r)(s-t-r-2) \\
 & + u_K(1+s)(1+t)(1-r)(s+t-r-2) + u_L(1-s)(1+t)(1-r)(-s+t-r-2) \\
 & + u_M(1-s)(1-t)(1+r)(-s-t+r-2) + u_N(1+s)(1-t)(1+r)(s-t+r-2) \\
 & + u_O(1+s)(1+t)(1+r)(s+t+r-2) + u_P(1-s)(1+t)(1+r)(-s+t+r-2)) \\
 & + \frac{1}{4}(u_Q(1-s^2)(1-t)(1-r) + u_R(1+s)(1-t^2)(1-r) \\
 & + u_S(1-s^2)(1+t)(1-r) + u_T(1-s)(1-t^2)(1-r) \\
 & + u_U(1-s^2)(1-t)(1+r) + u_V(1+s)(1-t^2)(1+r) \\
 & + u_W(1-s^2)(1+t)(1+r) + u_X(1-s)(1-t^2)(1+r) \\
 & + u_Y(1-s)(1-t)(1-r^2) + u_Z(1+s)(1-t)(1-r^2) \\
 & + u_A(1+s)(1+t)(1-r^2) + u_B(1-s)(1+t)(1-r^2))
 \end{aligned}$$

Geometry of SOLID186 is shown in Figure 28 [53]. All turbine parts are bonded at connections. Base of the tower is also constrained in all DOFs.

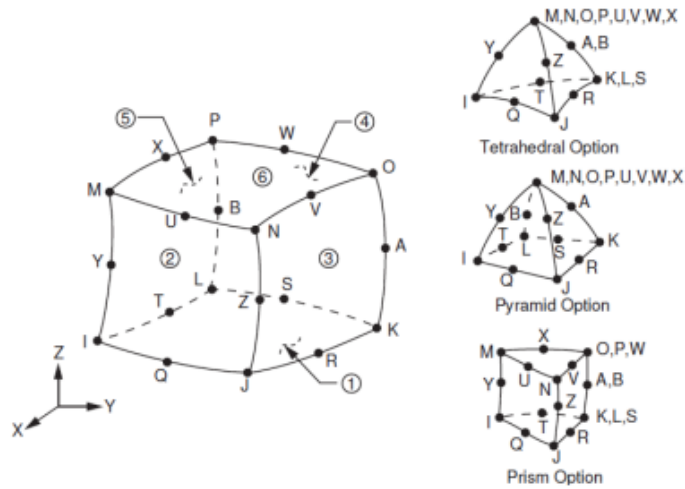


Figure 28. SOLID186 element [53]

Validation Analysis

Validation analysis is performed using the Block Lanczos method explained in Chapter 3. Analysis includes 200 frequencies. Effective mass of these frequencies is found to include more than 90% of the total mass. The first 50 natural modes are given in Table 5. X direction is parallel to the rotor's axis, Y direction is perpendicular to the rotor axis, and Z direction is parallel to the tower. Table 5 also gives the ratio of effective mass to total mass in the load direction (Y direction). Effective mass of frequencies associated with rotor blades are very small and near zero. First three mode shapes of the tower are shown in Figure 30.

Transient analysis is performed using the generalized HHT- α method described in Chapter 3. Like any transient analysis, it is important to keep time steps sufficiently small to produce stable results. In this analysis a time step of 0.02 second is found to be sufficient. This time step size is capable of capturing vibration frequencies of 50 Hz and lower. Same time step size will be maintained throughout this study. The analysis is performed using the damping value of 0.86% calculated in the experimental test. Figure 29 shows numerical transient results along with experimental results. Peak numerical acceleration happens at $t=28.7$ s and is equal to 0.287 g.

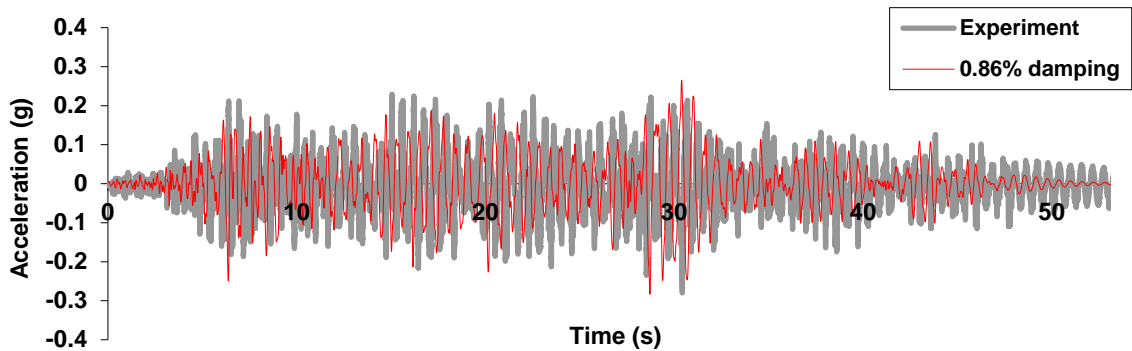


Figure 29. Experimental and numerical transient results with 0.86% damping

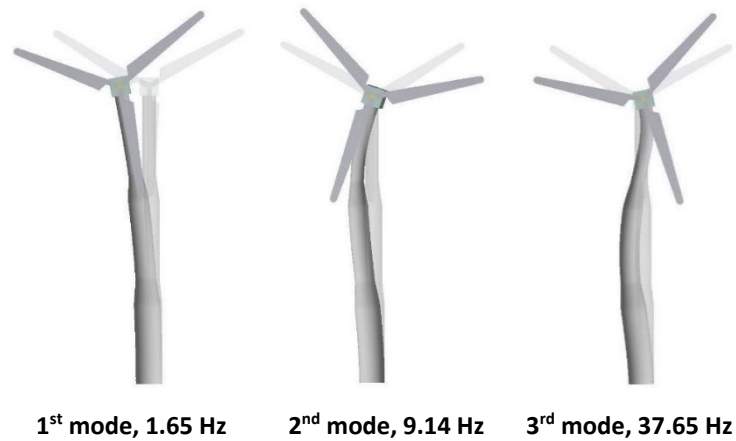


Figure 30. First three mode shapes of the validation model

Validation Results

First and second mode shapes of the numerical analysis are identical to the experimental mode shapes. First and second numerical natural frequencies are 3% and 24% lower than experimental values respectively. Considering the effective mass of first and second modes include 61% and 14% of the total mass respectively, the error caused by the second mode is less significant than the first mode. Also in the time domain, peak numerical acceleration response is 2.5% higher and occurs 1.8 second earlier than the experimental value. Considering the small difference between numerical and experimental results (less than 5%), the numerical method is found to be accurate.

Table 5. Natural modes of validation model

Mode	Frequency (Hz)	Effective/total mass in the Y direction	Mode	Frequency (Hz)	Effective/total mass in the Y direction
1	1.6487	0.6135	26	31.2939	0
2	1.6526	0	27	34.2832	0
3	6.5107	0	28	34.2846	0
4	6.5121	0	29	37.6473	0.0534
5	8.2190	0.0037	30	38.1891	0
6	9.1414	0.1438	31	38.1894	0
7	9.4813	0	32	40.0096	0
8	12.9994	0	33	40.0106	0
9	13.0019	0	34	40.2754	0
10	19.6885	0	35	40.6226	0
11	19.6919	0	36	40.6272	0
12	20.0233	0.0755	37	41.7566	0
13	20.9716	0	38	41.7569	0
14	20.9728	0	39	42.0233	0
15	21.2570	0	40	42.0241	0
16	21.2575	0	41	42.1334	0
17	21.8381	0	42	42.1355	0
18	25.5211	0	43	43.7569	0
19	25.5228	0	44	43.7637	0
20	27.1454	0	45	44.8066	0
21	27.1461	0	46	44.8075	0
22	27.2615	0	47	47.1785	0
23	27.2618	0	48	47.1817	0
24	31.1874	0	49	47.6629	0
25	31.2918	0	50	47.6639	0

Parametric Models

Geometry

Selection of wind turbine sizes for the parametric study is based on the capacity of wind turbines currently being used in the industry. In total, three turbine sizes are selected; a 1 MW and a 5MW utility scale turbines, and the 65kW industrial scale turbine from the experimental study described above. The hub heights of these turbines range from 22.6 to 90 m (74.1 to 295.3 ft). Towers are truncated steel cones with

constant thickness through the height ranging from 5.3 to 27 mm (0.21 to 1.06 in.) and increased diameter at the base. Mass of nacelle is ranging from 2,400 to 240,000 kg (164 to 16,445 slug) and mass of rotor blades and hub is ranging from 6,400 to 110,000 kg (439 to 7537 slug). Rotor blades in all turbines are three-bladed cantilevers and are made of epoxy reinforced with carbon fibers. Table 6 summarizes the physical properties of the three wind turbines. Detailed dimensions of the blades for the 1 MW and 5 MW turbines is given in Figure 31. Blade dimensions for the 65 kW turbine are given in Figure 24 and Figure 25.

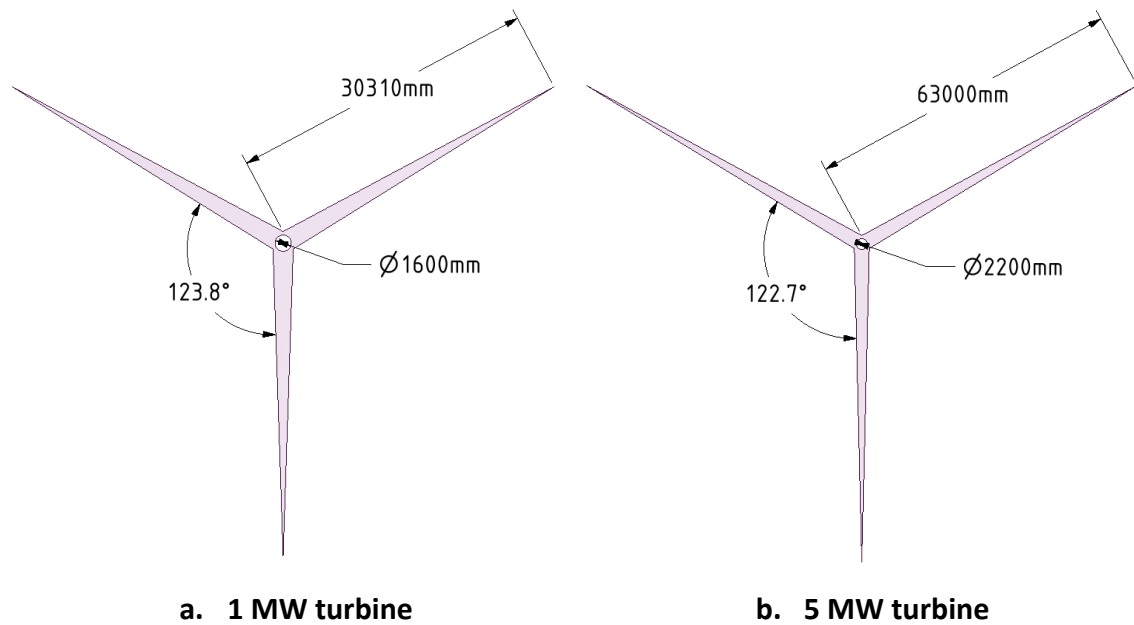


Figure 31. Blade dimensions for the 1 MW and 5 MW wind turbines

Material Properties

Material properties are identical to the ones used in validation model and are given in Table 3.

Table 6. Physical properties of parametric models

Property	65 kW Turbine	1 MW Turbine	5 MW Turbine
Hub diameter, length	0.4, 0.25 m 1.31, 0.82 (ft)	1.6, 0.5 m 5.25, 1.64 (ft)	2.2, 0.5 m 7.22, 1.64 (ft)
Hub height	22.6 m (74.1 ft)	61.14 m (200.6 ft)	90 m (295.3 ft)
Rotor blades diameter	16 m (105 ft)	60.62 m (198.8 ft)	126 m (413.4 ft)
Rotor blades mass	6,400 kg (439 slug)	42,000 kg (2878 slug)	110,000 kg (7537 slug)
Rotor blades thickness	60 mm (2.36 in.)	480 mm (18.9 in.)	550 mm (21.65 in.)
Nacelle width, height, length	1.45, 1.4, 3.28 m 4.76, 4.59, 10.76 (ft)	3.93, 3.93, 10.09 m 12.89, 12.89, 33.1 (ft)	3.93, 3.93, 10.09 m 12.89, 12.89, 33.1 (ft)
Nacelle mass	2,400 kg (164 slug)	53,700 kg (3680 slug)	240,000 kg (16,445 slug)
Tower diameter-outer, bottom	2.02 m (6.6 ft)	3.875 m (12.7 ft)	6 m (19.7 ft)
Tower diameter-outer, top	1.06 m (3.5 ft)	2.45 m (8 ft)	3.87 m (12.7 ft)
Tower length	21.9 m (71.8 ft)	57.19 m (187.6 ft)	88.5 m (290.3 ft)
Tower mass	1,900 kg (130 slug)	78,600 kg (5386 slug)	347,460 kg (23,809 slug)
Tower thickness	5.3 mm (0.21 in.)	18 mm (0.71 in.)	27 mm (1.06 in.)

Table 7. Number of nodes and element of the parametric model parts

Part	Element Type	65 kW Turbine		1 MW Turbine		5 MW Turbine	
		Elements	Nodes	Elements	Nodes	Elements	Nodes
Blades	Shell181	278	387	458	649	558	800
Hub	Solid186	28	199	44	287	21	180
Nacelle	Solid186	579	2073	593	2232	568	1910
Tower	Shell181	1760	12430	988	6981	1472	10384
Total	-	2645	15089	2083	10149	2619	13274

Meshing

Turbines are analyzed with detailed numerical models including the tower, rotor blades, and nacelle. Modeling tower details compared to an idealized model helps with considering the effect of stress concentration in the connections and stress distribution in the tapered sections. A detailed model also increases the accuracy of analysis by

realistically distributing the mass across the body. Meshing procedure is similar to validation model. Table 7 gives the number of nodes and elements for each part of the model.

Table 8. Natural modes of parametric models

Tower	X direction		Y direction		Z direction	
	Freq. (Hz)	Effective/total mass	Freq. (Hz)	Effective/total mass	Freq. (Hz)	Effective/total mass
65 kW	1.65	0.62	1.65	0.61	31.19	0.73
	9.48	0.15	9.14	0.14	21.84	0.02
	21.84	0.07	20.02	0.08	9.48	0.00
1 MW	0.43	0.73	0.43	0.73	11.67	0.70
	3.18	0.09	3.36	0.11	9.25	0.10
	9.25	0.03	7.49	0.05	15.42	0.02
5 MW	0.23	0.71	0.23	0.71	6.15	0.58
	2.20	0.10	1.51	0.11	4.81	0.13
	4.81	0.02	7.17	0.04	5.49	0.07

Parametric Analysis

Analyses of the towers are performed using the finite element analysis program, ANSYS Mechanical [53]. Geometry is assumed to be linear, with no local or global buckling. Connection surfaces are assumed to be in contact at all times which is no local separation happens between nodes. Towers are assumed to be fixed at the bottom. Soil-structure-foundation interaction will be studied separately in the Chapter 5.

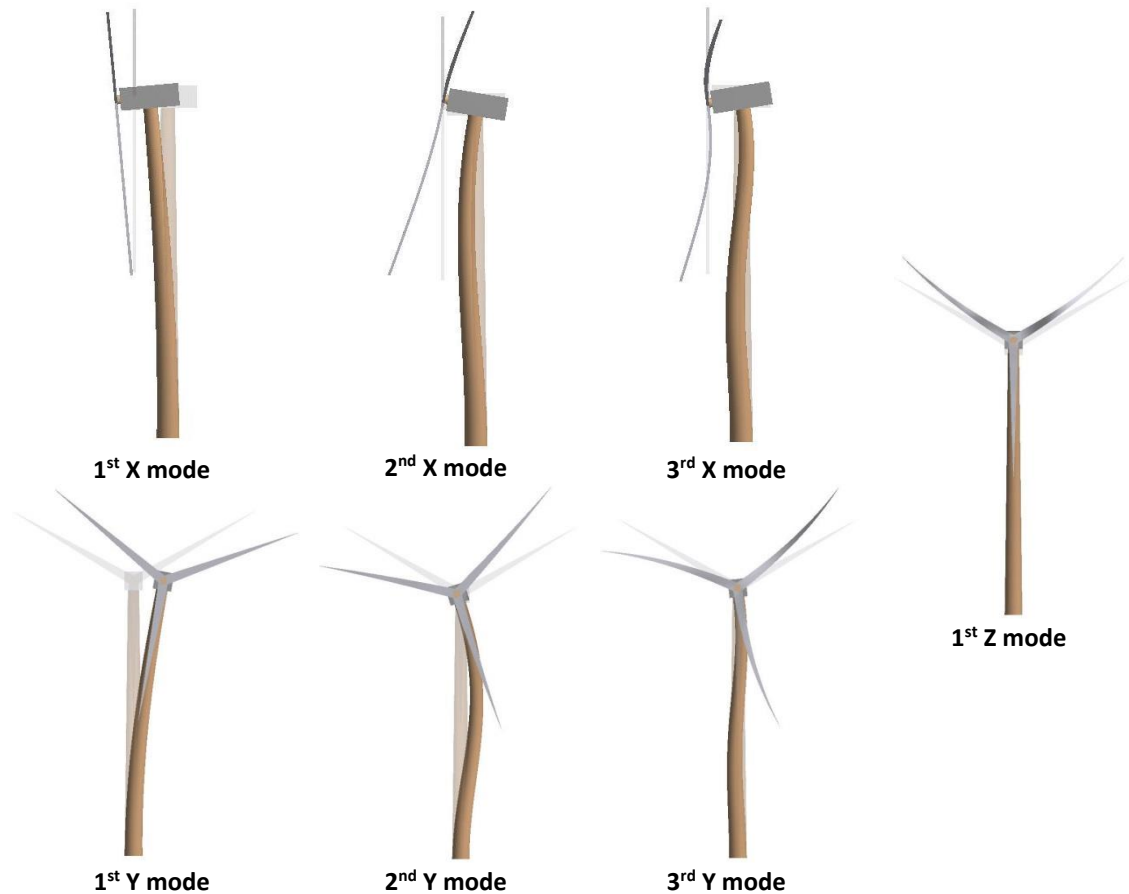


Figure 32. Horizontal and vertical mode shapes of parametric model towers

Modal Analysis

Parametric modal analysis is performed using the Block Lanczos method described in Chapter 3. Analysis includes 200 frequencies. Effective mass of these frequencies is found to include more than 90% of the total mass. The first three natural modes of the towers with highest ratio of effective to total mass are given in Table 8. X direction is parallel to the rotor's axis, Y direction is perpendicular to the rotor axis, and Z direction is parallel to the tower. Table 8 also gives the ratio of effective mass to total mass in all directions.

Figure 32 shows the first three mode shapes of the towers in horizontal directions, in addition to the first tower mode shape in the vertical direction.

Transient Analysis

Parametric transient analysis is performed using the generalized HHT- α method with a time step size of 0.02 second. The analyses are performed using three damping values of 0.5%, 1.0% and 2.0%. These damping values represent the uncertainty due to material and structural interaction with soil and air. For simplicity, a naming convention is used to include model, damping, and load properties in each analyzed response; The first number is the turbine capacity (1, 2, or 5 MW), the first letter is the material (s for steel), the second number is damping ratio (0.5, 1.0 or 2.0 %), the second letter is the earthquake (Landers, Imperial Valley, or Northridge), and the last letter is the direction of input loading and response (X, Y, or Z). In all analyses, the calculated response is in the direction of the earthquake load component. For example, 1S0.5-LX means response of the 1MW turbine with steel tower, with 0.5% damping, under horizontal component of the Landers earthquake in the X direction. For each analysis, complete transient analyses response is given in the Appendix.

First set of analyses is performed using the Landers earthquake on the 65 kW, 1 MW, and 5 MW turbines. Horizontal component of the earthquake is first applied in both X and Y directions separately and the acceleration response at the top of the nacelle is measured. The analysis is then repeated for different damping values. Figure 33 gives the acceleration response of the 1 MW turbine in the X and Y directions for three damping values. Next, vertical component of the Landers earthquake is applied in the Z direction and acceleration response is calculated for three damping values. Figure 34 gives acceleration response of the 1 MW turbine for three different damping values in the vertical direction. For the 5 MW turbine, the horizontal response is calculated with a damping ratio of 1%, the closest value to the current experimental data for wind turbines. Figure 35 shows the acceleration response of the 5 MW turbine in the X and Y directions for 1% damping ratio. Horizontal displacements are also calculated at top of the nacelle. Figure 36 gives the displacement response in the Y direction for 1 MW and 5

MW turbines with 1% damping. Vertical displacement at top of the nacelle is calculated with 1.0% damping under the same load. Figure 37 shows displacement in the Z direction at top of the nacelle for 1 MW and 5 MW turbines with 1% damping. Maximum stress in the structure is found to be located at the base of the tower, therefore, equivalent stress or von Mises stress is measured at the base of the towers. Figure 38 shows maximum von Mises stress at the tower base for 1 MW and 5 MW turbines with 1% damping under horizontal component of the load. To normalize the stress values, von Mises values are divided by the material yield strength. Figure 39 gives normalized von Mises stress at the tower base for 1 MW and 5 MW turbines with 1% damping under vertical component of the load. The analysis is repeated for Imperial Valley and Northridge earthquakes for 1% damping ratio. It should be noted that both 1 MW and 5 MW turbines experience above yield stress levels at the tower base under Imperial Valley load. Therefore, results should be interpreted accordingly. Table 9 summarizes the peak acceleration and deformation response at top of the nacelle and the maximum von Mises stress at tower base for all models. Complete transient analyses response is given in Appendix.

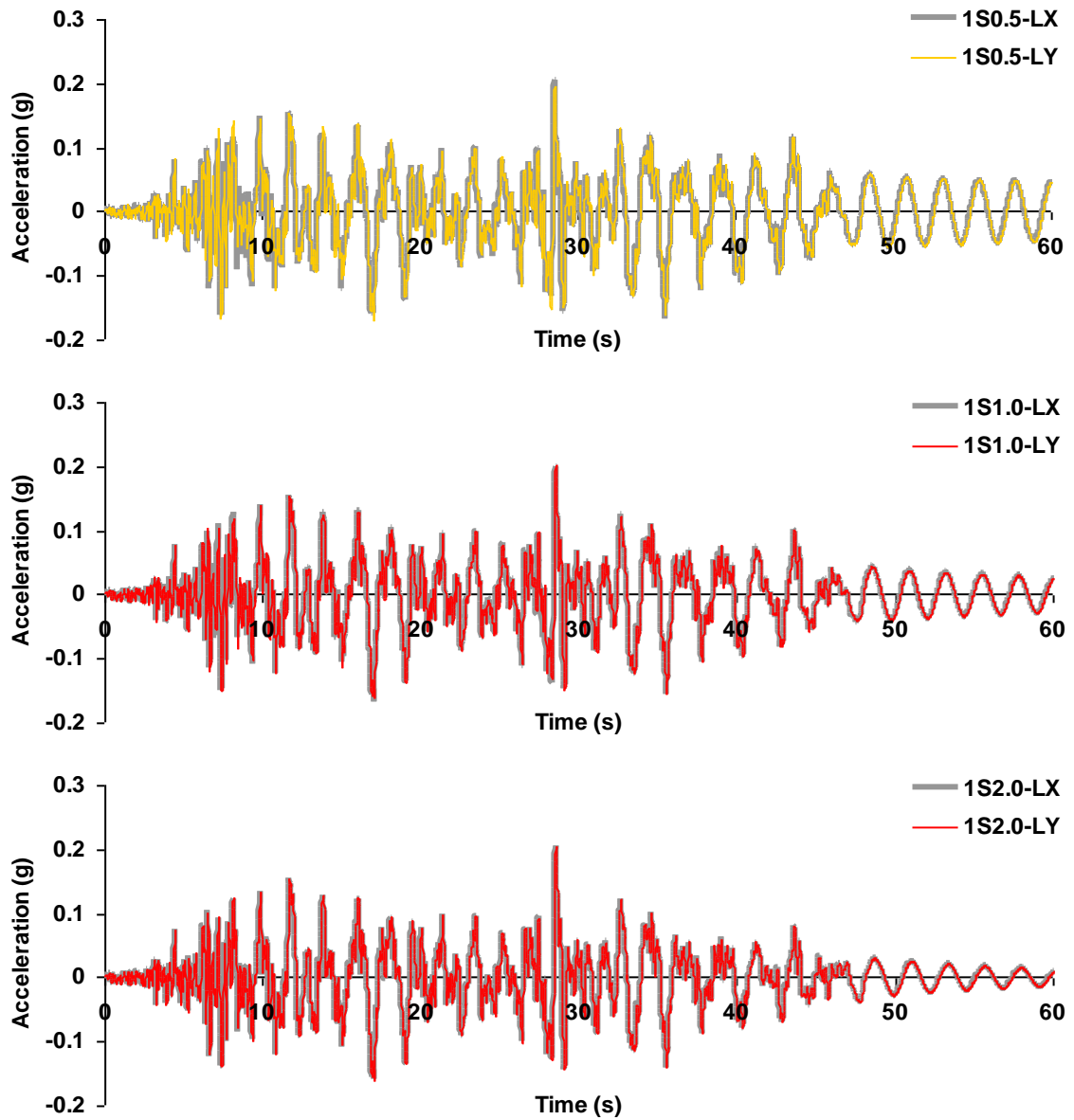


Figure 33. Acceleration response at top of the nacelle in the X and Y directions for the 1 MW turbine with 0.5%, 1%, and 2% damping ratios

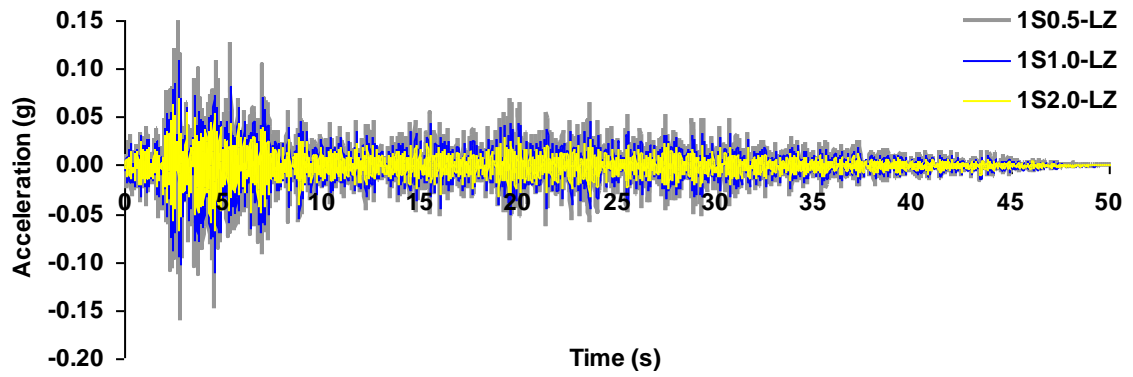


Figure 34. Acceleration response in the Z direction for 0.5%, 1%, and 2% damping ratios

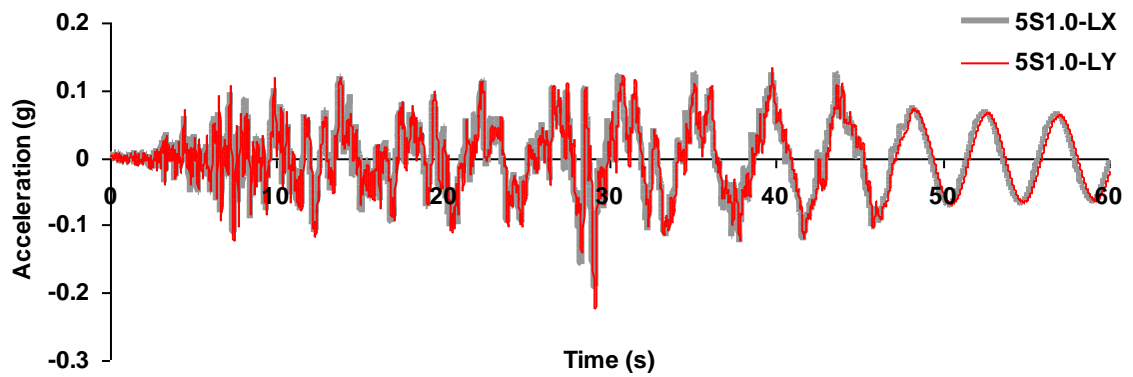


Figure 35. Acceleration response at top of the nacelle in the X and Y directions for the 5 MW turbine with 1% damping ratio

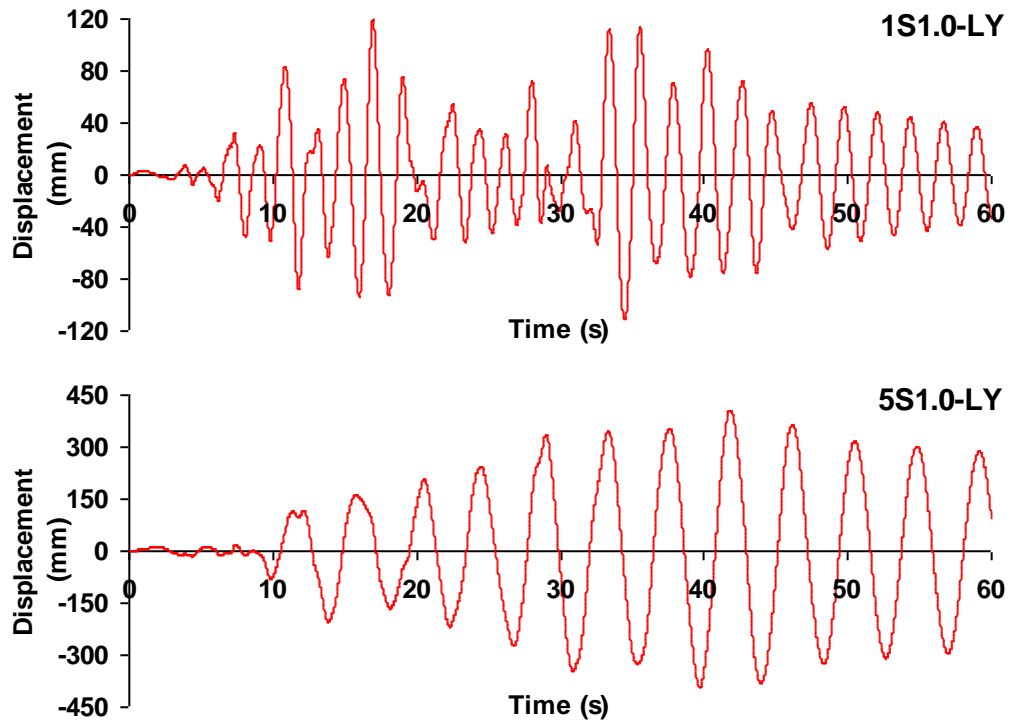


Figure 36. Displacement at top of the nacelle in the Y direction with 1.0% damping

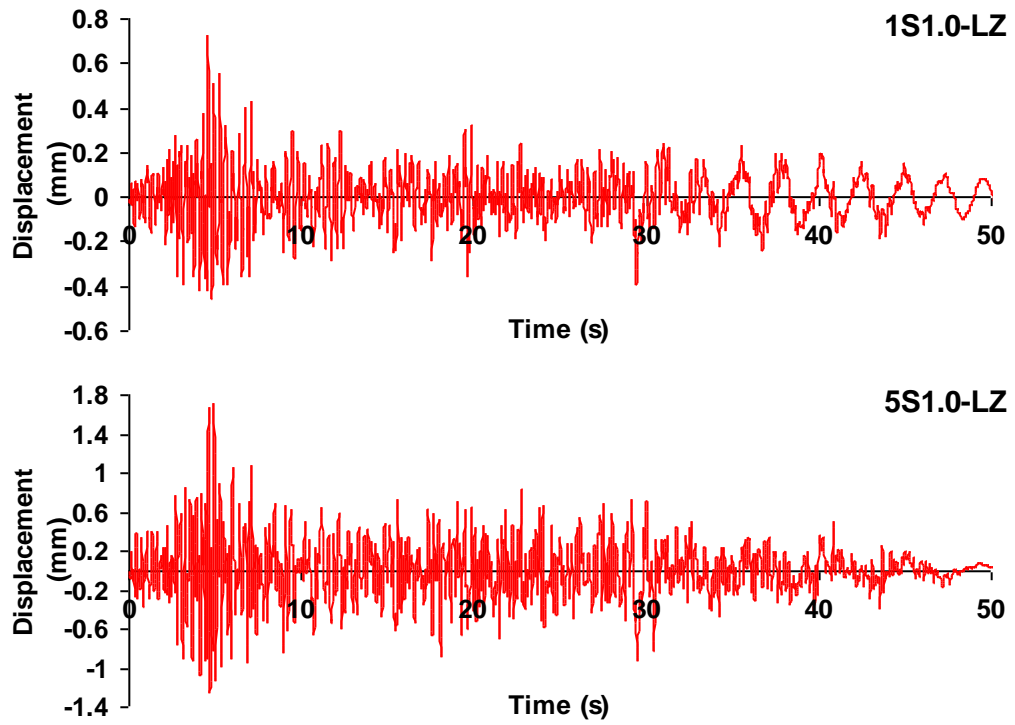


Figure 37. Displacement at top of the nacelle in the Z direction with 1.0% damping

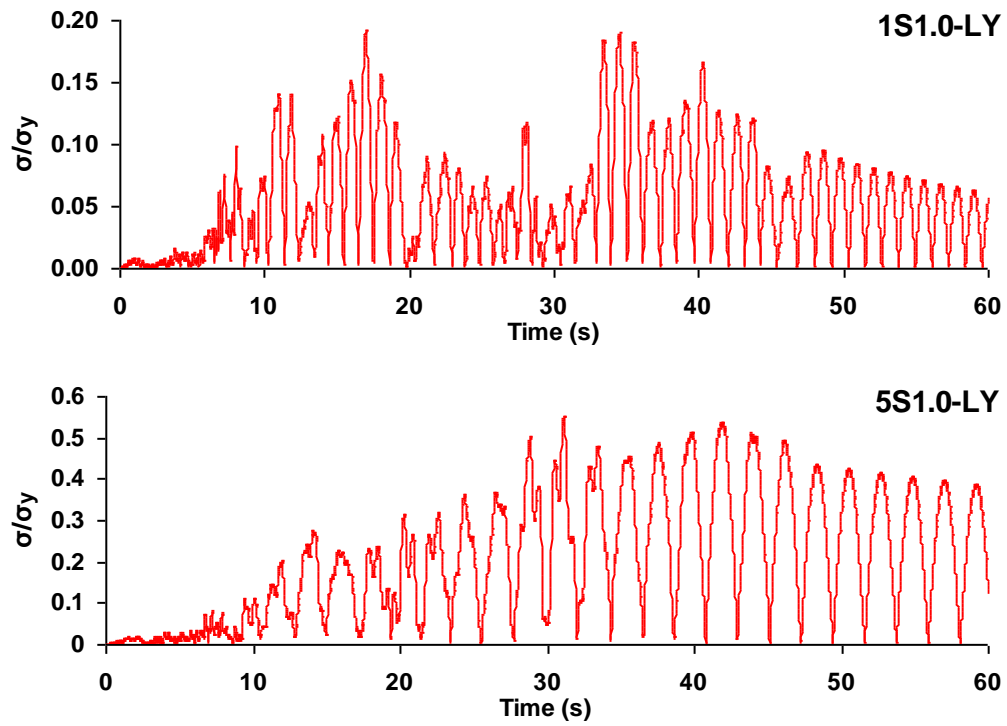


Figure 38. $\sigma_{\text{von Mises max}}/\sigma_y$ at tower base

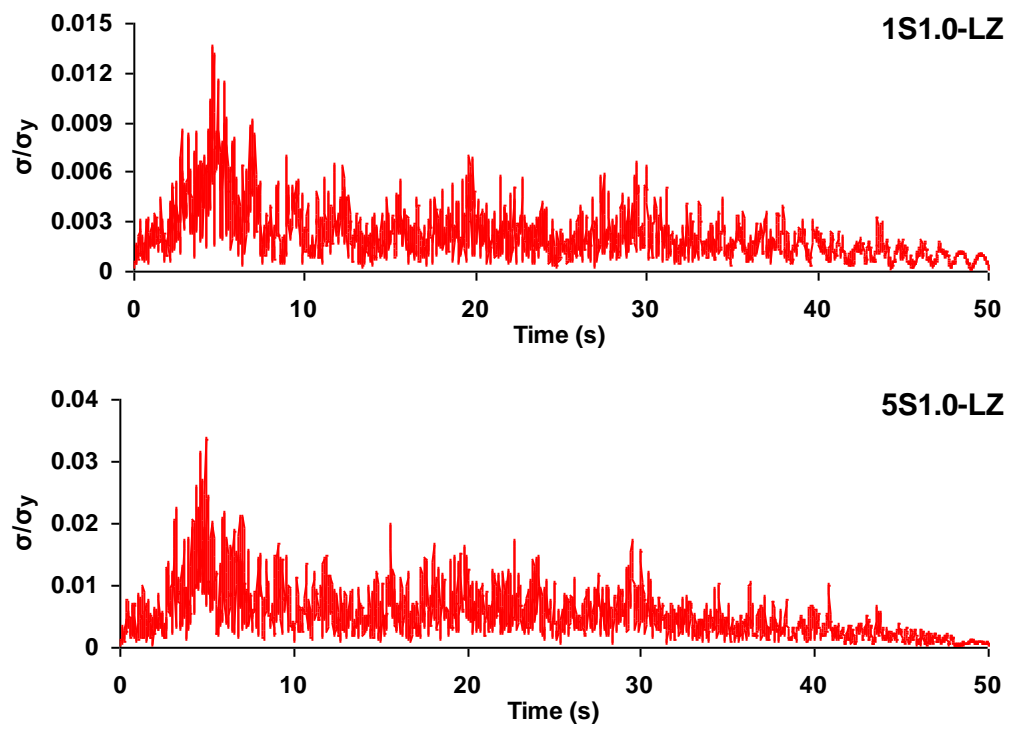


Figure 39. $\sigma_{\text{von Mises max}}/\sigma_y$ at tower base

Table 9. Peak acceleration and deformation response at top of the nacelle and maximum von Mises stress at tower base

Analysis	a_{max} (g)			δ_{max} (mm)			σ_{max} (MPa)		
	X	Y	Z	X	Y	Z	X	Y	Z
0.65S0.5-L	0.352	0.300	-	35.75	32.05	-	51.41	46.97	-
0.65S1.0-L	0.284	0.284	-	28.57	29.18	-	42.35	42.60	-
0.65S2.0-L	0.220	0.278	-	25.03	26.09	-	37.35	38.27	-
0.65S1.0-I	-	1.097	-	-	72.12	-	-	107.15	-
0.65S1.0-N	-	0.701	-	-	67.29	-	-	95.61	-
1S0.5-L	0.206	0.198	0.161	127.76	128.18	0.94	53.26	52.66	4.75
1S1.0-L	0.203	0.199	0.107	118.91	119.43	0.73	47.39	48.09	3.42
1S2.0-L	0.204	0.204	0.068	114.18	114.71	0.50	44.78	45.36	2.32
*1S1.0-I	-	0.642	-	-	720.21	-	-	303.99	-
1S1.0-N	-	0.523	-	-	234.92	-	-	100.17	-
5S0.5-L	0.193	0.230	0.298	450.38	446.90	2.29	154.12	156.82	10.67
5S1.0-L	0.189	0.222	0.235	409.58	405.99	1.73	135.88	137.71	8.44
5S2.0-L	0.187	0.207	0.181	341.77	338.77	1.32	112.06	113.69	6.89
*5S1.0-I	-	0.444	-	-	1212.00	-	-	404.29	-
5S1.0-N	-	0.405	-	-	330.93	-	-	108.28	-

* Analyses with stress level above yield

CHAPTER 5

SOIL-STRUCTURE INTERACTION

This chapter studies the effects of soil-structure interaction on the seismic response of horizontal axis wind turbines with truncated cone steel towers and frequency based designed foundations. Four types of foundations are studied; spread foundations, mono piles, pile groups with cap, and anchored spread foundations. Different foundation types are added to wind turbines with different capacities. Soil is modeled both implicitly (subgrade reaction modulus) and explicitly. Soil-foundation-wind turbine models are then analyzed in both frequency and time domains. Recommendations are given to simplify the design of wind turbines.

Frequency Based Design

In the analysis and design of wind turbines, tower design is usually controlled by its frequency limits to prevent interference with turbine operational frequencies [54]. Figure 40 shows allowable frequency range in a typical frequency design problem. Natural frequencies (f_{n1} , f_{n2} , etc.) should be separated from operational frequencies (f_{op1} , f_{op2} , etc.) with a safety margin. Considering operational frequencies of utility scale wind turbines typically range from 0.1 Hz for larger turbines to 0.5 Hz for smaller ones, natural frequency of these turbine should be above this range to prevent resonance. In other words, ratio of natural to operational frequency must be greater than 1 preferably with a 10% safety margin. Recommended values for this factor of safety are between 1.1 and 2. If safety margin is not big enough, effect of soil-structure interaction can shift

the natural frequencies of the structure too close to operational frequencies and dynamic amplification can occur. Therefore, assuming a fixed tower base may not be conservative and it may be necessary to analyze the soil-structure interaction. In other words, unlike other structures, design of wind turbine foundations may not be governed by soil bearing capacity alone and can be affected by dynamic properties of the wind turbine.

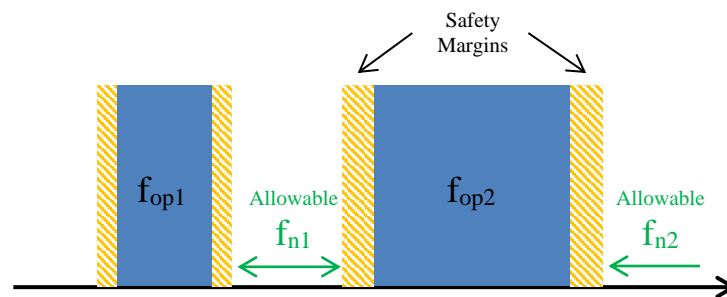


Figure 40. Allowable frequency range

Numerical Soil Models

To investigate the effects of soil-structure interaction, effect of soil can be included implicitly or explicitly. In implicit methods, effects of the soil are added to the analysis using springs and dampers without modeling the soil itself. Different implicit techniques use different assumptions and are suitable for specific problems. In an explicit method however, the soil itself is modeled with finite elements. The soil body should be large enough to be accurate and therefore it's slow compared to the implicit method. Implicit method is usually used in critical problems. Two common implicit techniques are linear soil pressure distribution and K-model [55]:

Linear Soil Pressure Distribution Model

In this method, soil pressure is assumed to be distributed linearly under the foundation. This soil pressure depends on the foundation forces only and nonlinear

reactions cannot be modeled. Linear soil pressure distribution model is a good approximation for stiffer foundations like column footings; however, it is conservative for flexible foundations.

K-Model

This implicit model simulates soil behavior by a series of elastic springs under foundation and results in nonlinear soil pressure distribution proportional to the foundation settlement. Stiffness of K-model springs are referred to as K or modulus of subgrade reaction. K-model is often used to analyze footings under single concentrated load. In K-model, K is a combination of soil and structure stiffness and therefore, in design problems it should be determined by trial and error. Figure 41 shows soil pressure distribution in K-model.

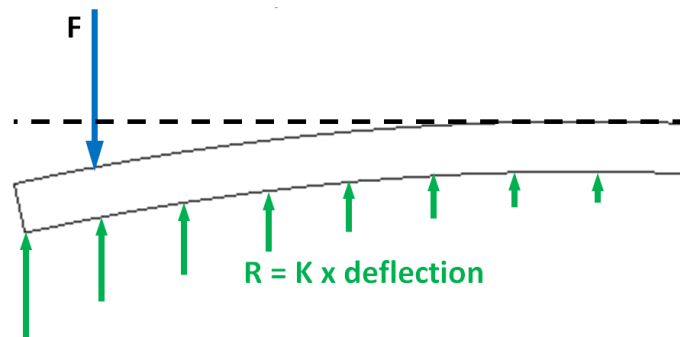


Figure 41. Soil pressure distribution in K-model

Explicit Model

This method is the most accurate way to analyze the soil-structure interaction. Soil body is modeled fully or partially and damping can be added to the structure, which results in a more realistic and economical design [54]. Depending on the size and complexity of the soil body, explicit model can be substantially slow and therefore, costly.

In this study only K-model and Explicit Soil model are used. Linear model is not used since it ignores the effects of foundation flexibility.

Foundation Types

Based on turbine properties and soil conditions, wind turbine foundations can have different design and configurations. These designs can be classified into four major categories; spread foundations, mono piles, pile groups with cap, and anchored spread foundations [56, 57].

Spread Foundation

Spread foundations are the cheapest and easiest types of foundations to build. If soil has enough bearing capacity, spread foundation is the first design choice. Spread foundations are usually rectangular, circular, or octagonal and made of reinforced concrete and/or steel. Overturning resistance usually comes from a combination of weight of the foundation and the backfill soil on the top. Figure 42 shows a spread foundation with pedestal.

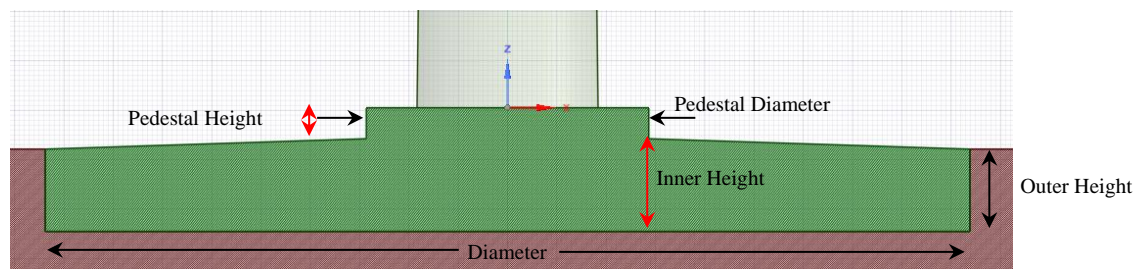


Figure 42. Spread foundation and pedestal

Mono Pile

In some cases, top soil cannot provide sufficient bearing capacity and using a pile can be a viable option. Mono piles may or may not bear on the bed rock and they transfer the wind turbine loads through a combination of bearing and frictional loads. Mono piles are usually made of reinforced concrete with or without steel pipe and the length can be $1/3$ to $2/3$ of the tower height [58]. Overturning resistance in mono piles is provided by axial and bending strength of the pile. Figure 44 shows the numerical model of the mono pile foundation.

Pile Group & Cap

Depending on the soil condition, it may be necessary to use two or more piles in a group configuration. Usually, all piles in a pile group are similar and connected with a cap. The wind turbine loads are applied on the cap and distributed to individual piles. Depending on the spacing of the piles, capacity of the pile group can be equal or less than the combination of individual piles. This is because of overlapping stress zone around the piles. Figure 44 shows the numerical model of the pile group & cap foundation.

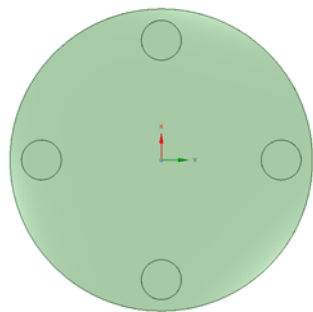
Anchored Spread Foundation

In cases where soil doesn't have enough bearing capacity and bedrock is easily accessible, spread foundations can be anchored to the bedrock. In this case, spread section is usually made of concrete. Anchors can be steel cables, helical steel shaft, or steel tendons [59]. Anchored spread foundations offer minimal footprint and are ideal for rock sites. Figure 44 shows the numerical model of the anchored spread foundation.

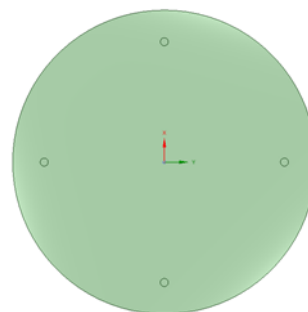
Parametric Models

Geometry

Parametric study of the soil-structure interaction is performed on three wind turbine capacities identical to those studied in Chapter 4. Explicit soil bodies are cuboid with square areas. Soil body size is determined using trial and error to dissipate 95% of the elastic energy within its boundaries. Further increase in the soil body size will have minimal effect on the analysis results. Four types of foundations are investigated, in addition to a fixed-base model without foundation. Spread foundations are circular slabs with pedestal, with varying thicknesses along the radius as shown in Figure 42. Mono piles also have a pedestal on top. Pile groups and anchors are in groups of four with each pile or anchor placed symmetrically relative to the center of the cap as shown in Figure 43. Dimensions of the soil bodies and foundations are given in Table 10.



Four symmetrical piles



Four symmetrical anchors

Figure 43. Placement of piles and anchors

Table 10. Dimensions of the soil bodies and foundations

Property	65 kW Turbine	1 MW Turbine	5 MW Turbine
Spread footing pedestal height	0.253 m (0.83 ft)	0.658 m (2.16 ft)	1.012 m (3.32 ft)
Spread footing pedestal diameter	2.314 m (7.59 ft)	6.016 m (19.74 ft)	9.256 m (30.37 ft)
Spread footing center height	0.758 m (2.49 ft)	1.971 m (6.47 ft)	3.032 m (9.95 ft)
Spread footing outer height	0.673 m (2.21 ft)	1.75 m (5.74 ft)	2.692 m (8.83 ft)
Spread footing diameter	7.576 m (24.86 ft)	19.698 m (64.62 ft)	30.304 m (99.42 ft)
Mono pile cap height	1.011 m (3.32 ft)	2.629 m (8.62 ft)	4.044 m (13.27 ft)
Mono pile cap diameter	2.314 m (7.59 ft)	6.016 m (19.74 ft)	9.256 m (30.37 ft)
Mono pile height	10 m (32.81 ft)	26 m (85.3 ft)	40 m (131.23 ft)
Mono pile diameter	2.02 m (6.63 ft)	5.252 m (17.23 ft)	8.08 m (26.51 ft)
Pile group height	10 m (32.81 ft)	26 m (85.3 ft)	40 m (131.23 ft)
Pile group diameter (each)	1 m (3.28 ft)	2.6 m (8.53 ft)	4 m (13.12 ft)
Anchor height	10 m (32.81 ft)	26 m (85.3 ft)	40 m (131.23 ft)
Anchor diameter	0.2 m (0.66 ft)	0.52 m (1.71 ft)	0.8 m (2.62 ft)
Pile/Anchor distance to cap center	3 m (9.843 ft)	15.6 m (51.181 ft)	24 m (78.74 m)
Soil depth	10.673 m (35.02 ft)	27.75 m (91.04 ft)	42.692 m (140.07 ft)
Soil square width	20 m (65.62 ft)	52 m (170.6 ft)	80 m (262.47 ft)

Material Properties

As mentioned, design of wind turbine foundations is often controlled by turbine operational and natural frequencies, in addition to the bearing capacity of the soil. Assuming a frequency-based design for foundations being investigated, the soil-foundation properties should be first adjusted to represent the realistic structural frequencies. Response of the structure is then analyzed to evaluate the effect of soil-structure interaction on the seismic response of the structure. To achieve this, E in explicit models and foundation properties are first selected. In K-models, K values are determined using trial and error. Next, displacement at top of the nacelle is calculated for each system. Mechanical properties of the explicit soil are given in Table 11.

Table 11. Mechanical properties of soil

Properties	Value
Angle of internal friction (Φ)	37°
Elasticity Module (E)	150 MPa (21,760 lbf/in ²)
Poisson's ratio (ν)	0.2
Unit weight (γ)	25,000 N/m ³ (159 lbf/ft ³)

Meshing

Meshing of turbines is like the procedure described in Chapter 4. Soil and foundations are meshed using SOLID186 elements. Contact between soil and foundation is modeled using bonded connection in ANSYS. The resulting finite element models of the 1 MW wind turbine with and without foundations are shown in Figure 44. Cross section of the pile group & cap foundation with explicit soil model is shown in Figure 45. The minimum element numbers needed for each model is determined by controlling the error in first natural frequencies obtained from modal analysis. Any further refinement in mesh size is found to have no significant effect on the accuracy. Table 12 gives the meshing summary for various parts of foundation-turbine models.

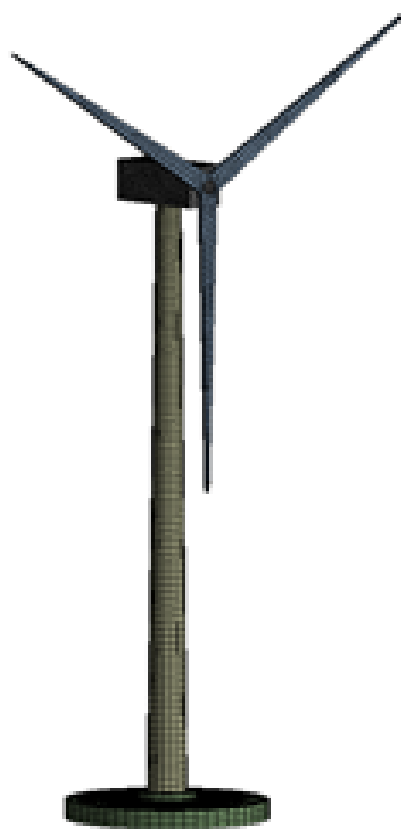
Table 12. Meshing summary

Part	Element Type	65 kW Turbine		1 MW Turbine		5 MW Turbine	
		Elements	Nodes	Elements	Nodes	Elements	Nodes
Tower	Shell181	2174	2195	1751	1768	1734	1751
Blades	Shell181	445	573	335	488	432	632
Nacelle & hub	Solid186	6606	10054	7592	11516	1816	2942
Spread foundation	Solid186	13634	58355	23560	99474	19026	80488
Mono pile	Solid186	28506	41871	29393	43122	27588	40527
Pile group & cap	Solid186	51533	80059	15984	71913	76876	49371
Anchored spread	Solid186	35132	160335	40941	184603	36407	165617

Parametric Analysis

Modal Analysis

Parametric modal analysis is performed using the Block Lanczos method described in Chapter 3. Analysis includes 100 frequencies. Effective mass of these frequencies is found to include more than 90% of the total mass. The first three natural frequencies of the systems with four types of foundations and three turbine sizes are given in Table 13, Table 14, and Table 15 respectively. X direction is parallel to the rotor's axis, Y direction is perpendicular to the rotor axis, and Z direction is parallel to the tower. Table 13, Table 14, and Table 15 also give a description of each mode shape. Frequencies are given for both K and explicit soil models. Frequency of model with no soil and foundation is also given as a reference.



(a) Spread foundation



(b) Mono Pile



(c) Pile Group & cap

(d) Anchor Spread

Figure 44. Meshing of 1 MW turbine with different foundation types

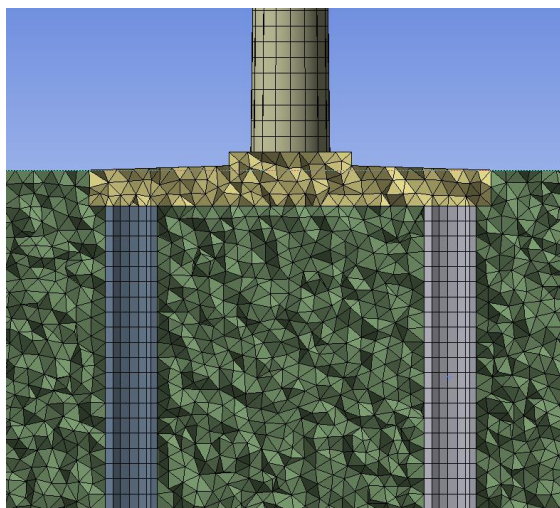


Figure 45. Meshing of pile group & cap foundation and explicit soil

Table 13. Natural frequencies and mode shapes of the 65 kW structure

Foundation Type	Mode	Frequency (Hz)		Mode Shape
		K-Model	Explicit	
None	1	1.65		1 st Translational X
	2	1.65		1 st Translational Y
	3	9.14		2 nd Translational Y
Spread	1	1.55	1.55	1 st Translational X
	2	1.59	1.59	1 st Translational Y
	3	7.96	3.74	2 nd Trans. Y-1 st Trans. Z
Mono-Pile	1	1.53	1.56	1 st Translational X
	2	1.64	1.60	1 st Translational Y
	3	8.42	6.73	2 nd Translational Y
Pile-Group & Cap	1	1.54	1.58	1 st Translational X
	2	1.64	1.62	1 st Translational Y
	3	8.38	4.08	2 nd Translational Y
Anchored Spread	1	1.52	1.56	1 st Translational X
	2	1.61	1.60	1 st Translational Y
	3	8.91	4.96	2 nd Translational Y

Table 14. Natural frequencies and mode shapes of the 1 MW structure

Foundation Type	Mode	Frequency (Hz)		Mode Shape
		K-Model	Explicit	
None	1	0.43		1 st Translational X
	2	0.43		1 st Translational Y
	3	3.18		2 nd Translational Y
Spread	1	0.42	0.42	1 st Translational X
	2	0.42	0.42	1 st Translational Y
	3	3.10	3.10	2 nd Translational Y
Mono-Pile	1	0.42	0.42	1 st Translational X
	2	0.42	0.42	1 st Translational Y
	3	3.09	3.11	2 nd Translational Y
Pile-Group & Cap	1	0.42	0.42	1 st Translational X
	2	0.42	0.42	1 st Translational Y
	3	3.10	2.80	2 nd Translational Y
Anchored Spread	1	0.42	0.42	1 st Translational X
	2	0.42	0.42	1 st Translational Y
	3	3.10	3.11	2 nd Translational Y

Table 15. Natural frequencies and mode shapes of the 5 MW structure

Foundation Type	Mode	Frequency (Hz)		Mode Shape
		K-Model	Explicit	
None	1	0.23		1 st Translational X
	2	0.23		1 st Translational Y
	3	1.51		2 nd Translational Y
Spread	1	0.23	0.22	1 st Translational X
	2	0.23	0.22	1 st Translational Y
	3	1.43	1.41	2 nd Translational Y
Mono-Pile	1	0.23	0.22	1 st Translational X
	2	0.23	0.23	1 st Translational Y
	3	1.42	1.39	2 nd Translational Y
Pile-Group & Cap	1	0.23	0.22	1 st Translational X
	2	0.23	0.23	1 st Translational Y
	3	1.42	1.36	2 nd Translational Y
Anchored Spread	1	0.22	0.22	1 st Translational X
	2	0.23	0.23	1 st Translational Y
	3	1.32	1.32	2 nd Translational Y

Transient Analysis

Parametric transient analysis is performed using generalized HHT- α method with a time step size of 0.02 second. The analyses are performed using horizontal component of Landers earthquake with a damping value of 1.0%. In all analyses, the measured response is in the direction of the earthquake load component. For each analysis, complete transient analyses response is given in Appendix. Horizontal component of the Landers earthquake is first applied in the X direction and acceleration response at top of the nacelle is measured. The analysis is then repeated for the Y direction. Figure 46 gives

the acceleration response at top of the nacelle in the X direction for 1 MW turbine with K soil and different foundation types. Table 16 summarizes the peak acceleration and deformation response at top of the nacelle and the maximum von Mises stress at tower base for all models. Complete transient analyses response is given in Appendix.

Table 16. Peak acceleration and deformation response at top of the nacelle and maximum von Mises stress at tower base for 1 MW system with K soil and different foundation types

Foundation Type	a_{\max} (g)		δ_{\max} (mm)		σ_{\max} (MPa)	
	X	Y	X	Y	X	Y
None (Fixed-base)	0.203	0.199	119	119	47	48
Spread	0.225	0.216	126	126	29	28
Mono pile	0.229	0.219	124	125	30	28
Pile group & cap	0.226	0.217	129	127	30	28
Anchored spread	0.226	0.219	131	128	31	28

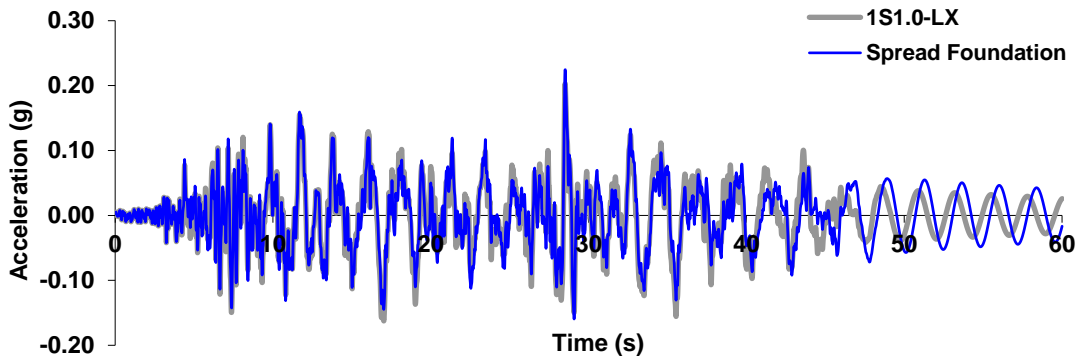


Figure 46. Comparison of acceleration response at top of the nacelle in the X direction for 1 MW system with K soil and different foundation types

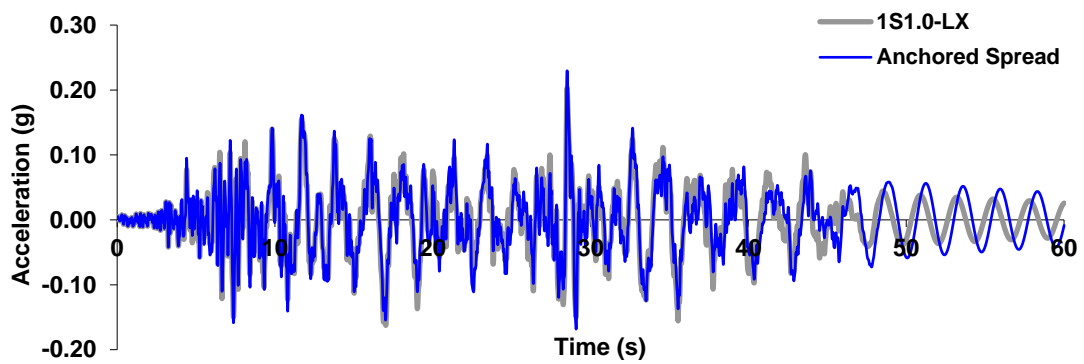
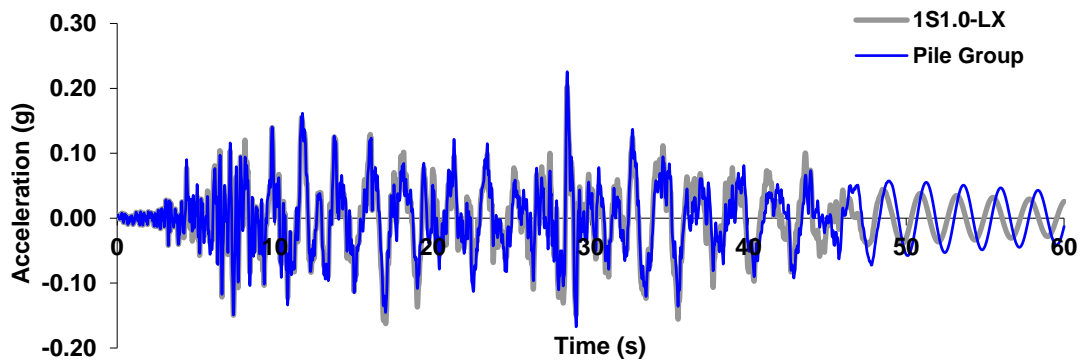
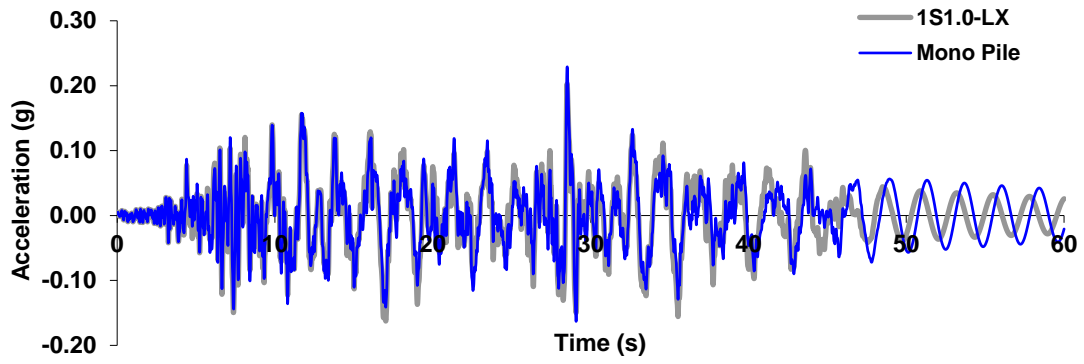


Figure 46 cont.

CHAPTER 6

RESULTS

This chapter categorizes the results of finite element analyses from Chapter 4 and 5 into six sections. Each section describes the results related to one of the objectives mentioned in Chapter 1.

Damping Effects

To evaluate the effects of damping on the seismic response of wind turbines, a selected set of results from parametric analyses performed in Chapter 4 are studied here. Summary of seismic responses presented in Table 9 are in terms of a_{\max} , δ_{\max} , and σ_{\max} von Mises. To compare the results for different load and turbine sizes, these results should first be normalized. Accelerations are normalized using PGA of corresponding loads. Displacement and stress are normalized using corresponding yield values (δ_y and σ_y). Table 17 lists normalized peak acceleration and deformation response at top of the nacelle and normalized von Mises stress at the tower base.

Table 18 presents the normalized maximum response for Landers earthquake. It's seen that except for acceleration of 1MW turbine in the Y direction, increasing the damping decreases the acceleration, displacement and stress in all turbines and directions. Figure 47 shows a portion of acceleration results for the 1MW turbine in the Y direction, in which acceleration reversal happens from $t=28.26$ s to 28.51 s. It is also observed that changes in the damping ratio has more effect on the acceleration response in the vertical direction compared to horizontal directions. It's because natural

frequencies of the 1MW and 5 MW turbines in the z direction (11.67 and 6.15 Hz) (Table 8) are closer to the frequency of Z component of earthquake (4.2 to 6.59 Hz) (Table 1) and therefore, acceleration response factor, R_a , is sensitive to damping. In the X and Y direction however, the natural frequencies are significantly smaller than the load frequency and the response is less dependent on the damping.

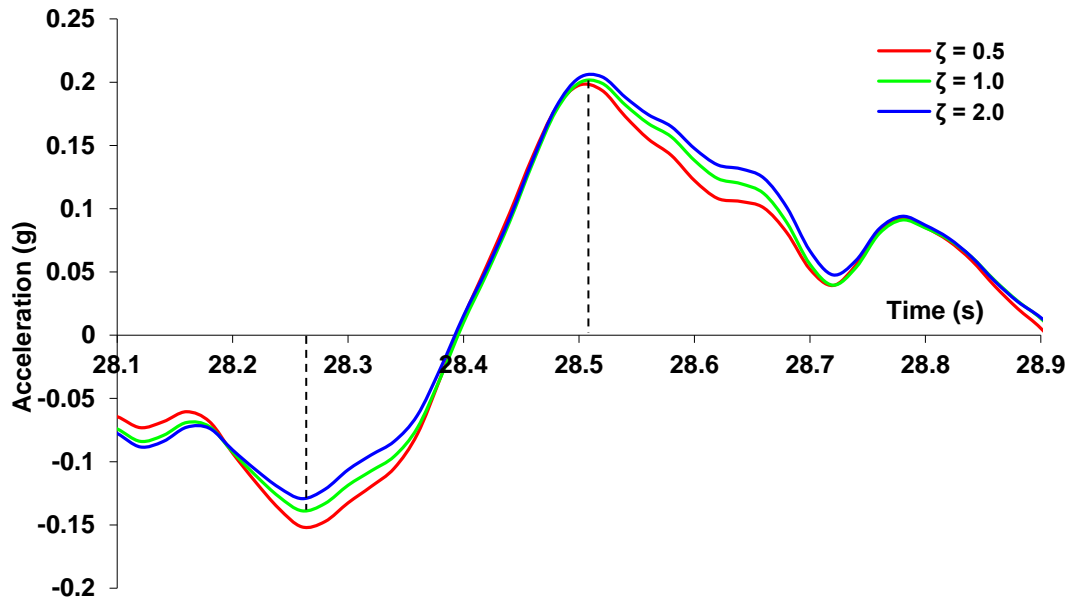


Figure 47. Reversal of acceleration in 1S2.0-L analysis

Table 17. Normalized peak acceleration and deformation response at top of the nacelle, and normalized von Mises stress at tower base for all analyses

Analysis	a_{max} / PGA			δ_{max} / δ_y			σ_{max} / σ_y		
	X	Y	Z	X	Y	Z	X	Y	Z
0.65S0.5-L	2.286	1.948	-	0.223	0.200	-	0.206	0.188	-
0.65S1.0-L	1.844	1.844	-	0.179	0.182	-	0.169	0.170	-
0.65S2.0-L	1.429	1.805	-	0.156	0.163	-	0.149	0.153	-
0.65S1.0-I	-	3.505	-	-	0.451	-	-	0.429	-
0.65S1.0-N	-	2.038	-	-	0.421	-	-	0.382	-
1S0.5-L	1.338	1.286	0.964	0.240	0.240	0.020	0.213	0.211	0.019
1S1.0-L	1.318	1.292	0.641	0.223	0.224	0.015	0.190	0.192	0.014
1S2.0-L	1.325	1.325	0.407	0.214	0.215	0.010	0.179	0.181	0.009
*1S1.0-I	-	2.051	-	-	1.351	-	-	1.216	-
1S1.0-N	-	1.520	-	-	0.441	-	-	0.401	-
5S0.5-L	1.253	1.494	1.784	0.630	0.625	0.035	0.616	0.627	0.043
5S1.0-L	1.227	1.442	1.407	0.573	0.568	0.027	0.544	0.551	0.034
5S2.0-L	1.214	1.344	1.084	0.478	0.474	0.020	0.448	0.455	0.028
*5S1.0-I	-	1.419	-	-	1.695	-	-	1.617	-
5S1.0-N	-	1.177	-	-	0.463	-	-	0.433	-

* Analyses with stress level above yield

Table 18. Effect of damping on normalized acceleration, deformation, and stress
(Landers earthquake)

Analysis	a_{\max}/PGA			δ_{\max}/δ_y			σ_{\max}/σ_y		
	X	Y	Z	X	Y	Z	X	Y	Z
0.65S0.5-L	<u>2.286</u>	<u>1.948</u>	-	<u>0.223</u>	<u>0.200</u>	-	<u>0.206</u>	<u>0.188</u>	-
0.65S1.0-L	1.844	1.844	-	0.179	0.182	-	0.169	0.170	-
0.65S2.0-L	1.429	1.805	-	0.156	0.163	-	0.149	0.153	-
1S0.5-L	<u>1.338</u>	1.286	<u>0.964</u>	<u>0.240</u>	<u>0.240</u>	<u>0.020</u>	<u>0.213</u>	<u>0.211</u>	<u>0.019</u>
1S1.0-L	1.318	1.292	0.641	0.223	0.224	0.015	0.190	0.192	0.014
1S2.0-L	1.325	<u>1.325</u>	0.407	0.214	0.215	0.010	0.179	0.181	0.009
5S0.5-L	<u>1.253</u>	<u>1.494</u>	<u>1.784</u>	<u>0.630</u>	<u>0.625</u>	<u>0.035</u>	<u>0.616</u>	<u>0.627</u>	<u>0.043</u>
5S1.0-L	1.227	1.442	1.407	0.573	0.568	0.027	0.544	0.551	0.034
5S2.0-L	1.214	1.344	1.084	0.478	0.474	0.020	0.448	0.455	0.028

Load Direction Effects

To evaluate the effects of load direction on the seismic response, a selected set of results from parametric analyses are studied here. First, normalized peak acceleration and deformation response at top of the nacelle and normalized von Mises stress at the tower base, given in Table 17, are filtered for Landers earthquake. Results are given in Table 19. For each turbine size, the response corresponding to the direction that has the highest value is underlined. It's seen that for the 1 MW turbine, normalized accelerations in the Z direction are smaller compared to horizontal directions. This is due to the fact the first natural frequency of the turbine and fundamental earthquake frequency are further from each other in the Z direction. In case of displacement and stress, Z direction has significantly lower values compared to X and Y directions. This is due to higher stiffness in the Z direction relative to X and Y directions. Horizontal

displacement and stress values are very close in X and Y directions for 1 MW and 5 MW turbines due to similarity of fundamental modes. For 65 kW turbine with 0.5% damping however, X direction has higher displacement and stress values. For acceleration, response of the 1 MW turbine is almost the same in the X and Y directions. For the 5 MW turbine, acceleration is greater in the Y direction compared to X. For 65 kW turbine, increasing the damping shifts the critical response from X direction to the Y direction. In the Z direction, both 1 MW and 5 MW turbines have significant accelerations. Acceleration in the Z direction is even higher than horizontal directions for 5 MW turbine with 0.5% damping ratio.

Table 19. Effect of load direction on normalized acceleration, deformation and stress (Landers earthquake)

Analysis	a_{max}/PGA			δ_{max}/δ_y			σ_{max}/σ_y		
	X	Y	Z	X	Y	Z	X	Y	Z
0.65S0.5-L	<u>2.286</u>	1.948	-	<u>0.223</u>	0.200	-	<u>0.206</u>	0.188	-
0.65S1.0-L	1.844	1.844	-	0.179	0.182	-	0.169	0.170	-
0.65S2.0-L	1.429	<u>1.805</u>	-	0.156	0.163	-	0.149	0.153	-
1S0.5-L	1.338	1.286	0.964	0.240	0.240	0.020	0.213	0.211	0.019
1S1.0-L	1.318	1.292	0.641	0.223	0.224	0.015	0.190	0.192	0.014
1S2.0-L	1.325	1.325	0.407	0.214	0.215	0.010	0.179	0.181	0.009
5S0.5-L	1.253	1.494	<u>1.784</u>	0.630	0.625	0.035	0.616	0.627	0.043
5S1.0-L	1.227	<u>1.442</u>	1.407	0.573	0.568	0.027	0.544	0.551	0.034
5S2.0-L	1.214	<u>1.344</u>	1.084	0.478	0.474	0.020	0.448	0.455	0.028

Resonance and Load Frequency Effects

To evaluate the effects of load properties and resonance on the seismic response, a selected set of results from parametric analyses are studied here. First, normalized peak acceleration and deformation response at top of the nacelle and

normalized von Mises stress at the tower base, given in Table 17, are filtered in Y direction for 1 MW and 5 MW turbines with 1% damping. The results are given in Table 20. Earthquake loads considered are Landers, Imperial Valley, and Northridge. This is to compare the resonance effect for different loads; one with similar dominant frequency as the natural mode of the structure, and the other one with a higher PGA. It's observed that responses are more critical under the Imperial Valley load for all turbines. Since Imperial Valley's PGA is less than Northridge, it is obvious that load frequency amplitudes can affect the response more than its PGA. In other words, depending on the load properties, resonance in wind turbines is possible. Figure 48 gives load amplitude vs. frequency for Landers, Imperial Valley, and Northridge earthquakes. First natural mode of 1 MW and 5 MW turbines are also shown in Figure 48. It's observed that the amplitude factor corresponding to the first natural mode of these turbines, is highest for Imperial Valley load.

Table 20. Effect of earthquake load properties (1% damping)

Turbine	1 st Freq. (Hz)	Earthquake Load			Transient Response		
		Y component	PGA (g)	Dominant Freq. (Hz)	a_{max} (g)	δ_{max}/δ_y	σ_{max}/σ_y
1S1.0	0.43	Landers	0.154	0.85	0.199	0.224	0.192
		Imperial Valley	0.313	0.59	<u>0.642</u>	<u>1.351</u>	<u>1.216</u>
		Northridge	0.344	1.06	0.523	0.441	0.401
5S1.0	0.23	Landers	0.154	0.85	0.222	0.568	0.551
		Imperial Valley	0.313	0.59	<u>0.444</u>	<u>1.695</u>	<u>1.617</u>
		Northridge	0.344	1.06	0.405	0.463	0.433

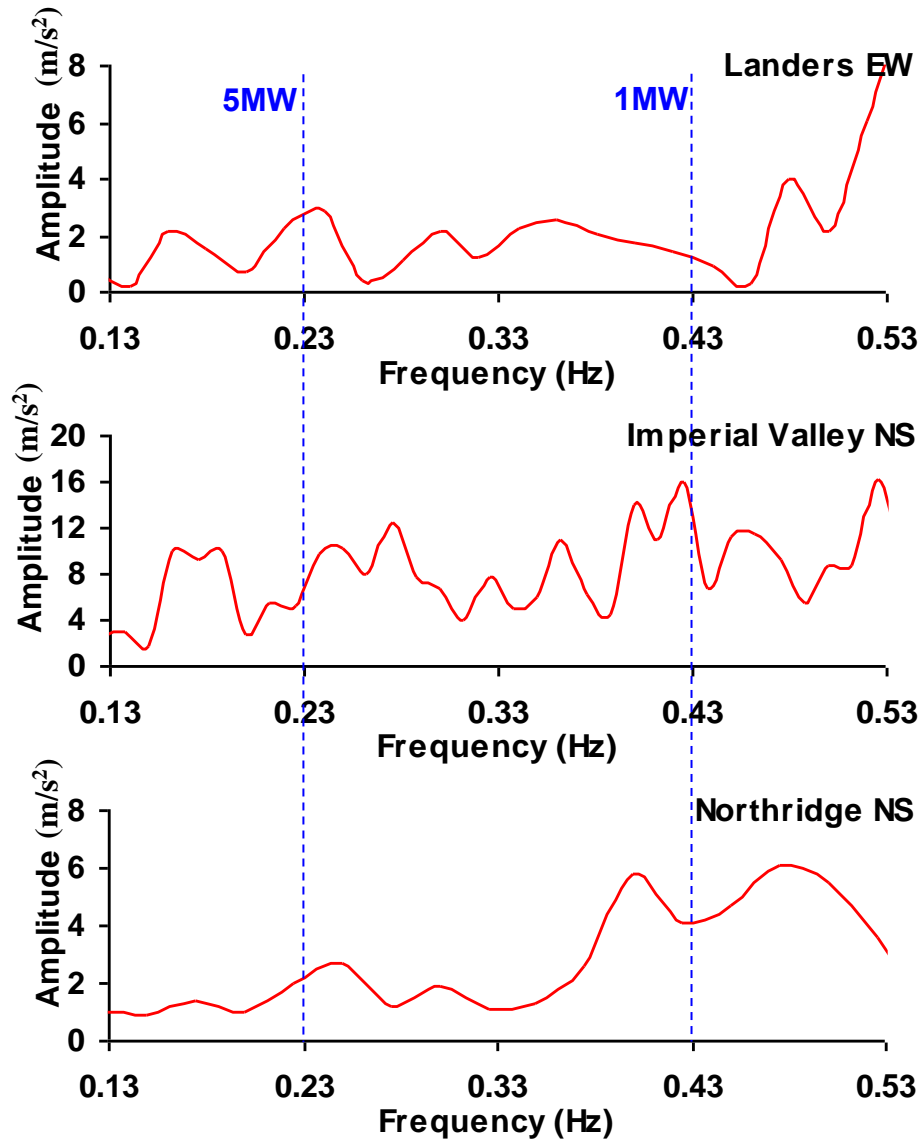


Figure 48. Amplitude vs. frequency for Landers, Imperial Valley, and Northridge loads

Turbine Size Effects

To evaluate the effects of turbine size on the seismic response, a selected set of results from parametric analyses are studied here. First, normalized peak acceleration and deformation response at top of the nacelle and normalized von Mises stress at the tower base, given in Table 17, are filtered for Landers earthquake. Results are given in

Table 21. It's observed that increasing the turbine size decreases the acceleration in the X direction for all damping values. In the Y direction however, acceleration at top of the 1 MW turbine is the lowest and 65 kW has the highest acceleration values. In the vertical direction, the 5 MW turbine has highest acceleration values. In case of normalized displacement and stress, values increase in all directions when increasing the size.

Table 21. Response comparison for different turbine sizes (Landers earthquake)

Analysis	a_{max}/PGA			δ_{max}/δ_y			σ_{max}/σ_y		
	X	Y	Z	X	Y	Z	X	Y	Z
0.65S0.5-L	<u>2.286</u>	<u>1.948</u>	-	0.223	0.200	-	0.206	0.188	-
0.65S1.0-L	<u>1.844</u>	<u>1.844</u>	-	0.179	0.182	-	0.169	0.170	-
0.65S2.0-L	<u>1.429</u>	<u>1.805</u>	-	0.156	0.163	-	0.149	0.153	-
1S0.5-L	1.338	1.286	0.964	0.240	0.240	0.020	0.213	0.211	0.019
1S1.0-L	1.318	1.292	0.641	0.223	0.224	0.015	0.190	0.192	0.014
1S2.0-L	1.325	1.325	0.407	0.214	0.215	0.010	0.179	0.181	0.009
5S0.5-L	1.253	1.494	<u>1.784</u>	<u>0.630</u>	<u>0.625</u>	<u>0.035</u>	<u>0.616</u>	<u>0.627</u>	<u>0.043</u>
5S1.0-L	1.227	1.442	<u>1.407</u>	<u>0.573</u>	<u>0.568</u>	<u>0.027</u>	<u>0.544</u>	<u>0.551</u>	<u>0.034</u>
5S2.0-L	1.214	1.344	<u>1.084</u>	<u>0.478</u>	<u>0.474</u>	<u>0.020</u>	<u>0.448</u>	<u>0.455</u>	<u>0.028</u>

Soil-Structure Interaction Effects

To evaluate the effects of soil-structure interaction on the seismic response of wind turbines, a selected set of results from parametric analyses performed in Chapter 5 are studied here. From results of modal analyses presented in Table 13,

Table 14, and Table 15 it is observed that adding soil and foundation has decreased the first and second natural frequency of the model with 65 kW turbine. This is due to the fact that fixed base towers have no rotation and therefore stiffer than the models with soil and foundation. In the model with 1 MW and 5 MW turbines, this change is small. Adding the soil and foundation is found to have more effect on the third natural frequency for all turbine sizes. This effect however, depends on the type of soil model and foundation used in the analysis. For 65 kW turbines, adding a spread foundation with explicit soil, causes the mode shape of third natural frequency to shift from second translational mode in the Y direction to first translational mode in the Z direction. This shift in the mode shapes wasn't seen in other analyses. Next, a comparison is made between natural frequencies of 65 kW, 1 MW, and 5 MW systems based on their soil models and foundation types. Figure 49 compares the first natural frequency of 65 kW turbine systems for different soil model and foundation types. The first natural frequency of reference fixed-base model is also given in Figure 49. For the 1 MW and 5 MW systems, the first natural frequencies are similar for all foundation types and soil models in Table 14 and Table 15.

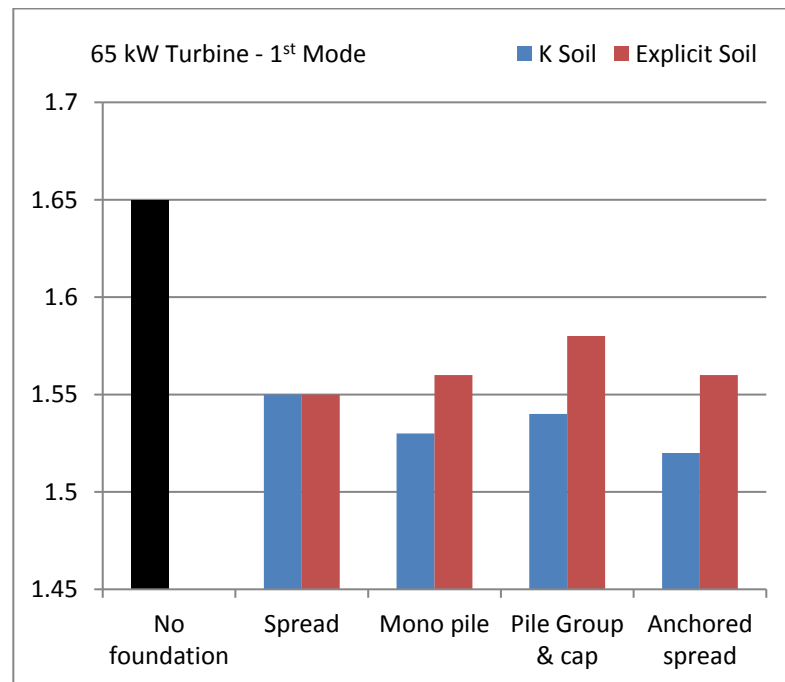


Figure 49. First natural frequency (Hz) of 65 kW system

Figure 50 compares the second natural frequency of 65 kW system for different soil model and foundation types. It is seen that K-models have higher second natural frequencies compared to explicit models. Among different types of foundations, pile group & cap have the highest second natural frequency and spread foundations have the lowest. Maximum overall difference between second natural frequencies is only 3.6%. In case of third natural frequency however, soil model and foundation types have a significant effect.

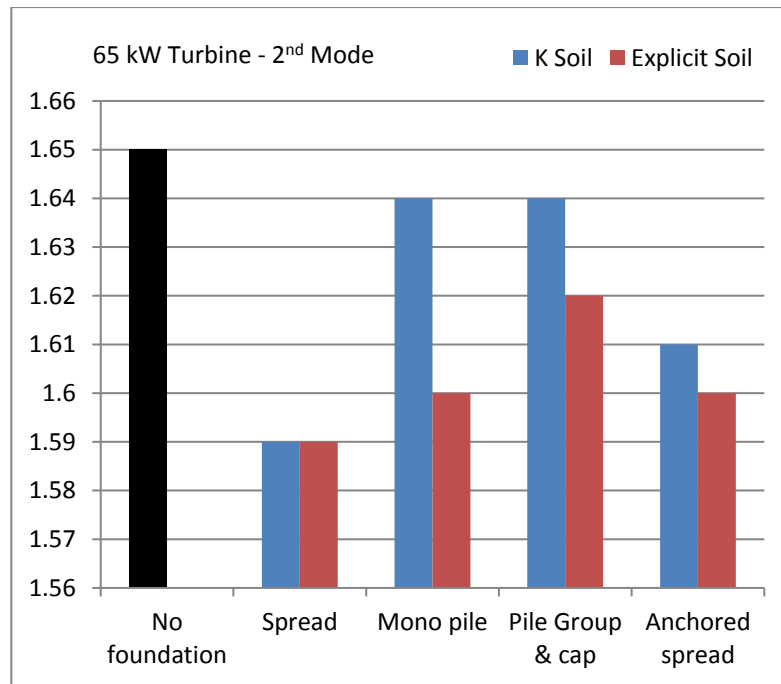


Figure 50. Second natural frequency (Hz) of 65 kW system

Figure 51, Figure 52, and Figure 53 compare the third natural frequency of 65 kW, 1 MW, and 5 MW systems for different soil model and foundation types respectively. It is seen that for 65 kW and 1 MW systems with K soil model, the third natural frequency is consistent for all foundation types. For 5 MW system with K soil model however, the third natural frequency of anchored spread foundation is 7-8% lower compared to other foundation types and 13% lower compared to system with no

foundation. In case of 65 kW system with explicit soil, third natural frequencies vary for different foundation types. For 1 MW system with explicit soil, except for pile group & cap foundation, all foundation types have similar frequencies. For 5 MW turbine system with explicit soil, the third natural frequency of anchored spread foundation is 13% lower compared to system with no foundation and other frequencies vary for different foundation types. These differences are partly due to the accuracy of explicit soil model relative to the K model and partly because of different frequency shift that these foundation types cause.

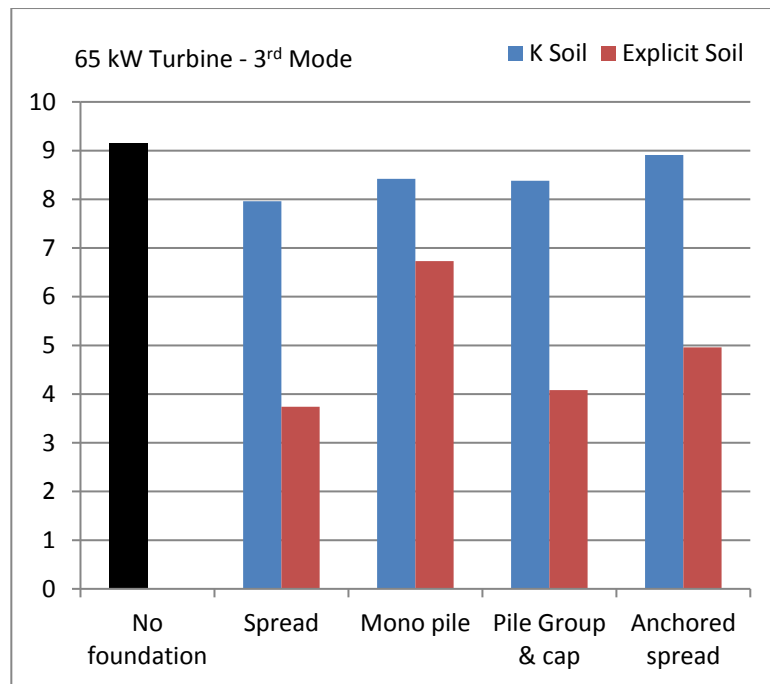


Figure 51. Third natural frequency (Hz) of 65 kW system

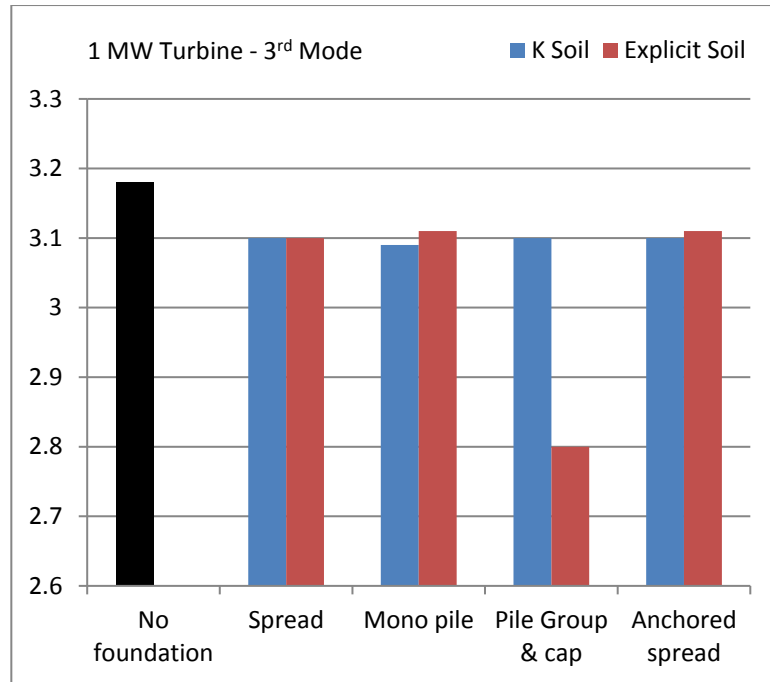


Figure 52. Third natural frequency (Hz) of 1 MW system

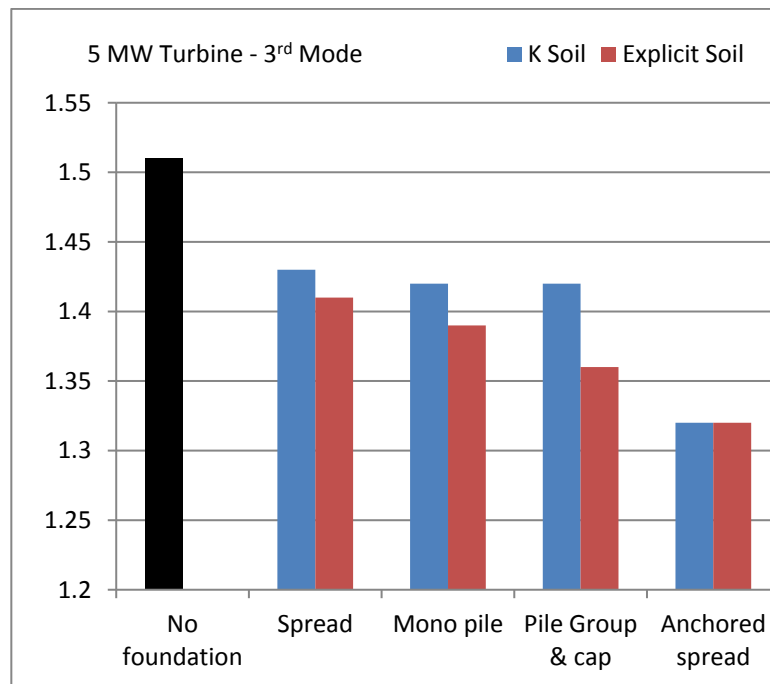


Figure 53. Third natural frequency (Hz) of 5 MW system

From results of transient analyses presented in Table 16, adding the effects of soil and foundation, has caused 8-13% increase in horizontal acceleration at top of the nacelle. Horizontal displacement at top of the nacelle are also increased 4-11%. The

increase is caused by rigid rotation of the foundation. In the X direction horizontal displacement at top of the nacelle is slightly higher. Table 22 lists the ratio of acceleration change for different foundations after foundation is added to the structure.

Table 22. Change in acceleration at top of the 1MW nacelle with soil & foundation

Foundation Type	Acceleration Change		Displacement Change	
	X	Y	X	Y
Spread	11%	8%	6%	6%
Mono pile	13%	10%	4%	5%
Pile group & cap	11%	9%	9%	6%
Anchored spread	11%	10%	11%	7%

Response Spectrum vs. Transient Analysis

In Chapter 2, a simplified method from IEC 61400 was mentioned in which the earthquake load on a wind turbine could be calculated. In this section, results of transient analyses for the Imperial Valley earthquake are compared to the values calculated using IEC 61400 method.

IEC 61400 recommended procedure includes the following steps:

1. Evaluate or estimate the site and soil conditions required by the relevant local standard.
2. Use the normalized design response spectrum and the seismic hazard-zoning factor to establish the acceleration at the first tower bending eigen-frequency assuming a damping of 1 % of critical damping.
3. Calculate the load for a system subject to the above acceleration in which the total rotor, nacelle, and 50 % of the tower mass is concentrated at the tower head.

Using ASCE 7-10 as the governing code [50]:

DHS is located on stiff soil which is classified as class D, therefore:

$$S_s = 2.26 \text{ g}, S_1 = 0.852 \text{ g}, S_{MS} = 2.26 \text{ g}, S_{M1} = 1.278 \text{ g}, S_{DS} = \frac{2}{3} S_{MS} = 1.506 \text{ g},$$

$$S_{D1} = \frac{2}{3} S_{M1} = 0.852 \text{ g}, T_0 = 0.2 S_{D1}/S_{DS} = 0.113 \text{ s}, \text{ and } T_s = S_{D1}/S_{DS} = 0.566 \text{ s}.$$

In which:

S_s is maximum considered earthquake (MCE) ground motion for 0.2 s spectral response acceleration (5% of critical damping),

S_1 is the mapped MCE spectral response acceleration at a period of 1 s (5% critical damping),

S_{MS} is the MCE spectral response acceleration at short periods adjusted for site class D (5% of critical damping),

S_{M1} is the MCE spectral response acceleration at a period of 1 s adjusted for site class D (5% of critical damping),

S_{DS} is the design spectral response acceleration parameter at short periods (5% of critical damping),

S_{D1} is the design spectral response acceleration parameter at a period of 1 s (5% of critical damping).

Design spectrum curve is constructed using the following formula:

$$T < T_0 \quad S_a = S_{DS} (0.4 + 0.6 T/T_0)$$

$$T_0 < T < T_s \quad S_a = S_{DS}$$

$$T_s < T < T_L \quad S_a = S_{D1}/T$$

$$T_L < T \quad S_a = S_{D1} T_L / T^2$$

The design spectrum for DHS (Desert Hot Springs station) is given in Figure 54.

From the spectrum, for 65 kW turbine with first period $T_1 = 0.61$ s, the 5% damped design spectral response acceleration is $S_5 = 1.506$ g. Similarly, for 1 MW turbine with $T_1 = 2.33$ s, $S_5 = 0.178$ g and for 5 MW turbine with $T_1 = 4.35$ s, $S_5 = 0.051$ g. Considering the 1% damping value suggested by IEC 61400, design spectrum should be scaled. This is achieved using the damping adjustment factor B [60]:

$$S_x = \frac{S_5}{B}$$

in which S_x is adjusted spectral acceleration and S_5 is the 5% damped spectral acceleration. Based on the recommended values, B for 1% damping is 0.75 therefore:

$$S_1 = \frac{S_5}{0.75}$$

Accelerations based on IEC 61400 design spectrum and transient methods are given in Table 23. Maximum moment demands from both methods are calculated and results are given in Table 24. Comparing the moment demand values for these two methods shows the IEC 61400 method is conservative for 65 kW and 1 MW turbines but underestimates the moment demand for 5 MW turbine. Considering that IEC assumes 1% damping, for smaller damping values the results will be underestimated even more.

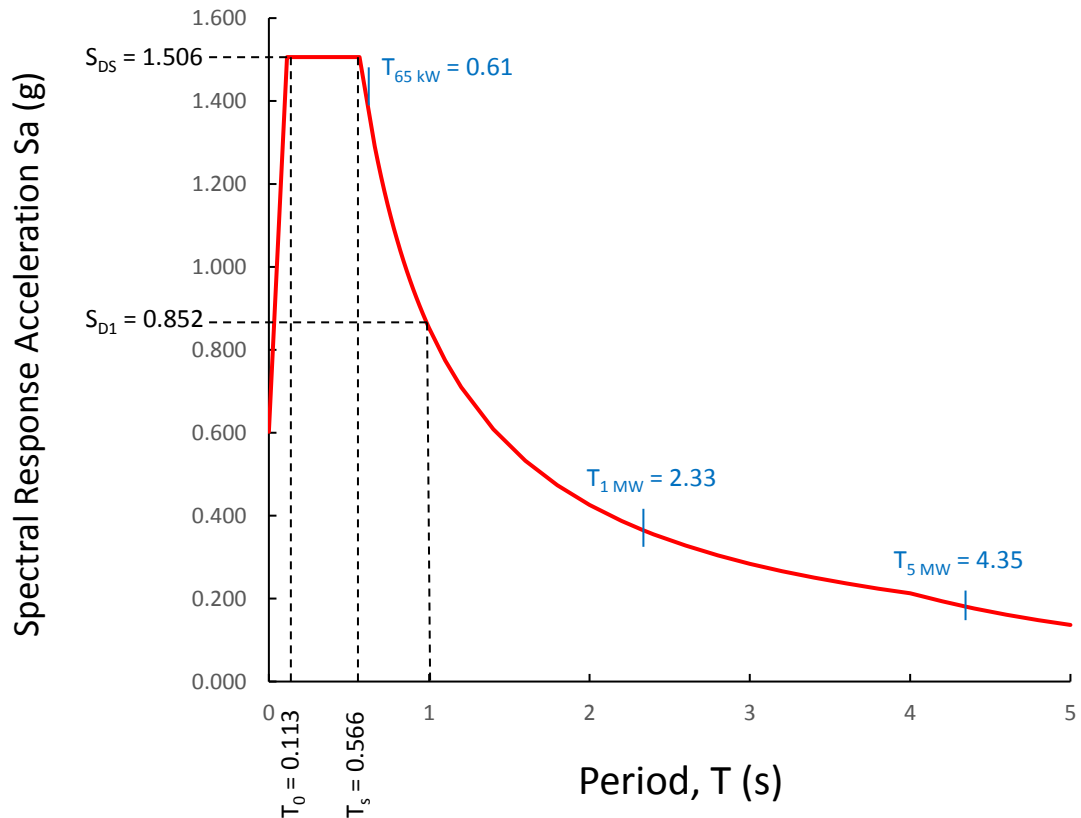


Figure 54. ASCE 7-10 design spectrum for DHS (stiff soil) (5% damping)

Table 23. Accelerations based on IEC 61400 design spectrum and transient methods

Turbine	1 st Frequency (Hz)	T ₁ (s)	Acceleration (g)		
			ASCE 5% damping	IEC 61400 S _a 1% damping	Transient a _{max} 1% damping
65 kW	1.65	0.61	1.398	1.864	0.284
1 MW	0.43	2.33	0.366	0.488	0.203
5 MW	0.23	4.35	0.180	0.240	0.222

Table 24. Moment demands based on IEC 61400 design spectrum and transient analysis

Turbine	Hub Height m (ft)	Concentrated Force kN (kip)	Moment Demand kN.m (kip.ft)	
			IEC 61400	Transient
65 kW	22.60 (74.1)	192 (43)	4,339 (3,186)	239 (176)
1 MW	61.14 (200.6)	314 (71)	19,198 (14,243)	11,725 (8,648)
5 MW	90.00 (295.3)	349 (78)	31,410 (23,033)	69,206 (51,044)

By interpolating the moment demand values, we can see that for values above 22,200 kN.m (16,348 kip), IEC 61400 predicts lower demands compared to FEA. Based on this three point case study, we can suggest the use of IEC 61400 for moment demands up to 22,200 kN.m (16,348 kip). Table 24 shows that the given IEC 61400 spectrum is not consistent with values from transient analysis. It's obvious that this underestimation can be addressed by first looking at the accuracy of current simplified lumped mass method, which can ignore the effects of higher structural modes which are important in the bigger turbines. Also, design spectrums specifically designed for wind turbines can be developed. Finally, a lower damping value can be proposed which can increase the calculated demand value.

CHAPTER 7

SUMMARY AND CONCLUSION

Summary

Current design concepts and their limitations were presented in Chapter 1 and Chapter 2. Chapter 1 presented a background in seismic analysis and outlined some of the existing problems in the field. It also defined scope and objectives of this research. A review of existing guidelines and articles on the seismic design of wind turbines was presented in chapter 2. It was discussed that displacement, acceleration, stress value, shear and moment demands were the basic design parameters. It was also discussed that wind turbine design goals are to provide enough strength capacity for the structure, while separating its operational and structural frequencies. Then theoretical formulations associated with time and frequency domain methods were presented in chapter 3. Using results of an experimental shake table on an industrial scale wind turbine, a finite element model was validated in chapter 4. Seismic response of wind turbines with different capacities was then analyzed and effect of different design parameters including damping, load direction, natural frequencies, and size was investigated. A comprehensive set of numerical analyses on wind turbines with 65 kW, 1 MW and 5 MW capacities were presented. Time history loads from Imperial Valley (1940), Northridge (1994), and Landers (1992) earthquakes were applied both at the bottom of towers and at the foundation level. The finite element method was used with Generalized HHT- α and Block Lanczos formulations. Finite element model was first validated using experimental test data. Numerical models based on modern wind

turbine designs were built. A parametric study was then performed using time and frequency domain methods to investigate the effects of different design variants. Effects of damping, load direction, load frequency amplitude, turbine capacity, and soil-structure interaction were investigated. In chapter 5, a series of modal and transient finite element analyses were performed on three horizontal axis tubular steel wind turbines towers on four types of foundations and the effects of soil was investigated using two different techniques. In chapter 6, accuracy of the response spectrum method (first mode approximation) suggested by codes was evaluated.

Overall, contributions of this dissertation to the seismic design of wind turbines can be arranged into two categories, design considerations and numerical analysis. In the design category, the accuracy of response spectrum method adopted by the design codes was evaluated for different wind turbine capacities. These results which weren't available before this research, provide a better understanding on the accuracy of this method and can be used as a source to update these codes. In the analysis category, this research adds a body of knowledge to the field of seismic engineering of wind turbines. The results of this category can be used to further study the dynamic behavior of wind turbines under seismic loads.

Conclusion

1. When different damping ratios were used in the transient seismic analysis, it was observed that the acceleration response in the vertical direction was more sensitive to these changes compared to horizontal directions. Therefore, it's recommended that in designing the connection of nacelle and tower for vertical earthquake loads, lower damping ratios be considered.
2. Different earthquake loads were applied in vertical direction and two horizontal directions; parallel and perpendicular to the rotor axis. It was observed that acceleration responses of 65 kW and 1 MW turbines in the horizontal directions were higher compared to vertical direction. It was also observed that for all

turbines, displacement and stress values in the horizontal directions were significantly higher compared to vertical direction. Displacement and stress values were close in both horizontal directions for 1 MW and 5 MW turbines. For 65 kW turbine with lower damping values however, displacement and stress values were higher in the direction parallel to the rotor axis. Acceleration response were similar in the horizontal directions for 1 MW turbine but 5 MW turbine had a higher acceleration response perpendicular to the rotor axis. For 65 kW turbine, increasing the damping shifted the critical response direction from parallel to rotor axis to perpendicular. In the vertical direction, both 1 MW and 5 MW turbines had significant accelerations. For 5 MW turbine with lower damping, vertical acceleration values were even higher than horizontal directions. Considering these findings, it's recommended that for the design of tower and nacelle-tower connection, horizontal earthquake component be considered both parallel and perpendicular to the axis of rotor blades. Maximum stress at the tower base and maximum acceleration at the nacelle level should be calculated in both horizontal directions. Also, because vertical earthquake component can create significant stress in the nacelle-tower connection, it's recommended to be considered in the design especially in larger turbines.

3. Landers, Imperial Valley, and Northridge earthquakes were applied at the tower base. It was observed that responses were significantly higher for the Imperial Valley load for all turbines even though its PGA is less than the Northridge earthquake load. Considering the proximity of the natural frequency of the structure and load, it's concluded that wind turbine natural frequency can be close enough to earthquake frequencies to cause resonance. Therefore, it's recommended to separate natural frequencies from both operational and load frequencies.
4. For different wind turbine sizes, it was observed that increasing the size decreased the acceleration in the direction parallel to the rotor axis for all damping values. In the direction perpendicular to the rotor axis however,

acceleration at top of the smallest tower had the highest values. In vertical direction, the largest turbine saw the highest acceleration values. Normalized displacement at the nacelle level and stress values at the tower base increased in all directions when turbine size increased. On the other hand, horizontal forces in the nacelle-tower connection were independent of turbine size and could be high even in smaller wind turbines. This study recommends to include horizontal forces in the design of connections even for small wind turbines.

5. Parametric study of the soil-structure interaction was performed on three wind turbine capacities. Turbines were modeled with a fixed base, also with four types of foundation; circular spread foundation, mono piles, pile groups with cap, and anchored spread foundations. Modal analysis results showed that including soil and foundation lowered the first and second natural frequencies of the model with 65 kW turbine but had minimal effect on those of the 1 MW and 5 MW turbines. For the third natural frequency however, adding the soil and foundation affected all models and depended on the type of soil model and foundation; for 65 KW turbines, adding a spread foundation with explicit soil, caused the mode shape of third natural frequency to shift from second translational in the horizontal direction perpendicular to the rotor axis to first translational mode in the vertical direction. A comparison was also made between natural frequencies of systems based on their soil models and foundation types. It was observed that systems with explicit soil had lower first frequencies compared to the models with K-model soil. For the 1 MW and 5 MW systems, the first natural frequencies were similar for all foundation types and soil models. For the second natural frequency of 65 kW, it was observed that K-models had higher second natural frequencies compared to explicit models. Among different types of foundations, pile group & cap had slightly higher second natural frequency and spread foundations had the lowest. For third natural frequency, soil model and foundation types had more effects. In the transient analyses, adding the effects of soil and foundation increased horizontal

acceleration and displacement at top of the nacelle. The increased displacement was mostly caused by the rigid rotation of the foundation and was slightly higher in the direction parallel to the rotor axis. This study concludes that for wind turbines that have a frequency-based foundation design, the soil can be modeled faster and easier using the K-model.

6. Based on IEC 61400, design spectral response accelerations were first calculated for all turbine sizes. Then maximum moment demands were compared for IEC 61400 and transient analyses methods. The results showed that IEC 61400 values were conservative for small wind turbines. For larger turbines however, the maximum demand suggested by IEC 61400 were smaller than what was seen in the transient method. This is a significant finding considering that size of modern wind turbines is increasing and they are being installed more frequently in seismic regions. This suggests the need for reevaluation of the current design standards for wind turbines. Based on this three point case study, we suggest the use of IEC 61400 for moment demands up to 22,200 kN.m (16,348 kip).

APPENDIX A
TRANSIENT ANALYSIS DATA FOR WIND TURBINES
WITHOUT FOUNDATIONS

65kW Tower

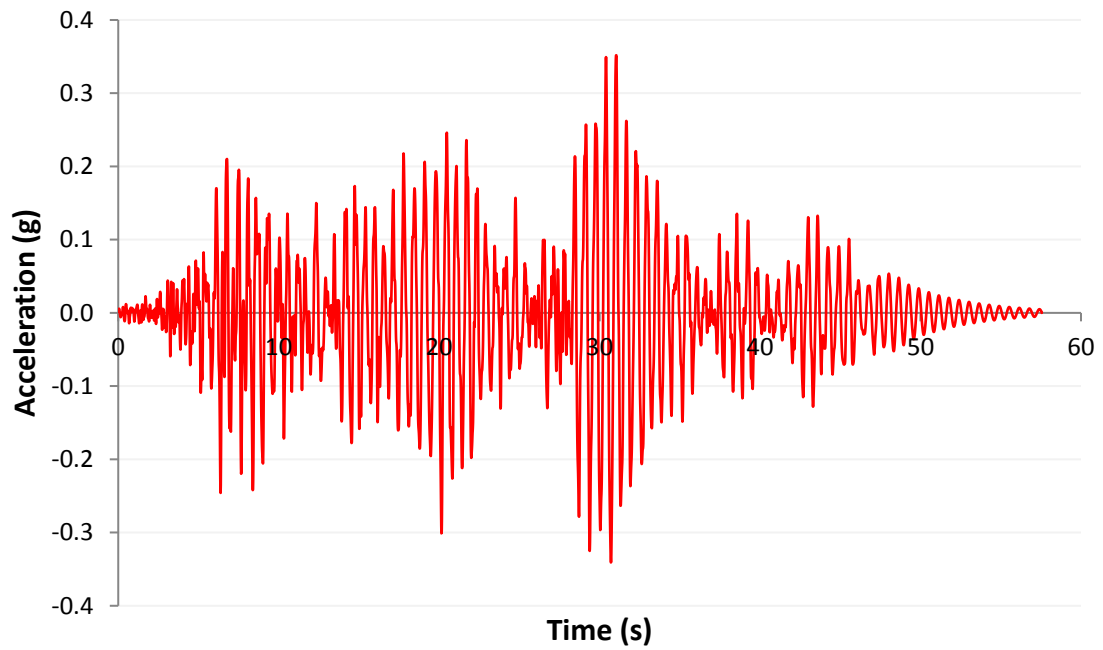


Figure A1. 0.65S0.5-LX acceleration

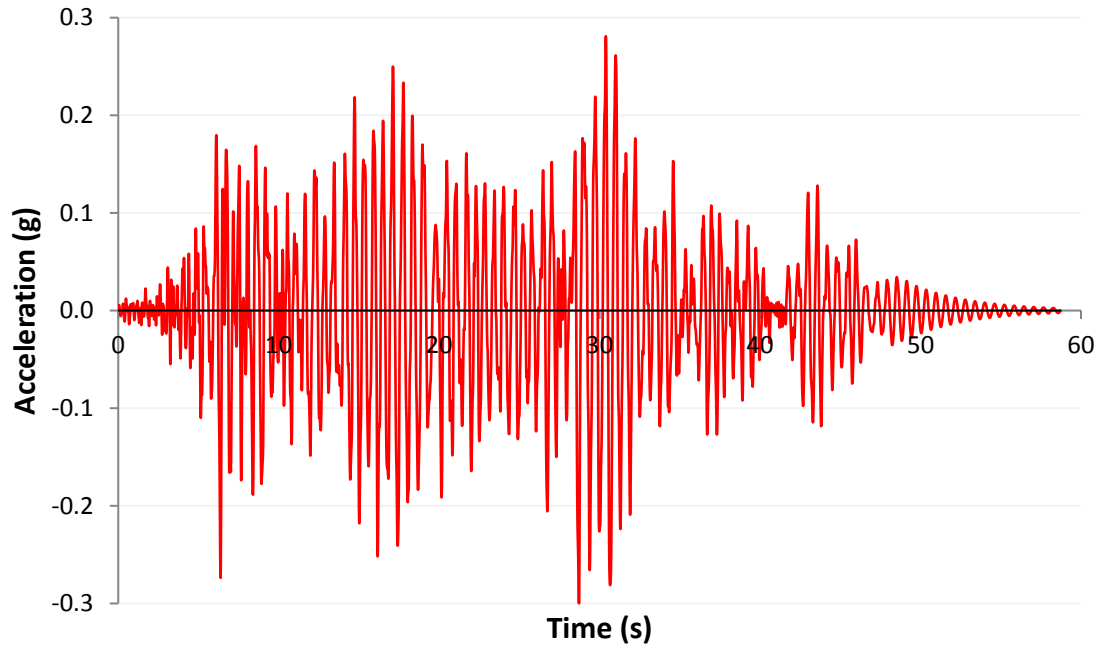


Figure A2. 0.65S0.5-LY acceleration

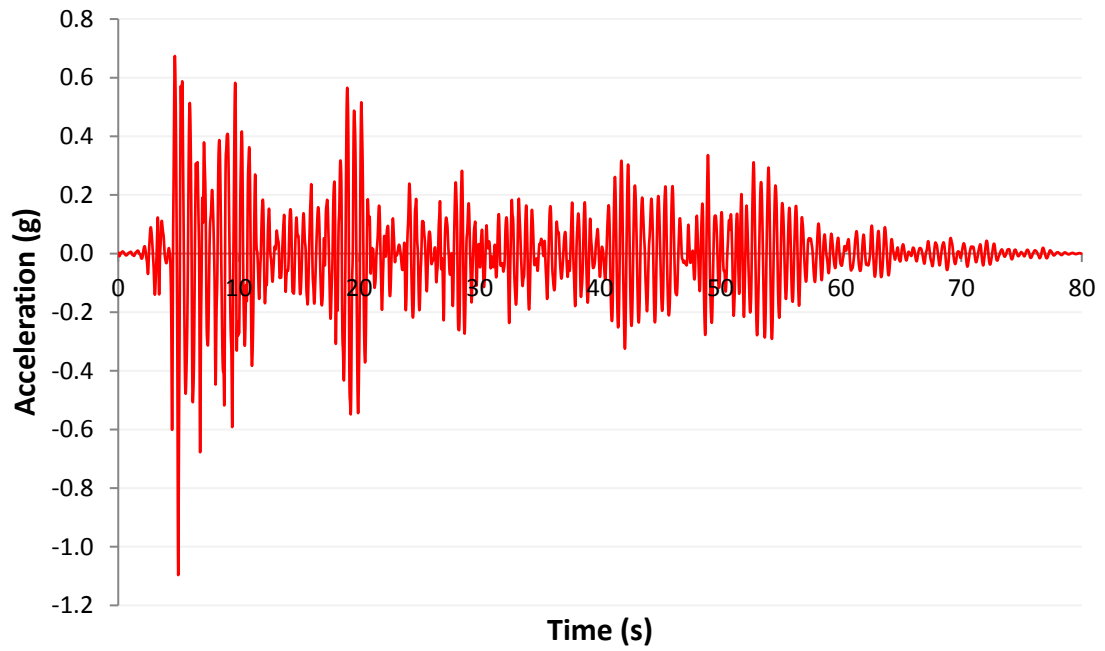


Figure A3. 0.65S1.0-IY acceleration

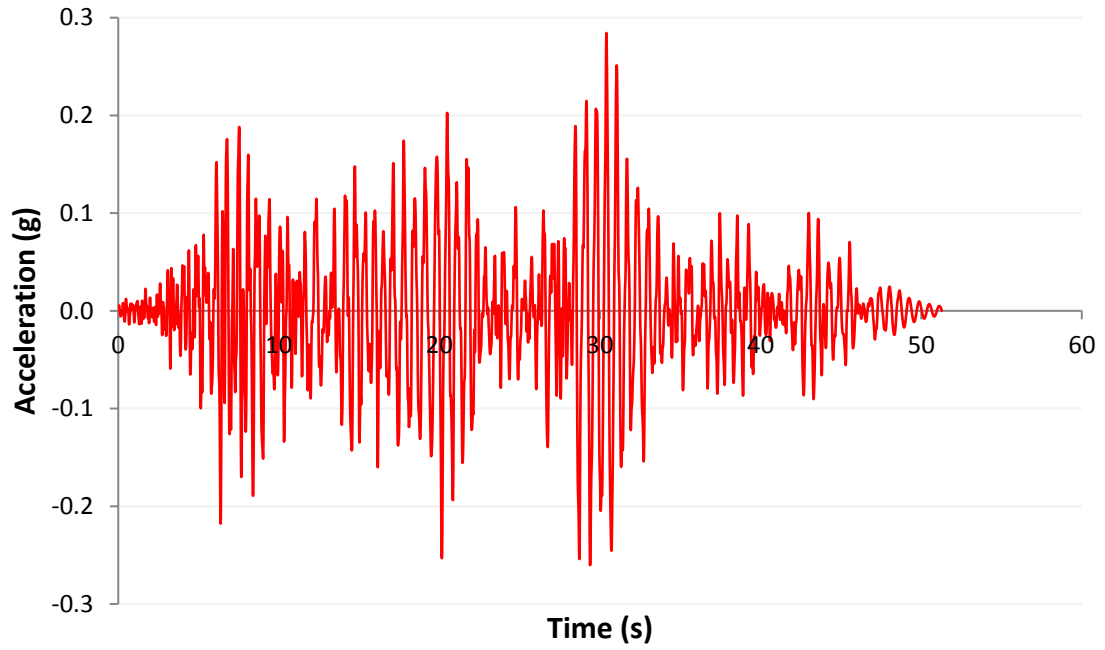


Figure A4. 0.65S1.0-LX acceleration

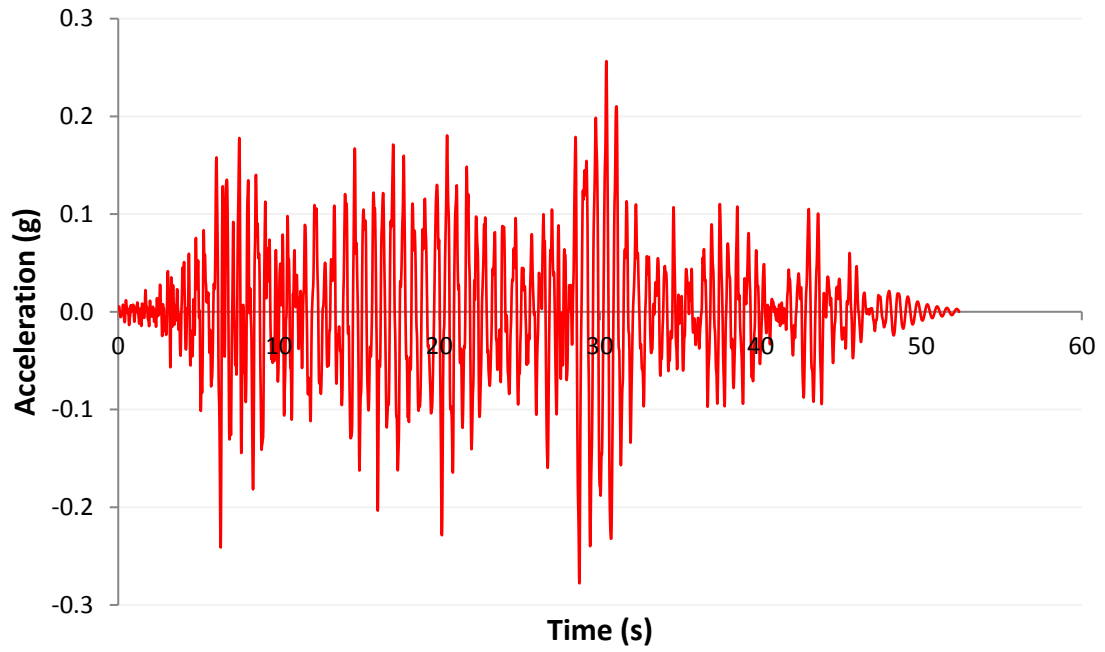


Figure A5. 0.65S1.0-LY acceleration

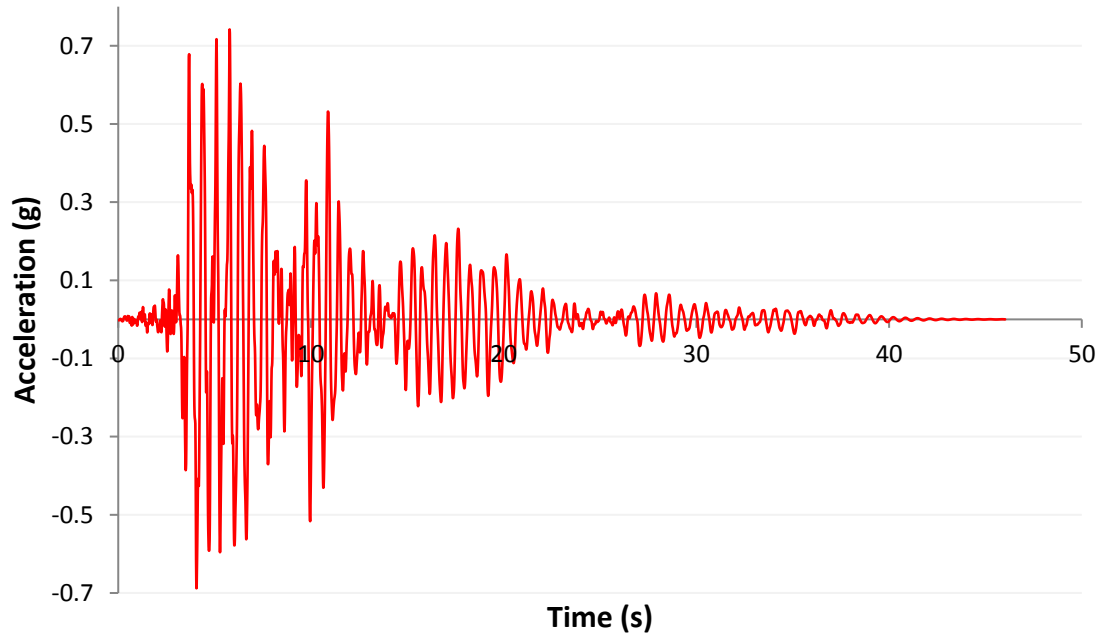


Figure A6. 0.65S1.0-NX acceleration

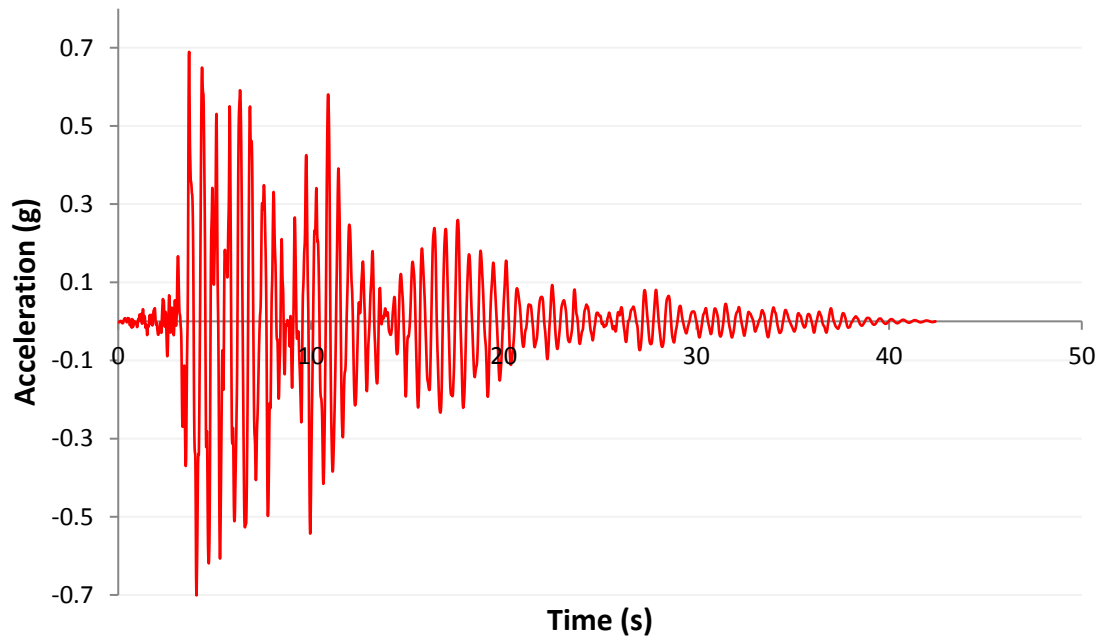


Figure A7. 0.65S1.0-NY acceleration

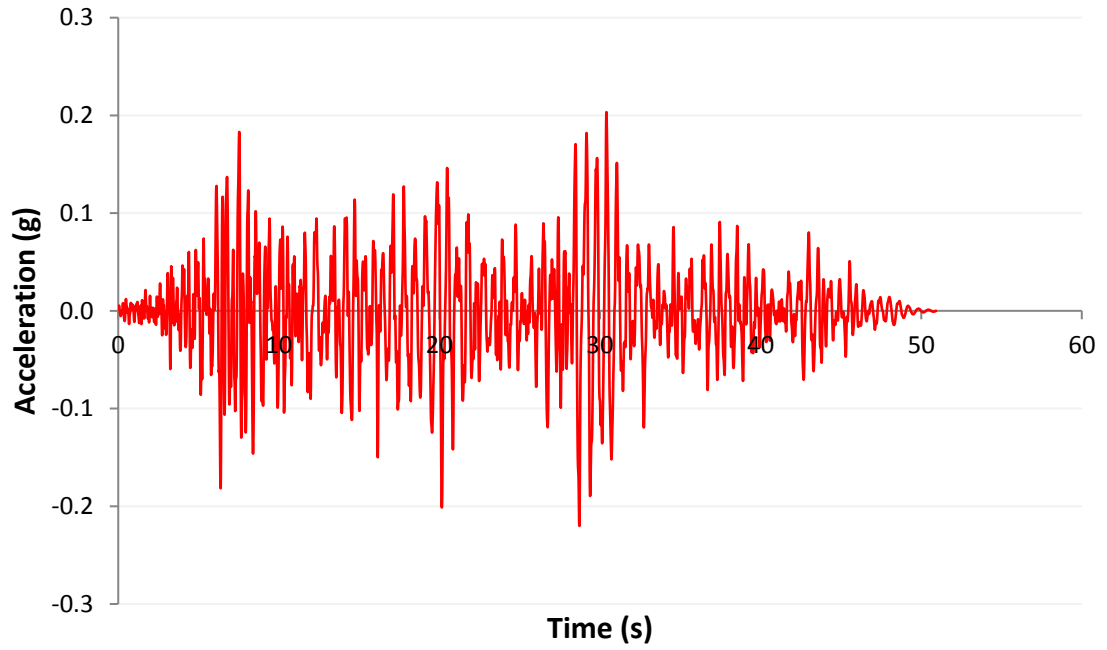


Figure A8. 0.65S2.0-LX acceleration

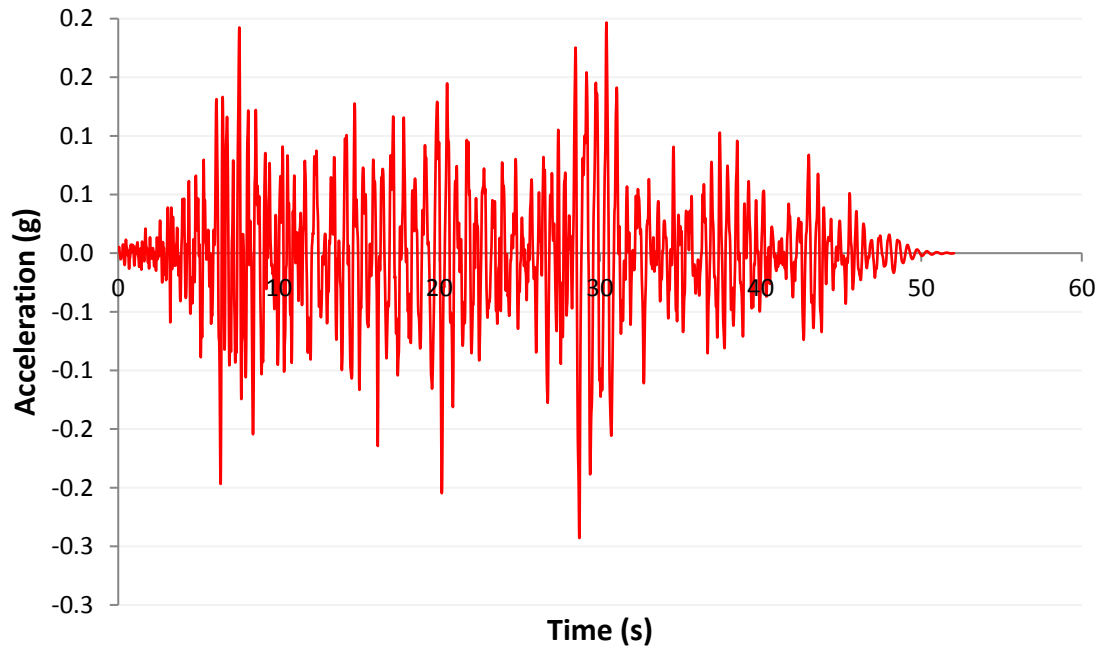


Figure A9. 0.65S2.0-LY acceleration

1MW Tower

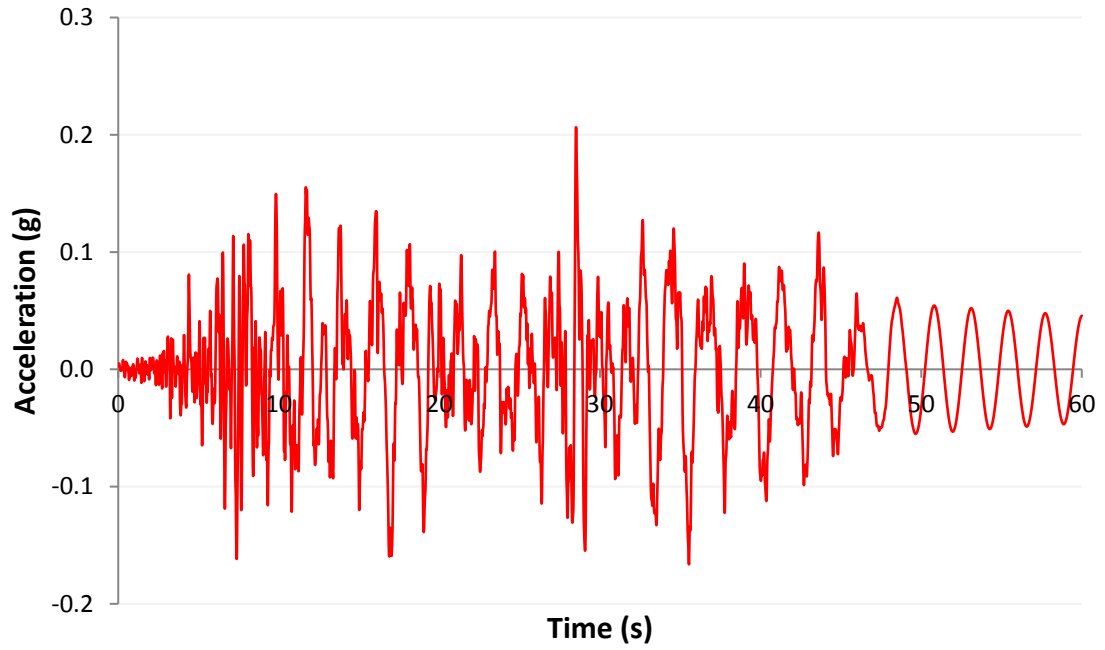


Figure A10. 1S0.5-LX acceleration

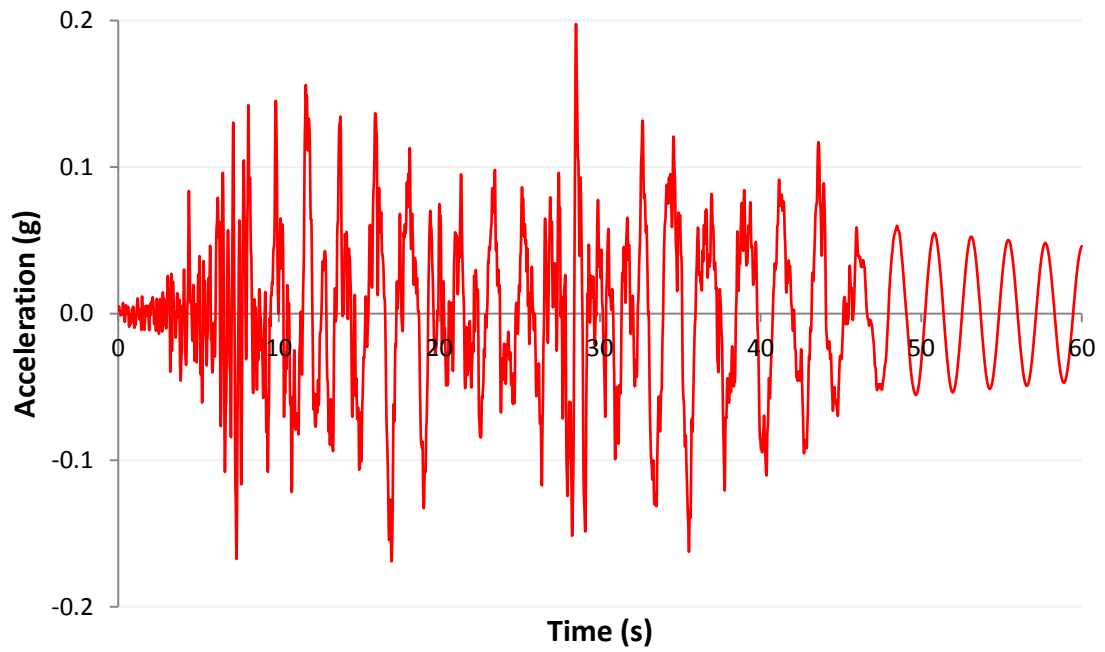


Figure A11. 1S0.5-LY acceleration

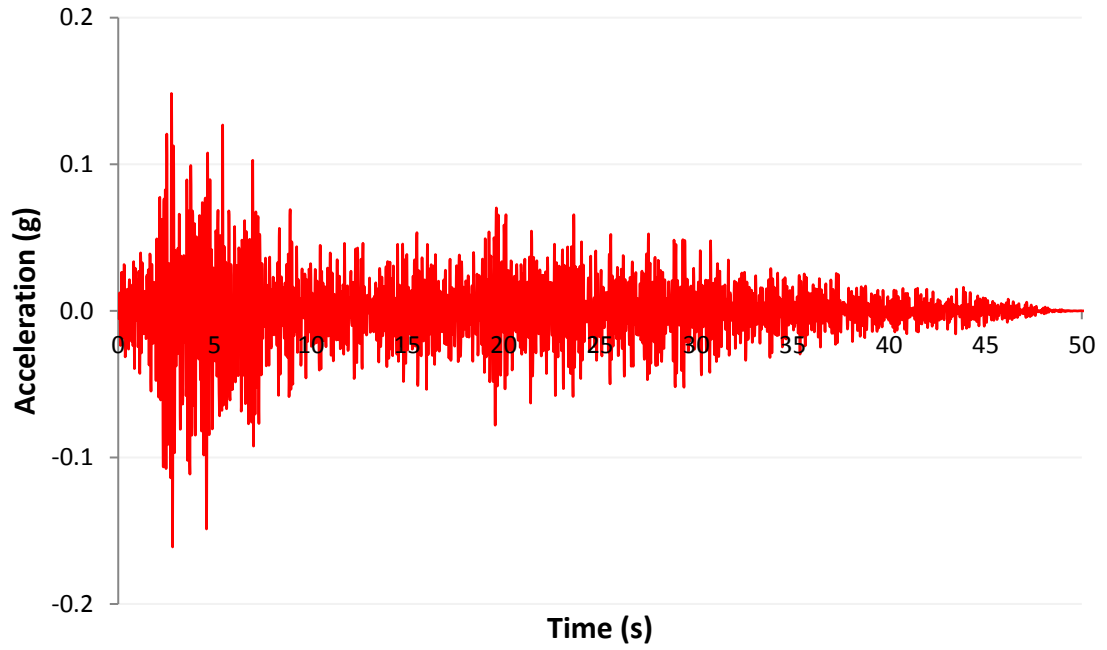


Figure A12. 1S0.5-LZ acceleration

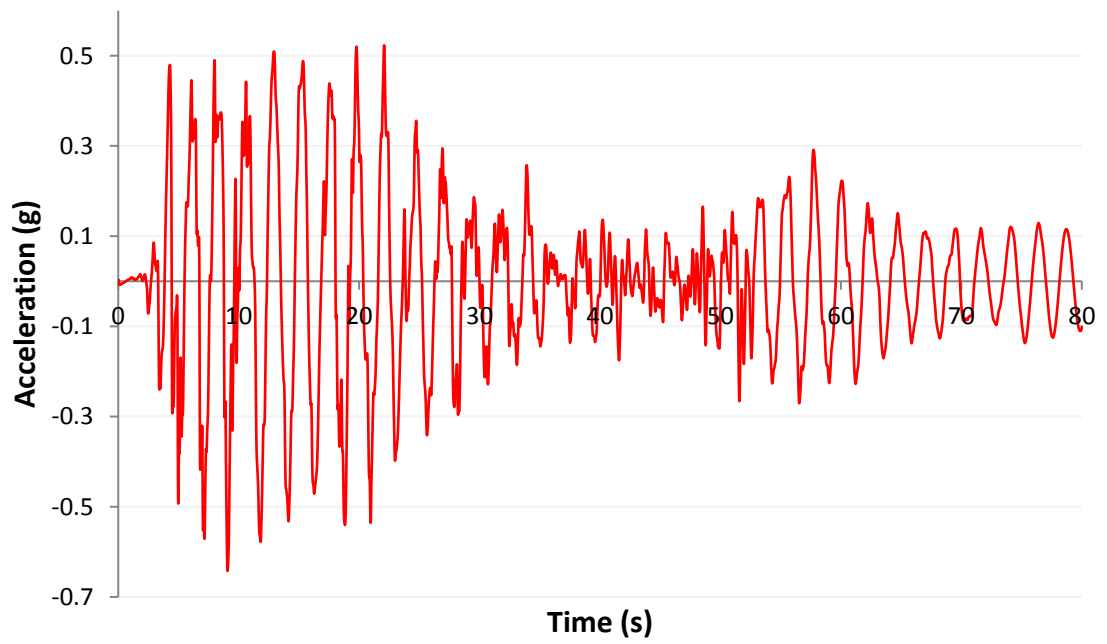


Figure A13. 1S1.0-IY acceleration

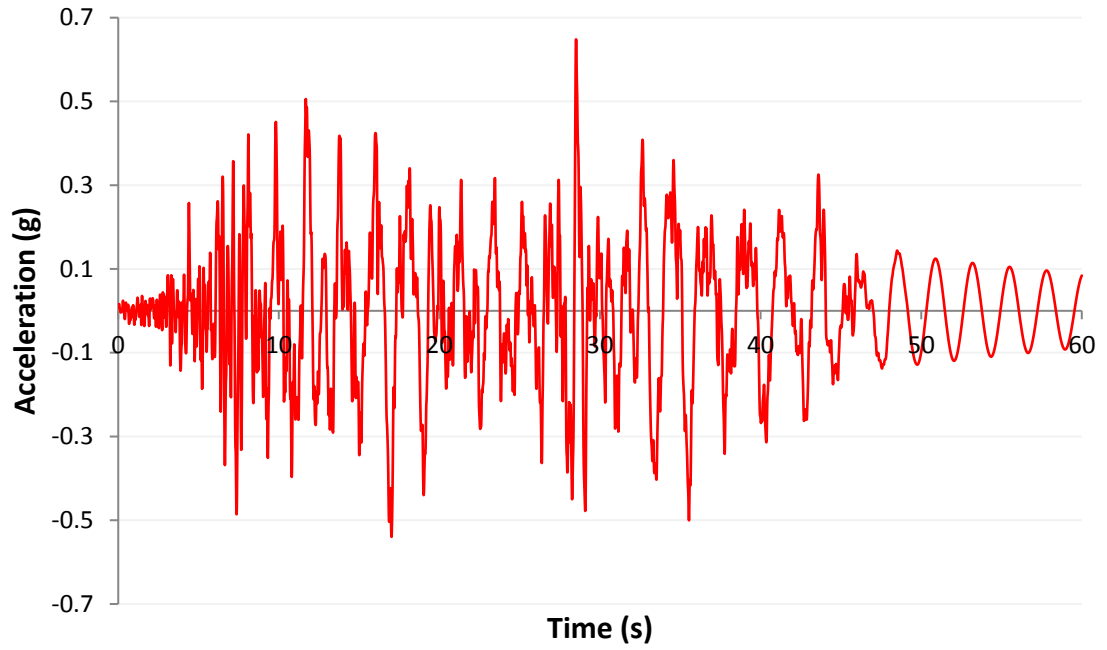


Figure A14. 1S1.0-L0.5Y acceleration

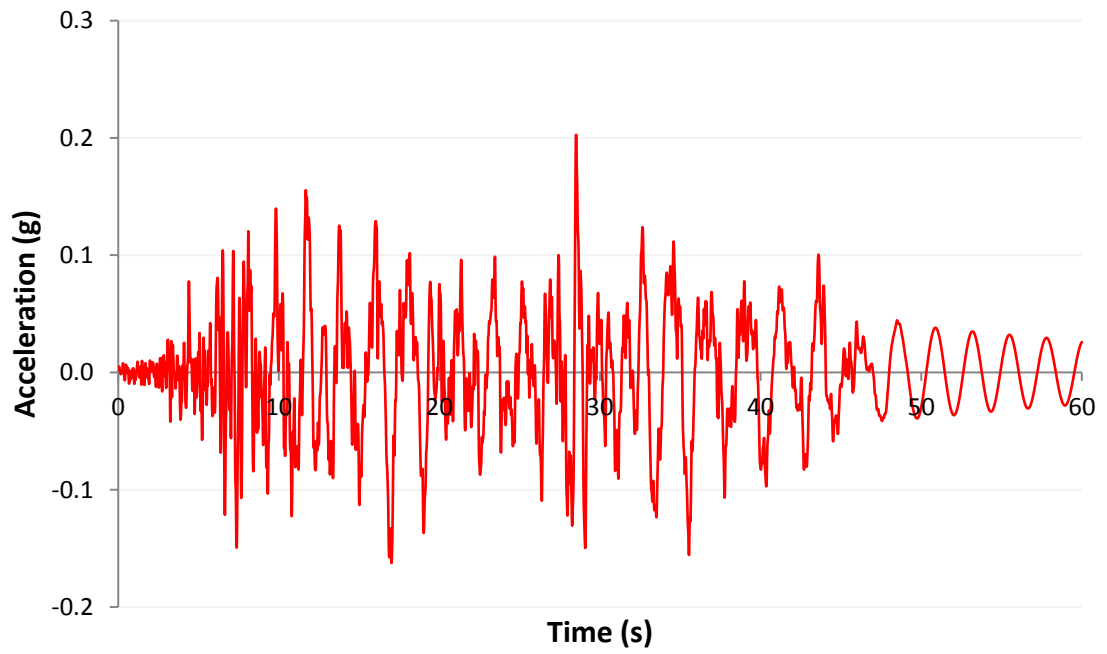


Figure A15. 1S1.0-LX acceleration

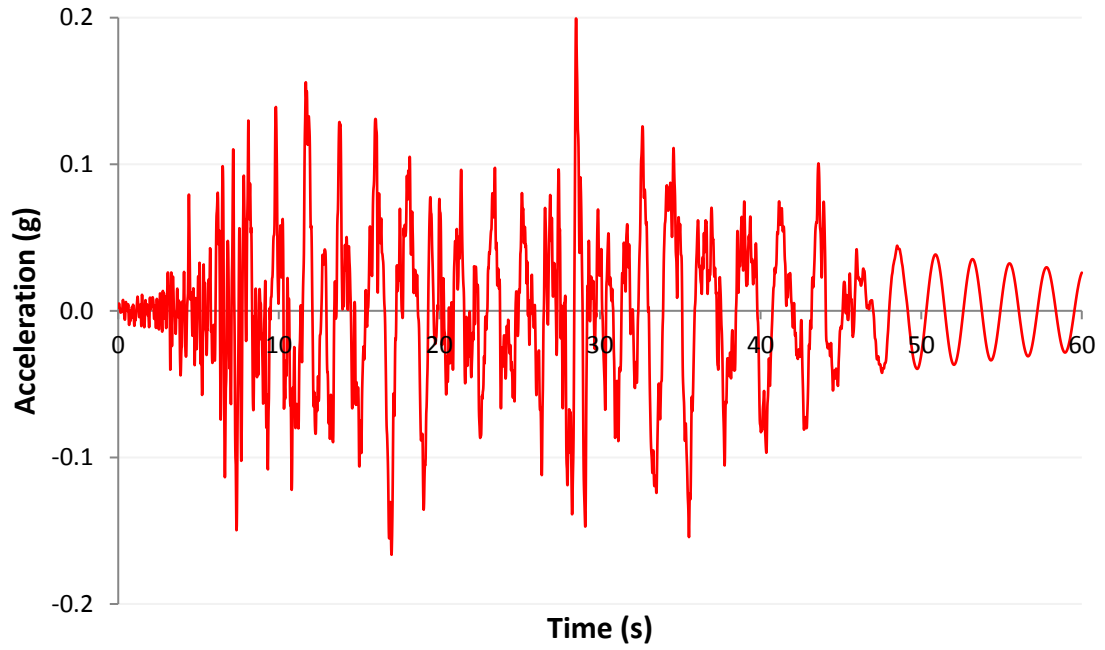


Figure A16. 1S1.0-LY acceleration

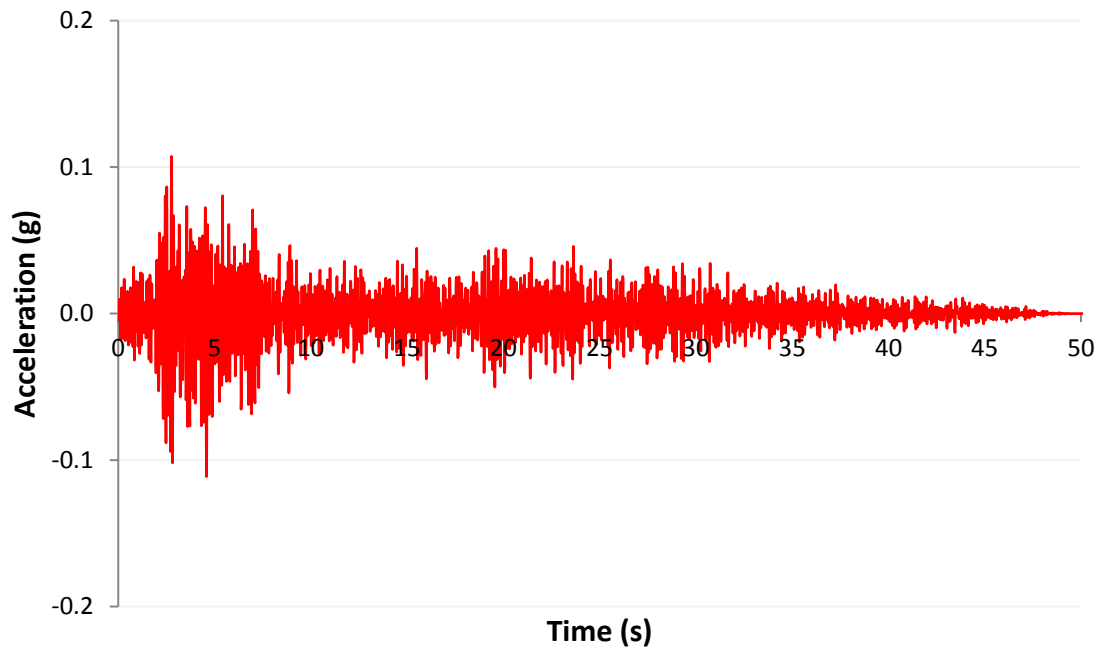


Figure A17. 1S1.0-LZ acceleration

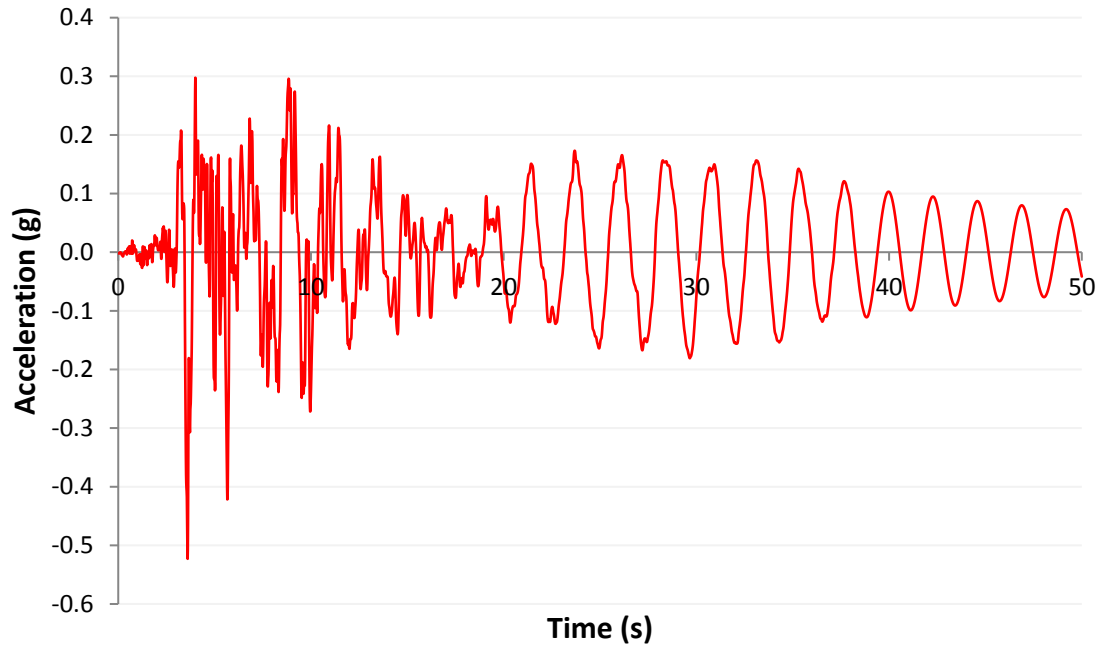


Figure A18. 1S1.0-NY acceleration

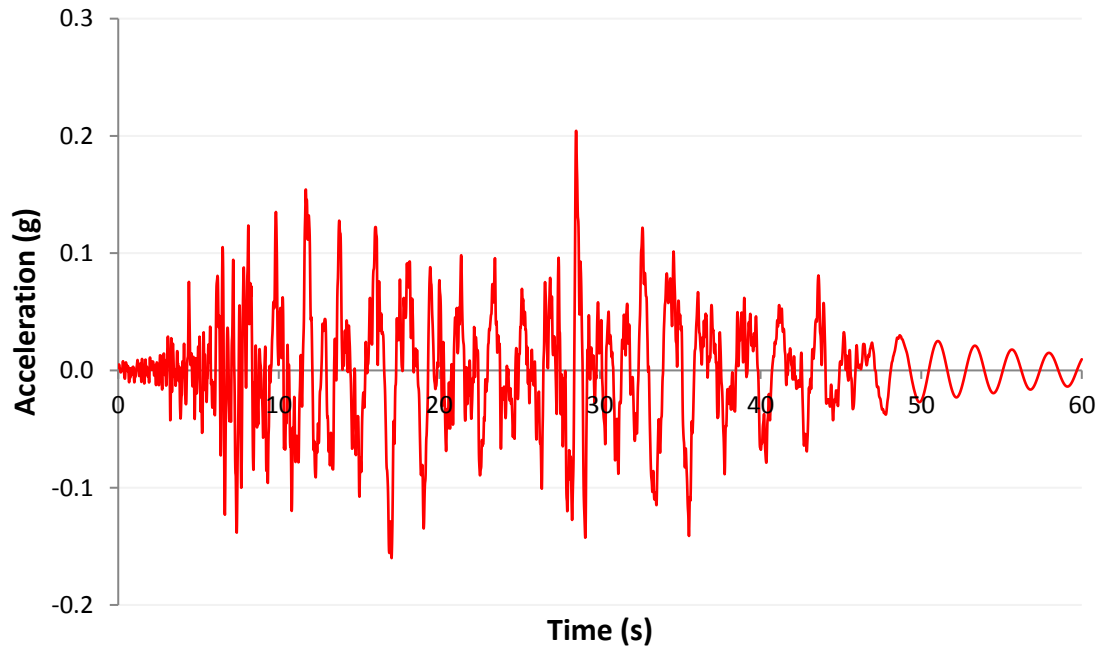


Figure A19. 1S2.0-LX acceleration

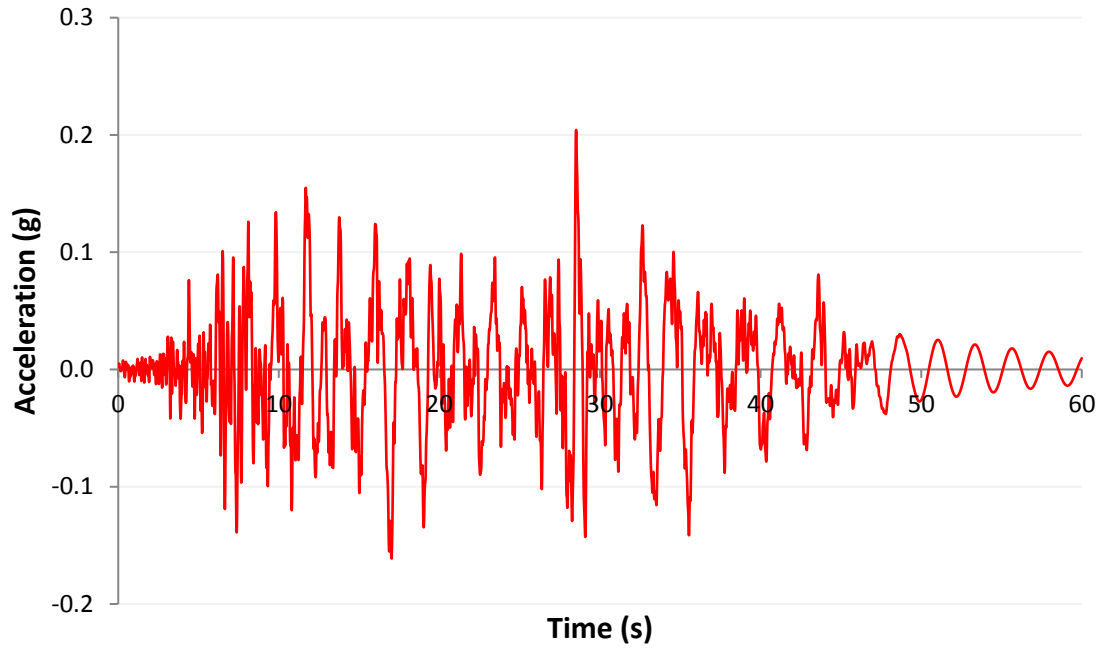


Figure A20. 1S2.0-LY acceleration

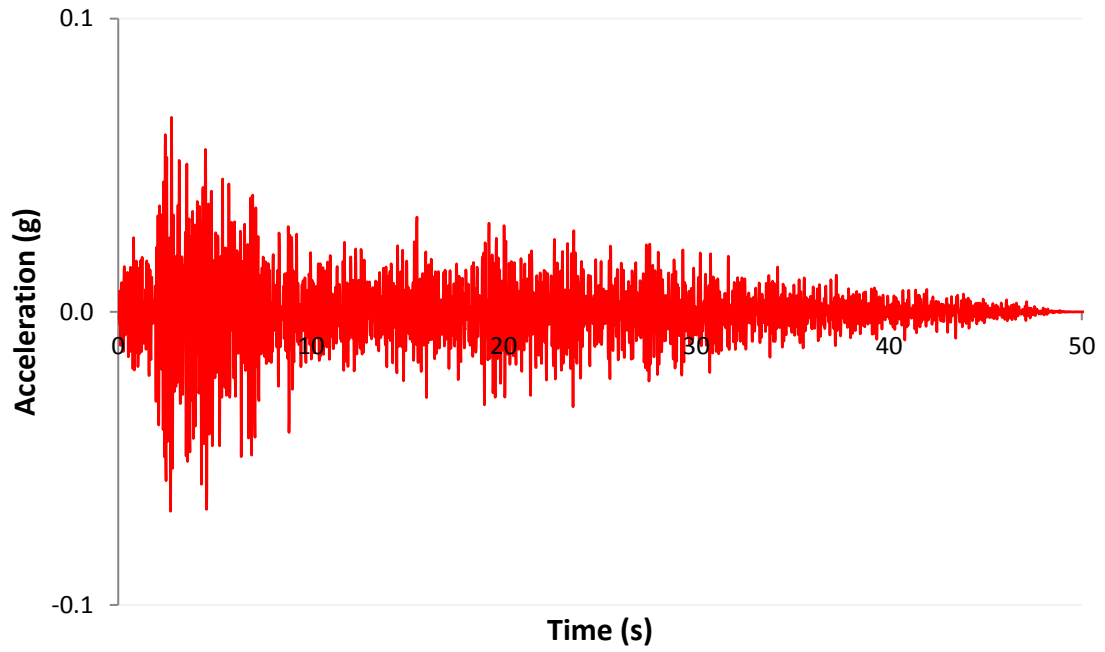


Figure A21. 1S2.0-LZ ACCELERATION

5MW TOWER

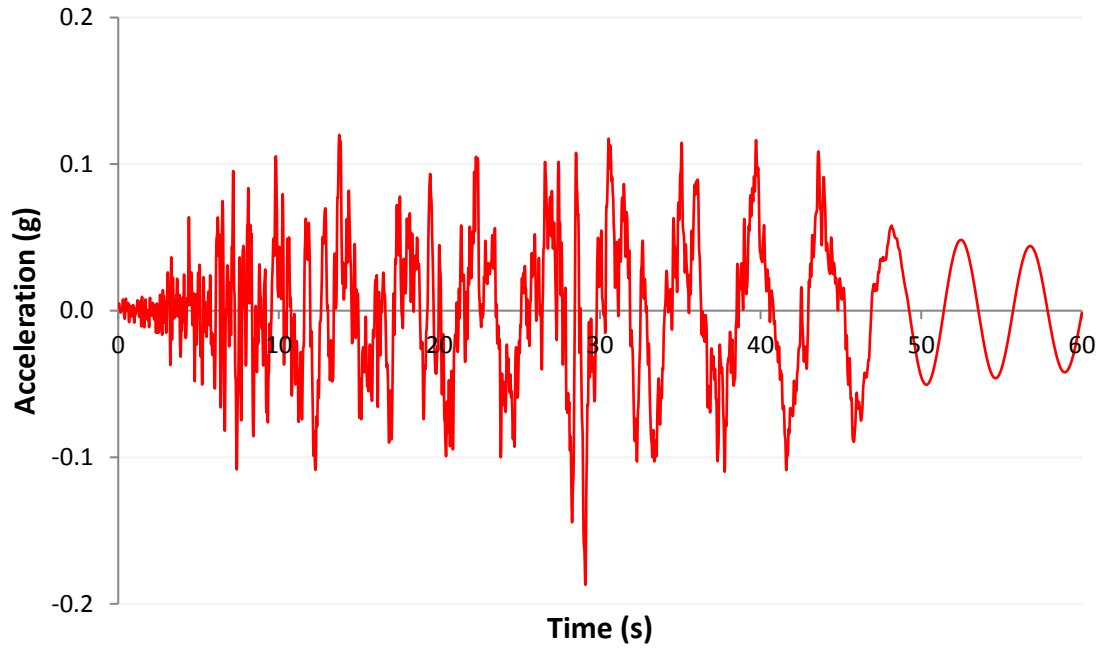


Figure A22. 5S0.5-LX acceleration

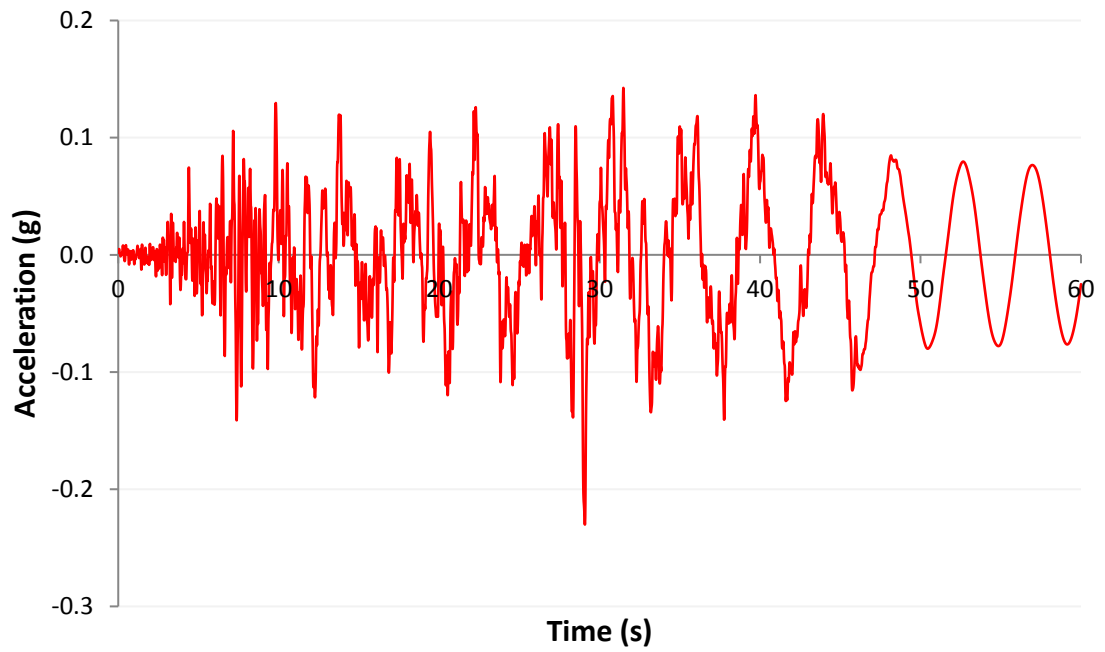


Figure A23. 5S0.5-LY acceleration

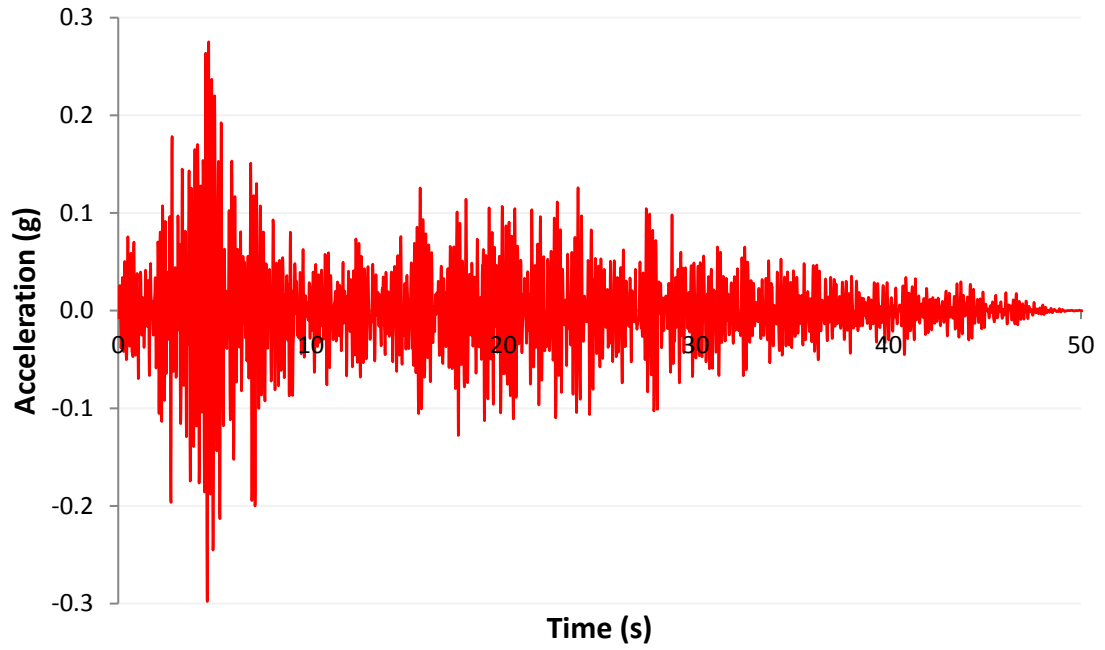


Figure A24. 5S0.5-LZ acceleration

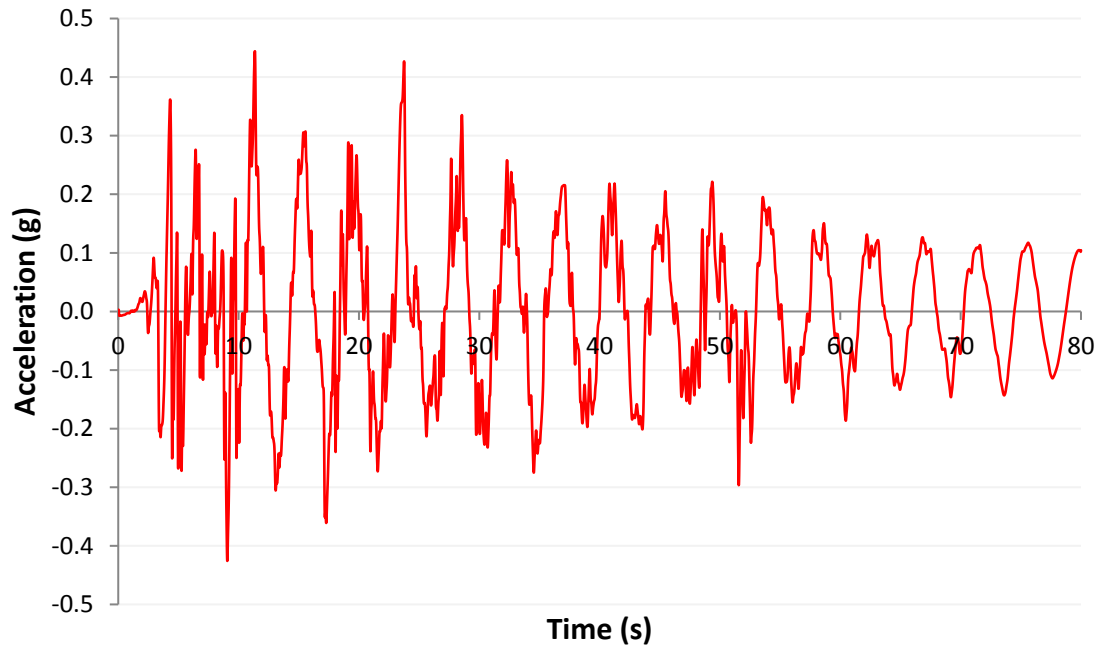


Figure A25. 5S1.0-IY acceleration

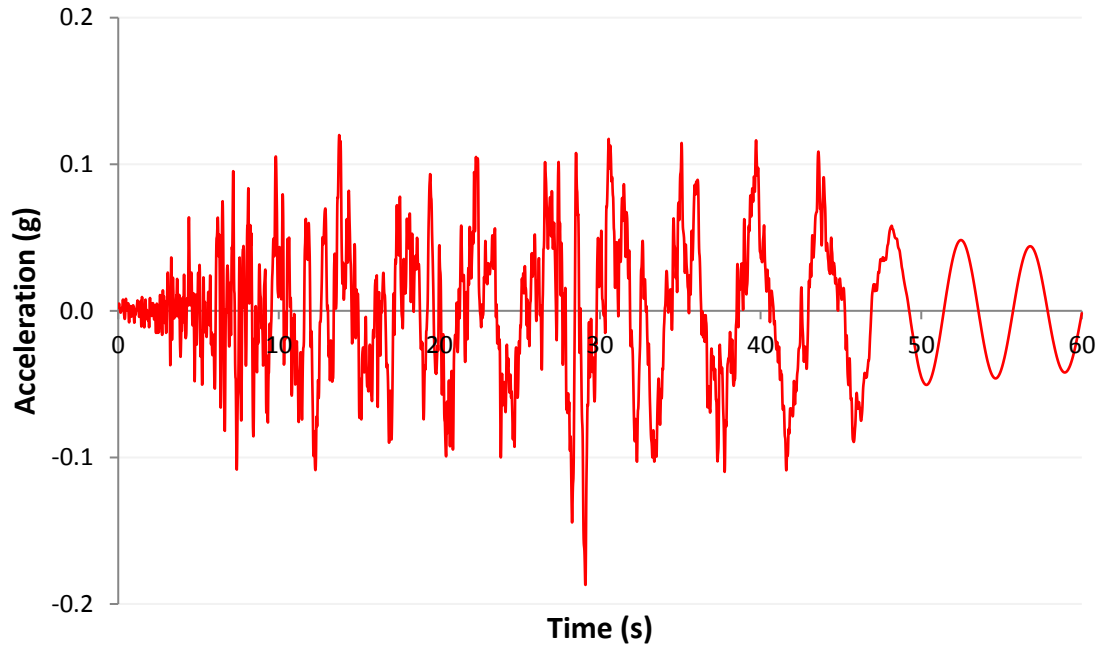


Figure A26. 5S1.0-LX acceleration

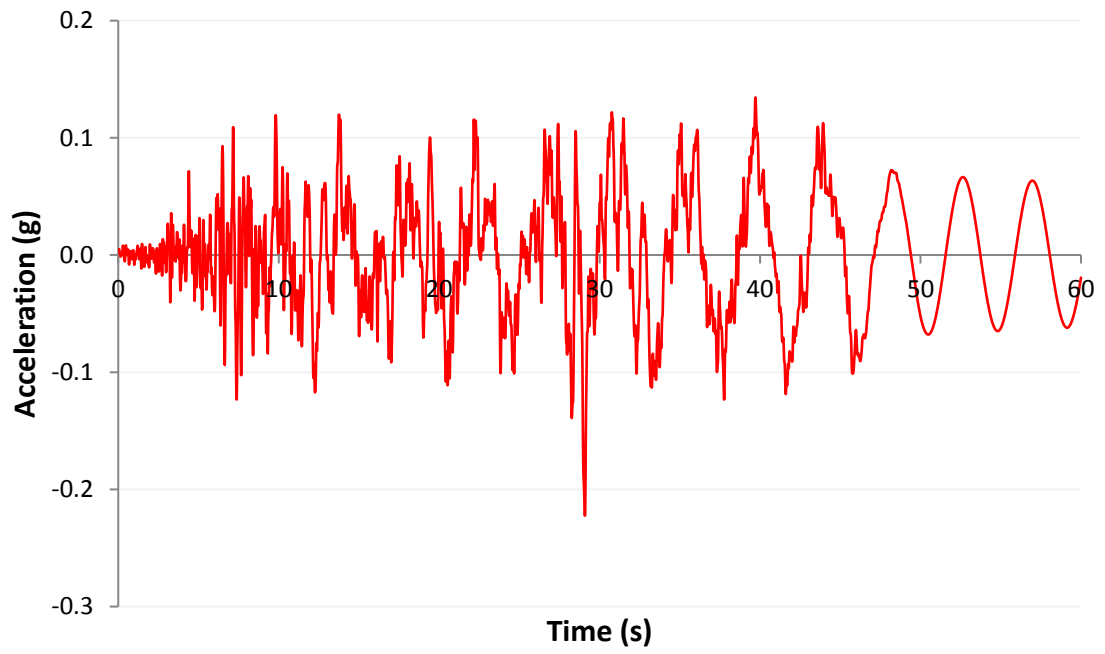


Figure A27. 5S1.0-LY acceleration

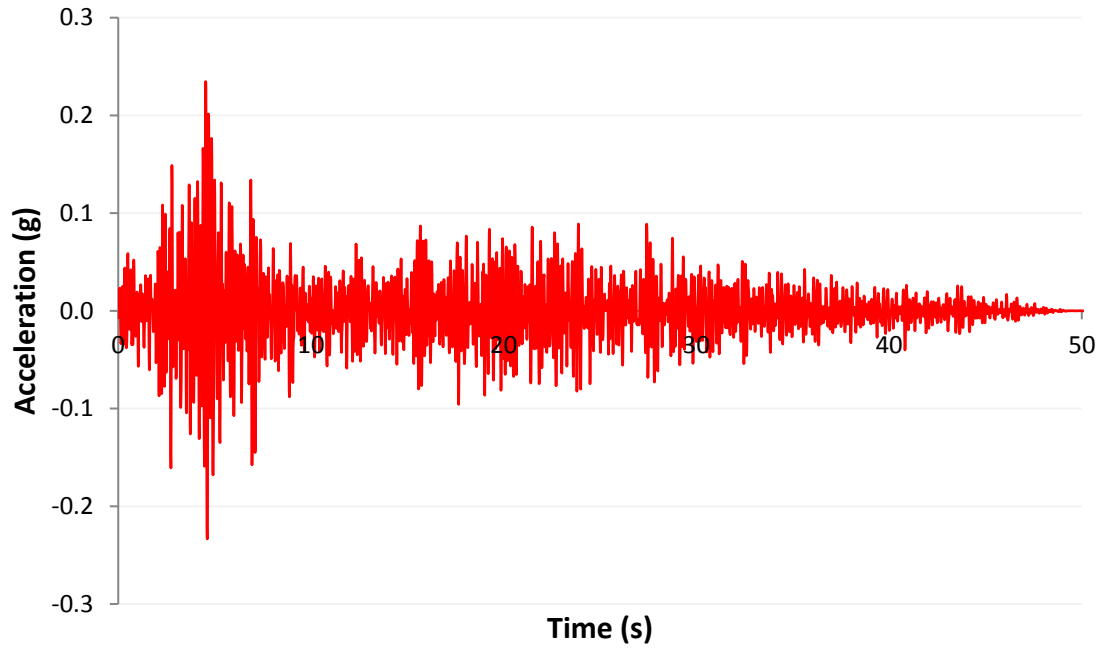


Figure A28. 5S1.0-LZ acceleration

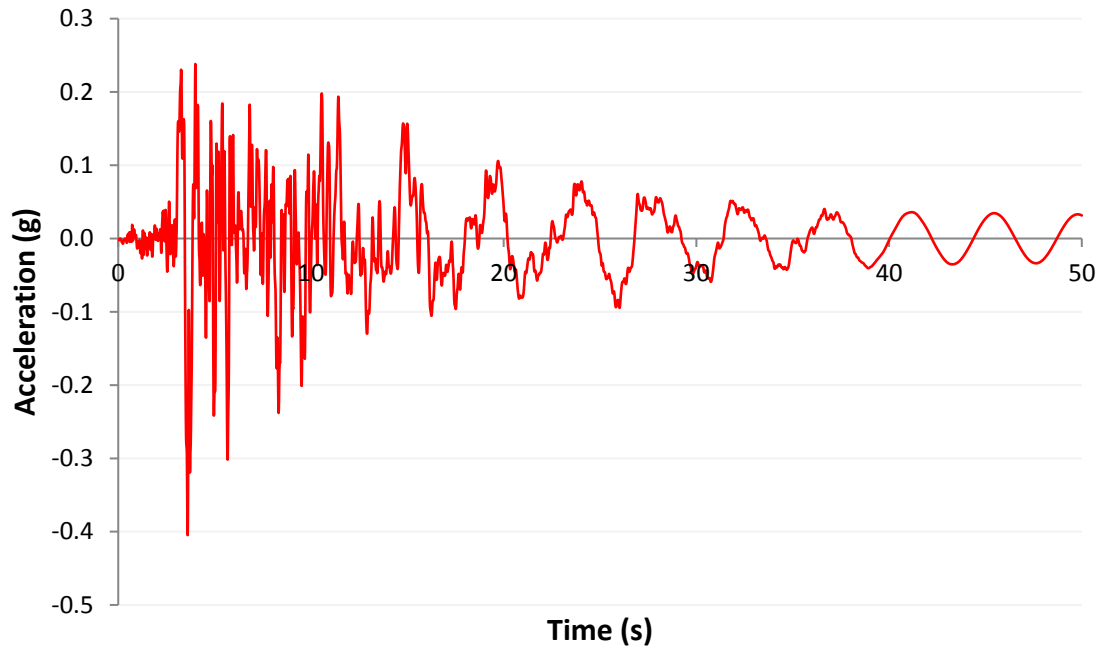


Figure A29. 5S1.0-NY acceleration

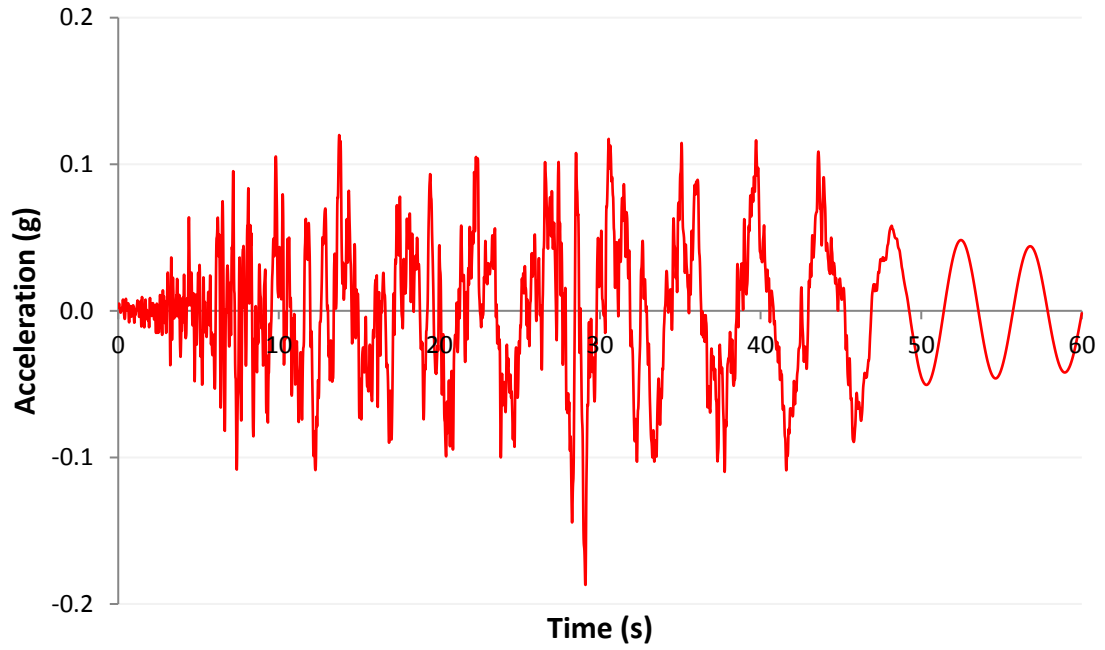


Figure A30. 5S2.0-LX acceleration

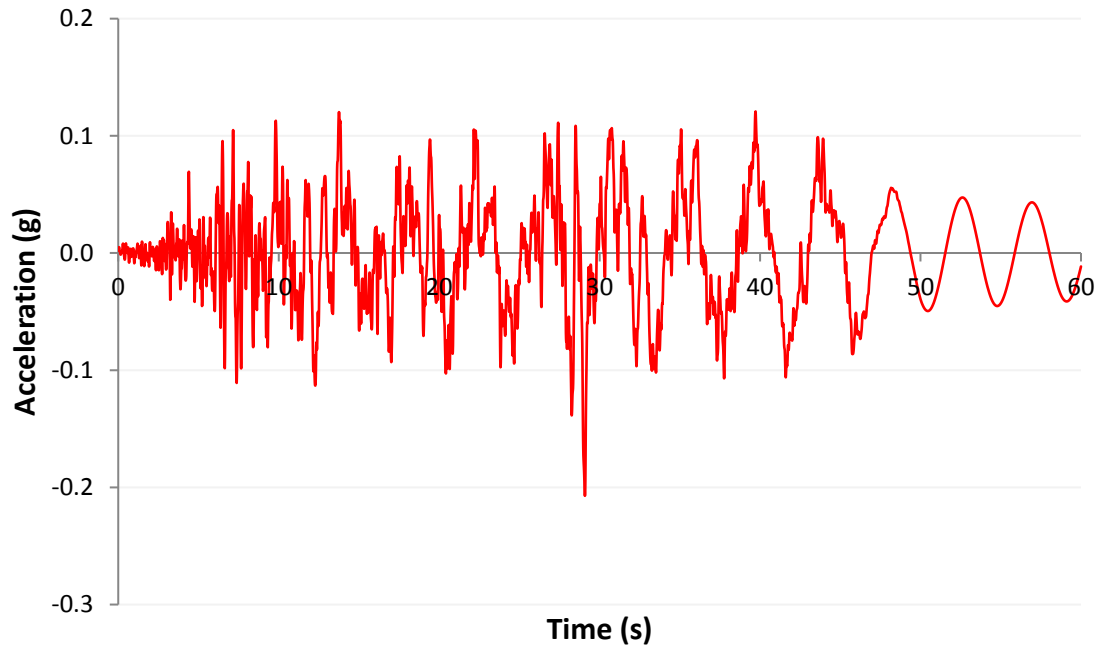


Figure A31. 5S2.0-LY acceleration

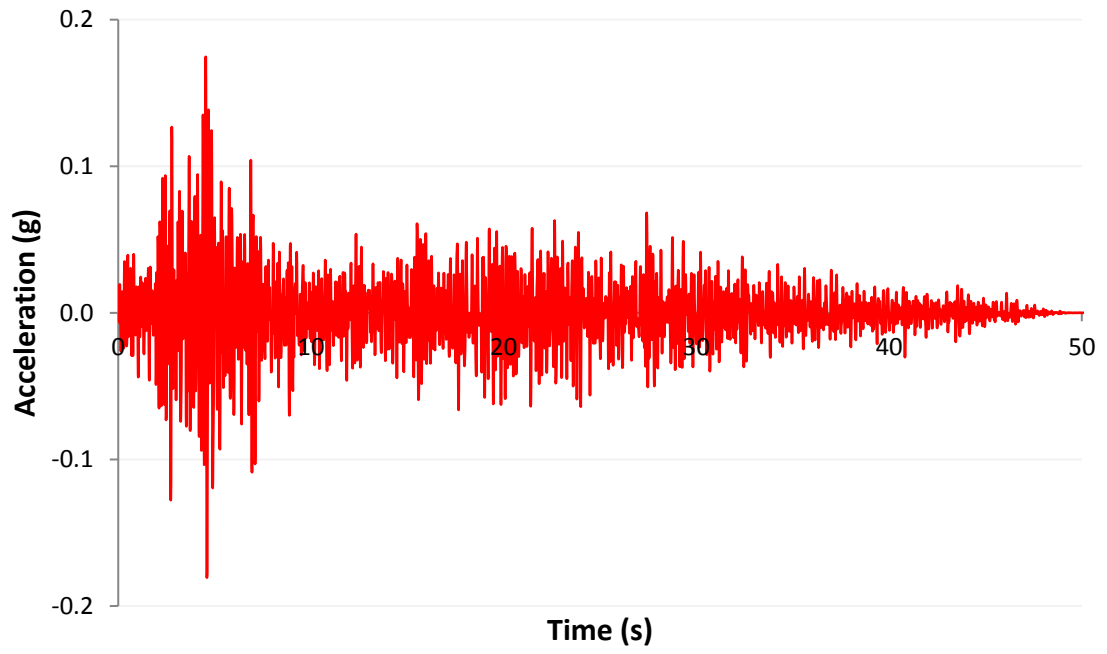


Figure A32. 5S2.0-LZ acceleration

APPENDIX B
TRANSIENT ANALYSIS DATA FOR WIND TURBINES
WITH FOUNDATIONS

1MW & Foundation

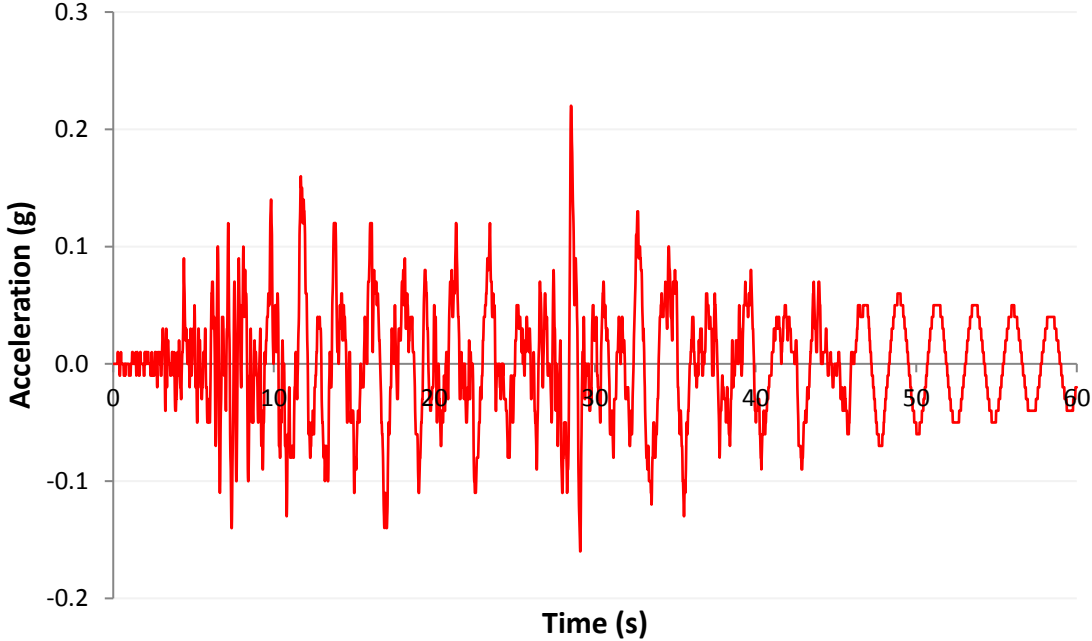


Figure B1. 1S1.0-LX & Spread foundation acceleration

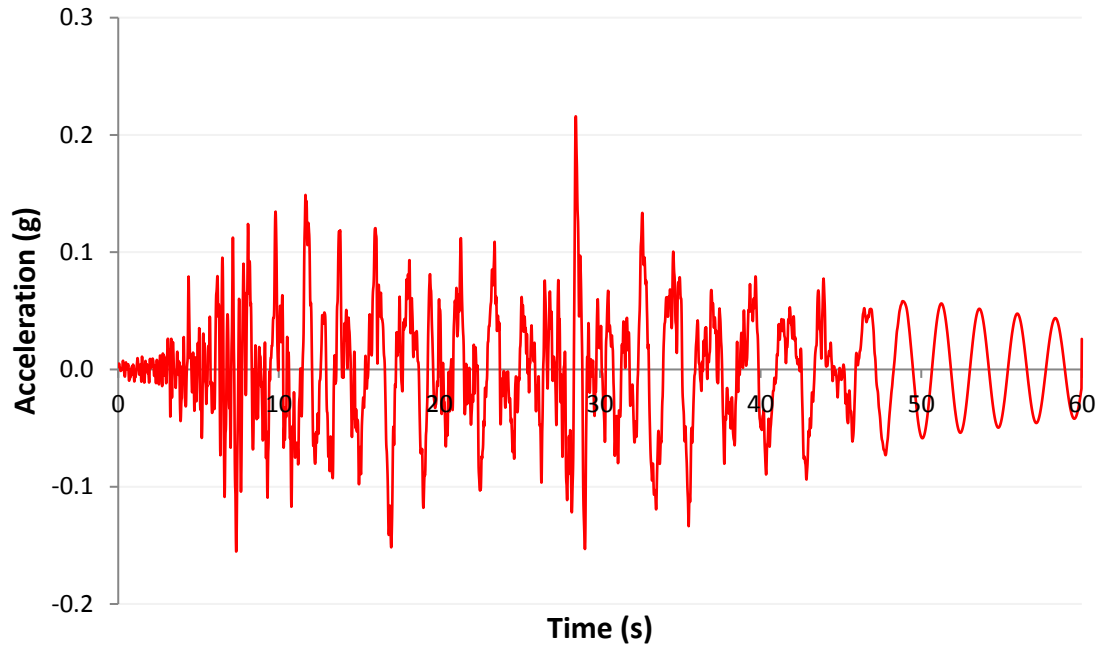


Figure B2. 1S1.0-LY & Spread foundation acceleration

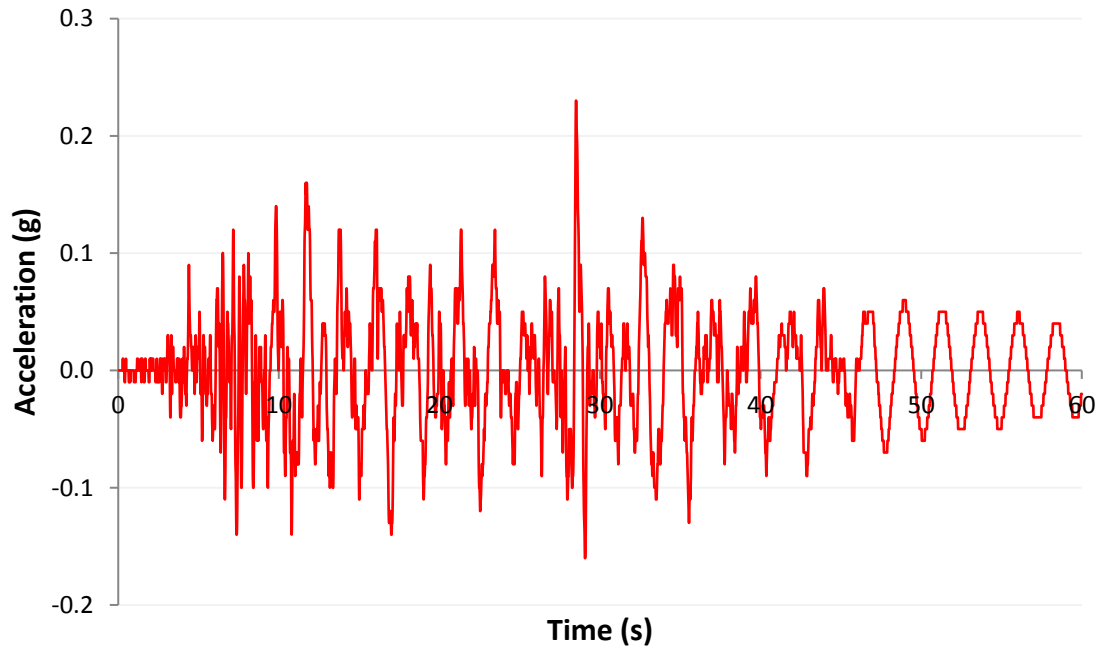


Figure B3. 1S1.0-LX & Mono pile foundation acceleration

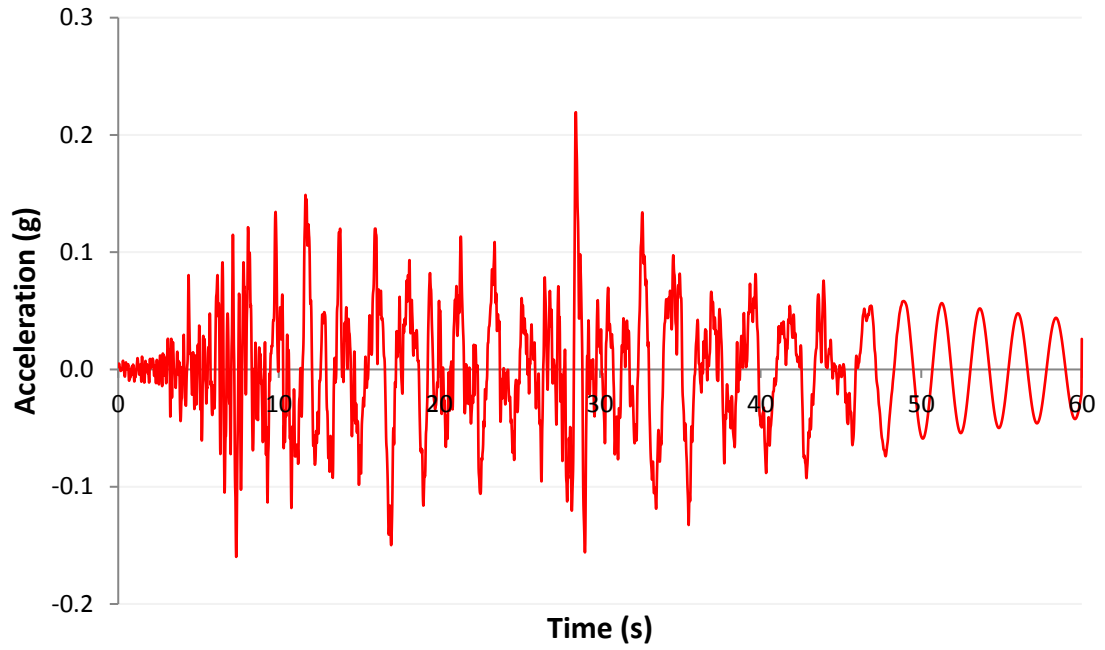


Figure B4. 1S1.0-LY & Mono pile foundation acceleration

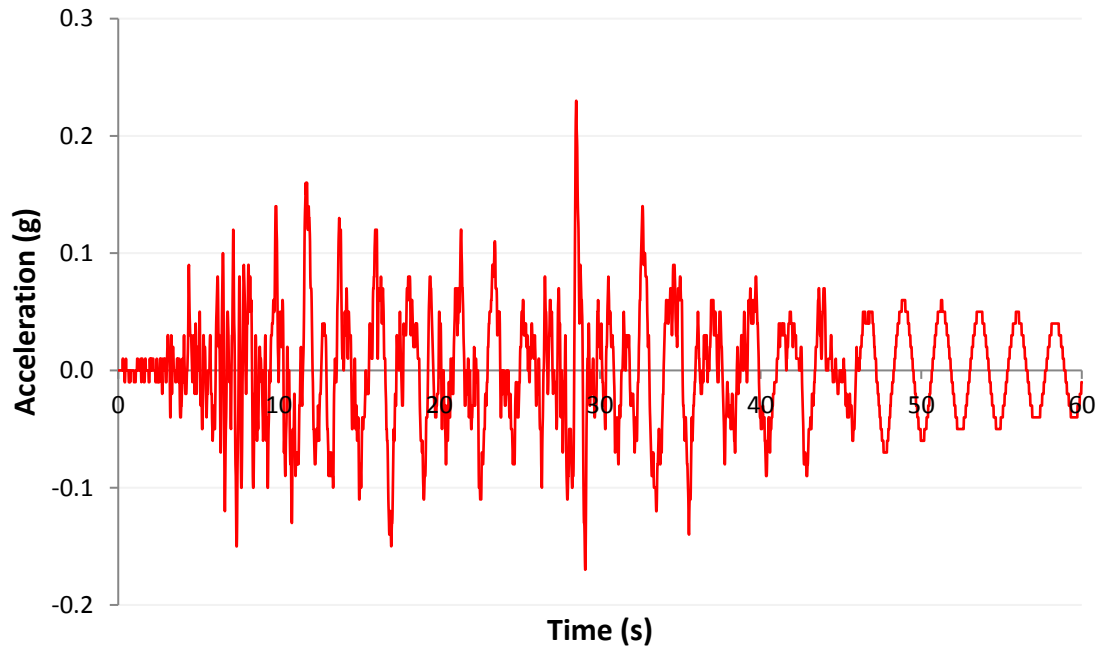


Figure B5. 1S1.0-LX & Pile group & cap foundation acceleration

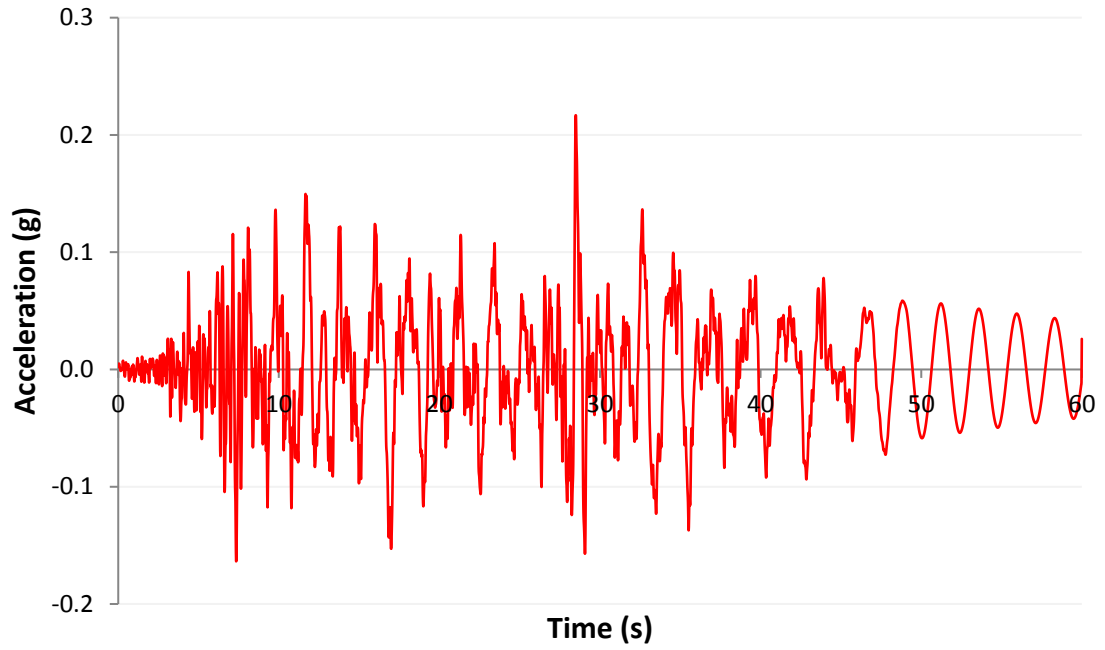


Figure B6. 1S1.0-LY & Pile group & cap foundation acceleration

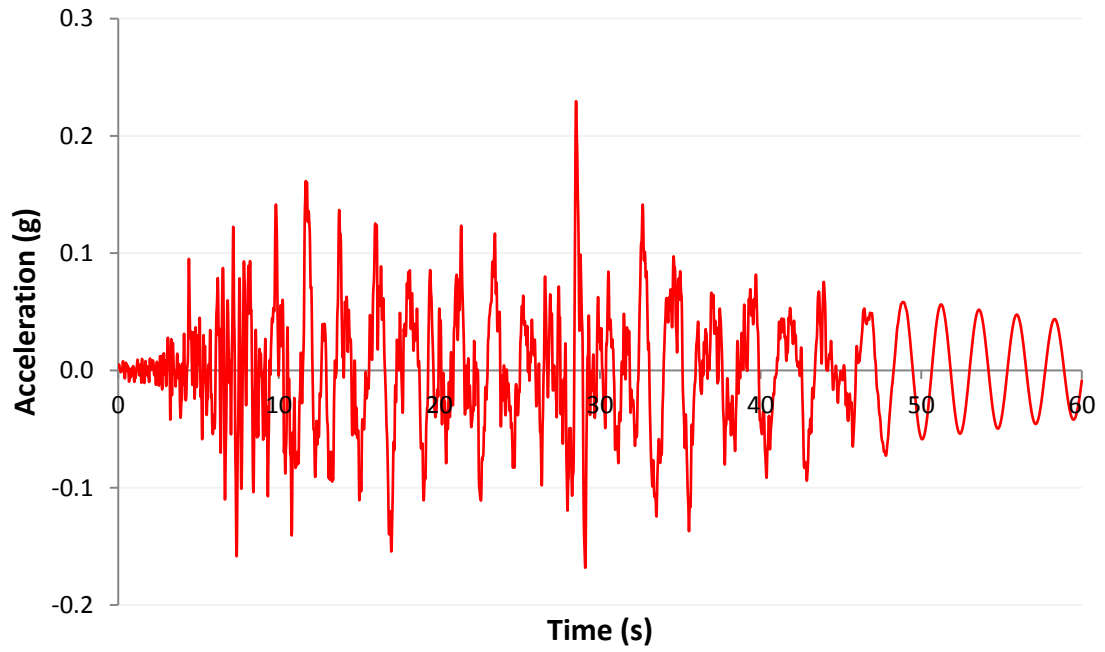


Figure B7. 1S1.0-LX & Anchored Spread foundation acceleration

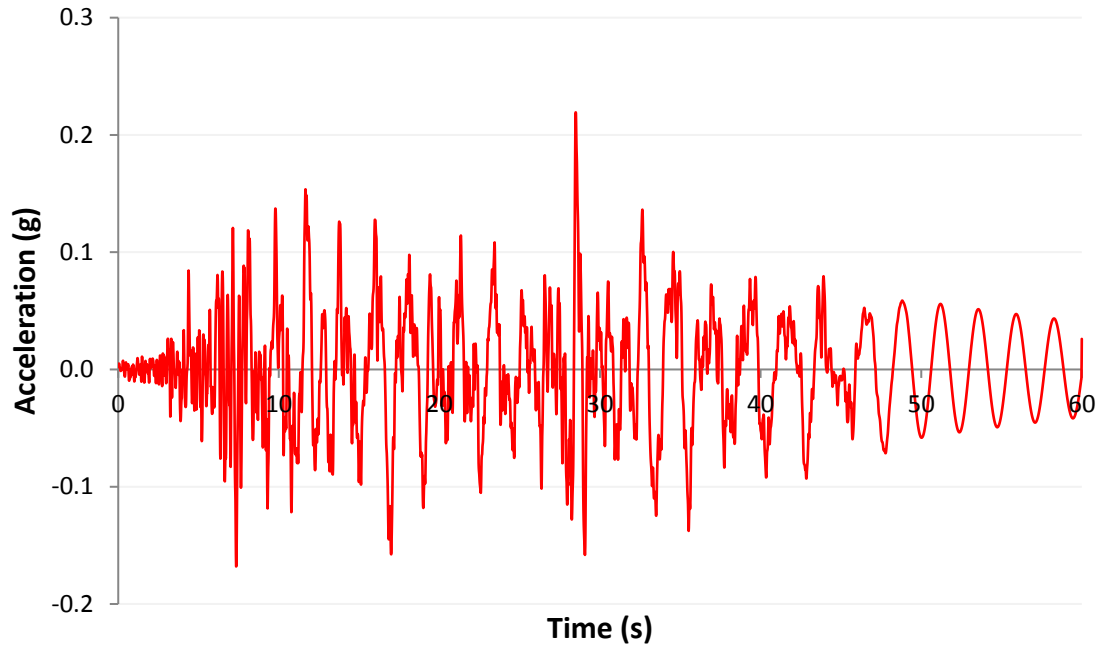


Figure B8. 1S1.0-LY & Anchored Spread foundation acceleration

REFERENCES

-
- 1 Chen, A. (2010) New Study Sheds Light on U.S. Wind Power Market. Lawrence Berkeley National Laboratory.
 - 2 Institute for Energy Research website
 - 3 Global Wind Energy Council (GWEC) (2015) Global Wind Report Annual Market Update
 - 4 Global Energy Concepts (2005) Wind Turbine Technology Overview
 - 5 The Renewable Energy Website, www.reuk.co.uk
 - 6 Vertical Axis Wind Turbines, www.newhomewindpower.com
 - 7 Vertical Axis Wind Turbines www.archiexpo.com
 - 8 Ancona, D. (2010) Wind Turbine - Materials and Manufacturing Fact Sheet. Office of Industrial Technologies, U.S. Department of Energy.
 - 9 howstuffworks.com
 - 10 Long, H. (2007) Truss Type Towers in Offshore Wind Turbines. Department of Civil and Transport Engineering, Norway.
 - 11 Harte, R. (2007) Structural Stability of Concrete Wind Turbines and Solar Chimney Towers Exposed to Dynamic Wind Action. *Journal of Wind Engineering and Industrial Aerodynamics* 95 (2007) 1079–1096.
 - 12 SLIM Transformer inside the World's Highest Wind Turbine (2008) Pauwels Business News.
 - 13 Zavitz, B. (2012) A New Measure of Wind Tower Scalability for Greater Hub Heights and Larger Turbines. Tindall Corporation White Paper Series No. WT-102.
 - 14 The Concrete Center (2005) Concrete Wind Towers.

-
- 15 Wind Powering America. Department of Energy, www.windpoweringamerica.gov
- 16 Singh, A.N. (2007) Concrete Construction for wind Energy Towers. The Indian Concrete Journal (pp. 43-49)
- 17 The Des Moines Register website
- 18 Prowell, I. (2010) Estimation of Seismic Load Demand for a Wind Turbine in the Time Domain. National Renewable Energy Laboratory (NREL/CP-500-47536).
- 19 Clough, R.W., and Penzien, J. (2003) Dynamics of Structures. McGraw-Hill, New York.
- 20 Hodges, D.H. (2002) Introduction to Structural Dynamics and Aeroelasticity, Cambridge University Press, Cambridge, U.K.
- 21 Wind Turbine Design Requirements IEC 61400 (2005) International Electrotechnical Commission Standards.
- 22 Guideline for the Certification of Wind Turbines (2010) Germanischer Lloyd (GL) GL2010.
- 23 Offshore Standard DNV-OS-J101, Design of Offshore Wind Turbine Structures, DET NORSKE VERITAS (2007).
- 24 Guidelines for Design of Wind Turbines, Det Norske Veritas and Wind Energy Department, Risø National Laboratory (2002).
- 25 Ritschel, U., and Warnke, I. , and Kirchner, J. , and Meussen, B. (2000) Wind Turbines and Earthquakes. 2nd World Wind Energy Conference (pp. 1-8).
- 26 Bazeos, N. , and Hatzigeorgiou, G. , and Hondros, I. , and Karamaneas, H. , and Karabalis, D. , and Beskos, D. (2002) Static, Seismic and Stability Analyses of a Prototype Wind Turbine Steel Tower. Journal of Engineering Structures 24(8) (pp. 1015–1025).
- 27 Eurocode 3 Design of Steel Structures (1996).
- 28 Kiyomiya, O., and Rikiji, and T., van Gelder, P. (2002) Dynamic Response Analysis of Onshore Wind Energy Power Units during Earthquakes and Wind. International Offshore and Polar Engineering Conference, Kitakyushu, Japan.

-
- 29 Lavassas, I. , and Nikolaidis, G. , and Zervas, P. , and Efthimiou, E. , and Doudoumis, I.N. , and Baniotopoulos, C.C. (2003) Analysis and Design of the Prototype of a Steel 1-MW Wind Turbine Tower. *Journal of Engineering Structures* (pp. 1097-1106).
- 30 Witcher, D. , and Hassan, G. (2004) Seismic Analysis of Wind Turbines in the Time Domain. *Wind Energy Journal*. *Wind Energy*. 2005; 8:81–91 (DOI: 10.1002/we.135)
- 31 Zhao, X. , and Maißer, B. (2006) Seismic Response Analysis of Wind Turbine Towers Including Soil-Structure Interaction. *Journal of Multi-body Dynamics* 220(1):53-61
- 32 Hänler, M. , and Ritschel, U. , and Warnke, I. (2006) Systematic Modelling of Wind Turbine Dynamics and Earthquake Loads on Wind Turbines. *European Wind Energy Conference and Exhibition, Athens, Greece*.
- 33 Zhao, X. , and Maißer, P. , and Wu, J. (2006) A New Multibody Modelling Methodology for Wind Turbine Structures Using a Cardanic Joint Beam Element. *Journal of Renewable Energy* (pp.532–546).
- 34 Bir, G. , and Jonkman, J. (2007) *Aeroelastic Instabilities of Large Offshore and Onshore Wind Turbines (NREL/CP-500-41804)*.
- 35 Prowell, I., and Veers, P. (2009) *Assessment of Wind Turbine Seismic Risk Existing Literature and Simple Study of Tower Moment Demand*
- 36 Prowell, I. (2009) *Experimental and Numerical Seismic Response of a 65 kW Wind Turbine. Journal of Earthquake Engineering* (13:1172–1190).
- 37 Prowell, I. , and Veletzos, M. , and Elgamal, A. (2008) *Full Scale Testing for Investigation of Wind Turbine Seismic Response*.
- 38 Prowell, I. , and Elgamal, A., and Lu, J. (2010) *Modeling the Influence of Soil-structure Interaction on the Seismic Response of a 5 MW Wind Turbine. Fifth International Conference on Recent Advances in Geotechnical Earthquake Engineering and Soil Dynamics*
- 39 Hongwang, M. (2012) *Seismic Analysis for Wind Turbines Including Soil-Structure Interaction Combining Vertical and Horizontal Earthquake. The 15th World Conference on Earthquake Engineering, Lisbon, Portugal*.

-
- 40 Kourkoulis, R.S., and Gelagoti, F.M., and Kaynia, A.M. (2012) Seismic Response of Offshore Wind Turbine Foundations. The 15th World Conference on Earthquake Engineering, Lisbon, Portugal.
- 41 Kjølraug, R.A., Kaynia, A.M., Elgamal, A., Seismic Response of Wind Turbines due to Earthquake and Wind Loading. Proceedings of the 9th International Conference on Structural Dynamics, Porto, Portugal.
- 42 Taddeia, F., Schauerb, M., Meinerzhagen, L., (2017) A Practical Soil-Structure Interaction Model for A Wind Turbine Subjected To Seismic Loads And Emergency Shutdown. X International Conference on Structural Dynamics 199 (2017) 2433–2438.
- 43 Time-History Dynamic Analysis of Concrete Hydraulic Structures, U.S. Army Corps of Engineers EM 1110-2-6051 (2003)
- 44 Zienkiewicz, O.C. , and Taylor, R.L. (2000) The Finite Element Method. Butterworth-Heinemann Publication.
- 45 Hughes, T.J.R. (1987) The Finite Element Method: Linear Static and Dynamic Finite Element Analysis. Dover Publications.
- 46 Hilber, H.M. , and Hughes, T.J.R. , and Taylor, R.L. (1977) Improved Numerical Dissipation for Time Integration Algorithm in Structural Dynamics. Journal of Earthquake Engineering and Structural Dynamics (Vol. 5. 283).
- 47 Wood, W.L. , and Bossak, M. , and Zienkiewicz, O.C. (1981) An Alpha Modification of Newmark Method. International Journal of Numerical Method in Engineering (Vol.15. p1562).
- 48 Chung, J. , and Hulbert, G.M. (1993) A time Integration Algorithm for Structural Dynamics With Improved Numerical Dissipation: the Generalized- α Method. Journal of Applied Mechanics (Vol. 60. 371).
- 49 NEHRP Recommended Provisions for Seismic Regulations for New Buildings and Other Structures (FEMA 450) 2003 Edition, The Building Seismic Safety Council
- 50 American Society of Civil Engineers and Structural Engineering Institute, Minimum Design Loads for Buildings and Other Structures (ASCE/SEI 7-10) (2010)
- 51 Chopra, A.K. (2012) Dynamics of structures - Theory and Applications to

Earthquake Engineering, Prentice Hall, New York.

52 Ancona, D. , and McVeigh, J. (2010) Wind Turbine - Materials and Manufacturing fact Sheet. Princeton Energy Resources International.

53 Mechanical APDL and Mechanical Applications Theory Reference (2010) ANSYS Inc.

54 Nicholson, J. (2011) Design of Wind Turbine Tower and Foundation Systems: Optimization Approach. Master's Thesis, University of Iowa, U.S.

55 Maunu, P. (2008) Design of Wind Turbine Foundation Slabs. Master's Thesis, Luleå University of Technology, Sweden.

56 Hassanzadeh, M. (2012) Cracks in Onshore Wind Power Foundations. Elforsk rapport 11:56.

57 Svensson, H. (2010) Design of Foundations for Wind Turbines. Master's Dissertation, Lund University, Sweden.

58 Marchegiani, E. (2005) AVEC foundation Design for Wind Turbines. Wind Energy Training Seminar.

59 Ashlock, J. , and Schaefer, V. (2011) Foundations for Wind Turbines.

60 Naeim, F. , and Kircher, C. (2001) On the Damping Adjustment Factors for Earthquake Response Spectra. Journal of The Structural Design of Tall Buildings (Vol. 10, 361-369)